

University of Nevada, Reno

**Nuclear Material Accountancy in High Temperature Molten Salt Using *In Situ* Raman Spectroscopy and Cyclic Voltammetry**

A dissertation submitted in partial fulfillment of the requirements for the degree of  
Doctor of Philosophy in Materials Science and Engineering

By

Vickram J. Singh

Dr. Dev Chidambaram/Dissertation Primary Advisor

Dr. Jeffrey LaCombe/Dissertation Co-Advisor

May, 2019

© by Vickram J. Singh 2019  
All Rights Reserved

**UNIVERSITY OF NEVADA RENO  
THE GRADUATE SCHOOL**

We recommend that the dissertation  
prepared under our supervision by

**VICKRAM J. SINGH**

entitled

**Nuclear Material Accountancy in High Temperature Molten Salt Using *In Situ* Raman  
Spectroscopy and Cyclic Voltammetry**

be accepted in partial fulfillment of the  
requirements for the degree of

DOCTOR OF PHILOSOPHY

Dev Chidambaram, Ph.D., Primary Advisor

Jeffrey LaCombe, Ph.D., Co-advisor

Qi An, Ph.D., Committee Member

Nicholas Tsoufanidis, Ph.D., Committee Member

Miles Greiner, Ph.D., Graduate School Representative

David W. Zeh, Ph.D., Dean, Graduate School

May 2019

## Abstract

As the world attempts to transition to more sustainable and environmentally friendly forms of energy, nuclear power has the potential to play a central role in meeting the growing energy needs of the planet. The security concerns associated with special nuclear materials and nuclear waste continue to hinder the growth of nuclear energy. High temperature molten salt systems have been proposed as an advanced, proliferation-resistant media for nuclear energy production, fuel reprocessing, and securing the nuclear weapons complex. A chemical-based sensing system was designed, constructed, and evaluated for nuclear material accountancy in high temperature molten chloride salt. Raman spectroscopy and cyclic voltammetry were utilized as sensing methods to study lanthanide concentration, diffusion kinetics, speciation, and coordination chemistry in the molten LiCl-KCl salt of eutectic composition.

*In situ* Raman spectroscopy was conducted using a custom-built, fiber-based system. A commercial system was modified through an iterative process to address the hands-free and extreme environmental requirements associated with the molten salt studies. The experimental system was designed and constructed with remote control and data acquisition capabilities for the high temperature environment. This system was used to investigate samarium speciation and coordination chemistry in the molten LiCl-KCl at 500 °C. Trivalent samarium was confirmed to be present as an octahedral  $\text{SmCl}_6^{3-}$  complex, in agreement with the literature. Raman spectra were analyzed for bond-specific vibration modes and fluorescence. The electroanalytical voltammetry system

coupled with the fiber-based Raman system was used to study divalent samarium ions. Divalent samarium was produced *in situ* using both chemical and electrochemical reduction protocols and analyzed using Raman spectroscopy. To our knowledge, this is the first Raman spectrum of divalent samarium in molten LiCl-KCl eutectic. Raman spectra of  $\text{CeCl}_3$  in molten LiCl-KCl was found to be identical to that obtained from  $\text{SmCl}_3$  in molten LiCl-KCl except for the fluorescence features. Spectra obtained from multi-analyte environment (mixture of Sm and Ce in molten LiCl-KCl) showed that differentiating mixed analytes is not possible without significant technological and design improvements and development of complex deconvolution protocols.

A cyclic voltammetry analysis protocol available in the literature was further developed for more accuracy. Collected data was analyzed using existing electrochemical relationship, the Randles-Sevcik equation, which was originally developed for aqueous, fully-reversible systems. The applicability of this empirical relationship was evaluated over a broad concentration range. Calculated diffusion coefficients were compared and contrasted to the existing literature.

The coupled spectroelectrochemical system was then employed to study the nature of samarium oxychloride formation in the molten LiCl-KCl- $\text{SmCl}_3$  system. A synthesis method reported in the literature was confirmed *in situ*, and the synthesized product was confirmed to be samarium oxychloride using solid state characterization methods.

In summary, this dissertation reports the construction and successful deployment of a combined Raman spectroscopy and electroanalytical system for nuclear material

accountancy in high temperature molten salt. The electroanalytical voltammetry system produced accurate and repeatable data in the low analyte concentration regime which was confirmed with the literature. The *in situ* Raman spectroscopy system was engineered, constructed and successfully tested for use in high temperature molten salt environments. The system designed in this dissertation can be deployed for use in studying single analyte in molten salt systems immediately.

## Dedication

To my parents and brother

For their unwavering support and love

## Acknowledgements

I thank my co-advisor, Dr. Jeffrey LaCombe, for his professional guidance and support in completing my course of study. His unique perspectives on leadership and overcoming adversity will undoubtedly serve me well throughout the rest of my professional career. I acknowledge my advisor Dr. Dev Chidambaram and my committee members Dr. Qi An, Dr. Nicholas Tsoulfanidis and Dr. Miles Greiner, for their time and scientific insights. I especially thank Dr. Nicholas Tsoulfanidis and Taylor Wilson for the unparalleled nuclear education they have provided to me. Their insights have not only educated me but inspired me to pursue an innovative career in the nuclear industry.

I thank my colleagues at MERLab for their support and friendship. I especially thank Dr. Augustus Merwin, Dr. David Rodriguez, and Zachary Karmioli for teaching me the fundamentals of electrochemistry and assisting with solid state materials characterization. I thank my best friend and lab mate Christopher Bruneau. The long nights, obstacles, and uncertainties we faced together have convinced me we are capable of chasing our most ambitious pursuits.

This work was supported by the United States Department of Energy (DOE) under contracts DE-NE0008236 and DE-NE0008572, and the United States Nuclear Regulatory Commission (NRC) under contract NRC-HQ-13-G-38-0027. I acknowledge Materials Characterization Nevada (MCNV) for assistance with solid-state characterization. Dr. Kenny Osborne and Ms. Nancy Hebron-Israel serve as the DOE and NRC award program managers, respectively.



# Table of Contents

<b>ABSTRACT</b> .....	<b>I</b>
<b>DEDICATION</b> .....	<b>IV</b>
<b>ACKNOWLEDGEMENTS</b> .....	<b>V</b>
<b>LIST OF TABLES</b> .....	<b>VIII</b>
<b>LIST OF FIGURES</b> .....	<b>IX</b>
<b>CHAPTER 1 INTRODUCTION</b> .....	<b>1</b>
1.1 NUCLEAR SECURITY AND NONPROLIFERATION .....	1
1.2 ADVANCEMENTS IN NUCLEAR TECHNOLOGY .....	2
1.3 NUCLEAR MATERIAL ACCOUNTANCY IN MOLTEN CHLORIDE SALTS .....	4
1.4 ELECTROANALYTICAL VOLTAMMETRY IN THE MOLTEN LiCl-KCl EUTECTIC .....	7
1.5 RAMAN SPECTROSCOPY IN THE MOLTEN LiCl-KCl EUTECTIC .....	12
1.6 SUMMARY .....	16
<b>CHAPTER 2 EXPERIMENTAL</b> .....	<b>18</b>
2.1 SPECTROELECTROCHEMICAL APPARATUS .....	18
2.2 CHEMICALS AND MATERIALS.....	21
2.3 SOLID STATE CHARACTERIZATION.....	22
<b>CHAPTER 3 SYSTEM DEVELOPMENT AND CALIBRATION</b> .....	<b>23</b>
3.1 RAMAN CALIBRATION .....	23
3.2 PRELIMINARY CHLORIDE SALT RAMAN .....	25
3.3 PRELIMINARY CV INVESTIGATIONS .....	27
3.4 AUTOMATED SYSTEM QUASI-REFERENCE CV STUDY .....	33
3.5 Ag AgCl REFERENCE ELECTRODE IMPLEMENTATION FOR CV .....	39
3.6 LOW CONCENTRATION CERIUM CV STUDY.....	43
<b>CHAPTER 4 <i>IN SITU</i> RAMAN SPECTROSCOPY OF SAMARIUM IONS IN MOLTEN LiCl-KCl EUTECTIC</b> .....	<b>47</b>
4.1 INTRODUCTION .....	47
4.2 EXPERIMENTAL .....	49
4.3 RESULTS AND DISCUSSION.....	52
4.4 CONCLUSIONS .....	63

<b>CHAPTER 5 CYCLIC VOLTAMMETRY OF SAMARIUM IONS IN THE MOLTEN LiCl-KCl EUTECTIC FOR DIFFUSION COEFFICIENT ANALYSIS .....</b>	<b>65</b>
5.1 INTRODUCTION .....	65
5.2 EXPERIMENTAL .....	68
5.3 RESULTS AND DISCUSSION.....	73
5.4 CONCLUSIONS .....	86
<b>CHAPTER 6 AN INVESTIGATION OF SYNTHESIZED SAMARIUM OXYCHLORIDE IN MOLTEN LiCl-KCl EUTECTIC AND ITS NUCLEAR MATERIAL MANAGEMENT IMPLICATIONS .....</b>	<b>88</b>
6.1 INTRODUCTION .....	88
6.2 EXPERIMENTAL .....	91
6.3 RESULTS AND DISCUSSION.....	96
6.4 CONCLUSIONS .....	106
<b>CHAPTER 7 OTHER RELEVANT RESULTS .....</b>	<b>107</b>
7.1 MULTI-ANALYTE STUDY.....	107
7.2 LiCl-KCl-ZrCl <sub>4</sub> RAMAN SPECTROSCOPY .....	111
<b>CHAPTER 8 DISCUSSION OF RESULTS .....</b>	<b>113</b>
8.1 EVALUATION OF SPECTROELECTROCHEMICAL SYSTEM.....	113
8.2 NUCLEAR MATERIAL ACCOUNTANCY APPLICATIONS.....	115
<b>CHAPTER 9 CONCLUSIONS AND FUTURE WORK .....</b>	<b>117</b>
9.1 CONCLUSIONS .....	117
9.2 FUTURE WORK .....	119
<b>REFERENCES .....</b>	<b>121</b>
<b>APPENDIX.....</b>	<b>132</b>
A.1 OXYCHLORIDE SYNTHESIS METHOD.....	132
A.2 TECHNICAL MEETING ABSTRACTS .....	135
A.3 UNIVERSITY OF NEVADA, RENO 2016 GRADUATE STUDENT POSTER CONTEST .....	142
A.4 UNIVERSITY OF NEVADA, RENO 2018 3 MINUTE THESIS .....	143

## List of Tables

<b>Table 1</b> An experimental electroanalytical sequence developed by Tylka et al. employed for accurate and repeatable CV acquisition .....	10
<b>Table 2</b> Diffusion coefficients from the literature obtained measured in environmental conditions similar to this study for trivalent cerium and trivalent samarium at concentrations below 5 wt. % [47, 49, 57-59] .....	11
<b>Table 3</b> Expected Raman mode values from the literature are reported for solid state, molten, and eutectic mixtures of NaNO <sub>3</sub> and KNO <sub>3</sub> [66].....	24
<b>Table 4</b> Raman modes and associated intensities for molten eutectic NaNO <sub>3</sub> /KNO <sub>3</sub> were reported by Janz et al. [66].....	24
<b>Table 5</b> Results obtained using the fiber system were compared to the literature values published by Janz et al. [66]. .....	25
<b>Table 6</b> Diffusion coefficient results for trivalent cerium from this study were compared with the recent literature. ....	46
<b>Table 7</b> Comparison of previously published Nd <sup>2+</sup> vibration modes and Sm <sup>2+</sup> modes reported in this study .....	56
<b>Table 8</b> Comparison of neodymium vibration modes from the literature, chemically reduced divalent samarium modes and electrochemically reduced divalent samarium modes .....	63
<b>Table 9</b> Electroanalytical sequence obtained from Tylka et al. and adjusted for SmCl <sub>3</sub> analysis .....	72
<b>Table 10</b> Summary of the molten SmCl <sub>3</sub> -LiCl-KCl samples analyzed in this work, their respective SmCl <sub>3</sub> concentrations measured using ICP-OES, and WE surface area values determined using the immersion step method.....	78
<b>Table 11</b> Diffusion coefficient results and associated error values from this study compared with the available literature. ....	84
<b>Table 12</b> Migration contribution results with respect to Sm <sup>3+</sup> transference for all sample concentrations.....	85
<b>Table 13</b> EDS chemical analysis results for both precipitate morphologies observed in SEM images indicated approximately 1:1 Sm:Cl atomic ratio values. ....	97
<b>Table 14</b> Summary of advantages, disadvantages, and synergies of the SPEC system's analytical components.....	114

## List of Figures

<b>Figure 1</b> A proposed pyrochemical reprocessing flowsheet for the LWR fuel cycle illustrating the many unit operations that may require NMA [37].....	6
<b>Figure 2</b> A Jablonski diagram illustrating the differences between Raman scattering, Rayleigh scattering and sample fluorescence as they relate to energy states modified from Harris et al. [64] .....	13
<b>Figure 3</b> Point group $O_h$ Raman active modes of vibration for a molecule similar to an $[LnCl_6]^{3-}$ complex – $\nu_1$ , $\nu_2$ , and $\nu_5$ modes Raman active, modified from Ferraro [63] .....	15
<b>Figure 4</b> Spectroelectrochemical system constructed and tested for simultaneous voltammetric and spectroscopic studies in the molten LiCl-KCl eutectic.....	20
<b>Figure 5</b> Broad sweep results indicated the presence of Raman modes and were compared with the available literature. ....	25
<b>Figure 6</b> Working distance of the fiber-based Raman had a pronounced effect on spectral quality in terms of signal-to-noise ratio. ....	26
<b>Figure 7</b> The installation of quartz discs between the Raman objective and molten salt sample significantly decreased signal magnitude. ....	27
<b>Figure 8</b> Preliminary investigations produced a collection of CVs obtained at varying $SmCl_3$ concentrations and peak current vs. concentration results. Repeatability and the theoretically linear relationship between peak current and scan rate were evaluated...	29
<b>Figure 9</b> The preliminary repeat study after implementation of the adjusted experimental procedure increased repeatability of CV scans. ....	30
<b>Figure 10</b> Preliminary attempt at immersion experiment for determining working electrode surface area produced the expected linear correlation but large amounts of error in current response. ....	31
<b>Figure 11</b> CVs taken with a direct and indirect connection to cell leads using an aqueous electrochemical system inspired a drift away from extension cable use. ....	33
<b>Figure 12</b> Cyclic voltammetry of 1.0 wt. % $SmCl_3$ solvated in the molten LiCl-KCl eutectic at 500 °C and analyzed according to the Randles-Sevcik equation. ....	34
<b>Figure 13</b> Cyclic voltammetry of 2.0 wt. % $SmCl_3$ solvated in the molten LiCl-KCl eutectic at 500 °C and analyzed according to the Randles-Sevcik equation. ....	35
<b>Figure 14</b> Cyclic voltammetry of 3.0 wt. % $SmCl_3$ solvated in the molten LiCl-KCl eutectic at 500 °C and analyzed according to the Randles-Sevcik equation. ....	36
<b>Figure 15</b> Cyclic voltammetry of 4.0 wt. % $SmCl_3$ solvated in the molten LiCl-KCl eutectic at 500 °C and analyzed according to the Randles-Sevcik equation. ....	37

<b>Figure 16</b> Cyclic voltammetry of 5.0 wt. % $\text{SmCl}_3$ solvated in the molten LiCl-KCl eutectic at 500 °C and analyzed according to the Randles-Sevcik equation. ....	38
<b>Figure 17</b> Peak current varied in a relatively linear fashion with respect to concentration as a result of the quasi-reference study. ....	39
<b>Figure 18</b> Cyclic voltammetry of 1.0 wt. % $\text{SmCl}_3$ in molten LiCl-KCl eutectic maintained at a temperature of 500 °C produced relatively linear trends with respect to scan rate and immersion depth of the WE. ....	40
<b>Figure 19</b> Cyclic voltammetry of 3.0 wt. % $\text{SmCl}_3$ in molten LiCl-KCl eutectic maintained at a temperature of 500 °C produced relatively linear trends with respect to scan rate and immersion depth of the WE. ....	41
<b>Figure 20</b> Cyclic voltammetry of 5.0 wt. % $\text{SmCl}_3$ in molten LiCl-KCl eutectic maintained at a temperature of 500 °C produced relatively linear trends with respect to scan rate and immersion depth of the WE. ....	41
<b>Figure 21</b> Cyclic voltammetry of 7.0 wt. % $\text{SmCl}_3$ in molten LiCl-KCl eutectic maintained at a temperature of 500 °C produced relatively linear trends with respect to scan rate and immersion depth of the WE. ....	42
<b>Figure 22</b> Peak current concentration results with (left) and without (right) the 7.0 wt. % data set suggested limits in the Randle-Sevcik's applicability or the manifestation of migration at higher analyte concentration.....	43
<b>Figure 23</b> CVs obtained from 1.0 wt. % $\text{CeCl}_3$ melt at various scan rates were clean and exhibited relatively consistent spacing.....	44
<b>Figure 24</b> Peak current versus scan rate data from preliminary 1.0 wt. % $\text{CeCl}_3$ sample exhibited a linear correlation as expected. ....	44
<b>Figure 25</b> CVs obtained from a repeat 1.0 wt. % $\text{CeCl}_3$ experiment indicated the presence of unexplained redox peaks not associated with typical $\text{CeCl}_3$ data .....	45
<b>Figure 26</b> CVs obtained from a 2.0 wt. % $\text{CeCl}_3$ melt indicated the presence of unexplained redox peaks as well.....	46
<b>Figure 27</b> SPEC setup employed for dual Raman spectroscopy and electrochemical studies. ....	51
<b>Figure 28</b> Raman polarized (VV) and depolarized (HV) spectra of 5 mol % trivalent samarium in LiCl-KCl eutectic. ....	53
<b>Figure 29</b> Reduced Raman spectra of isotropic and anisotropic components associated with trivalent samarium in LiCl-KCl eutectic at 500 °C. ....	54
<b>Figure 30</b> Polarized (VV) and depolarized (HV) Raman spectra of 0.01 mol % $\text{SmCl}_3$ in LiCl-KCl eutectic 30 minutes after the addition of an equimolar amount of $\text{Sm}^0$ at 500 °C. ...	55

<b>Figure 31</b> Raman spectra obtained during the chemical reduction of trivalent samarium by equimolar samarium metal addition for 60 minutes from 0.01 mol % SmCl <sub>3</sub> in LiCl-KCl eutectic salt at 500 °C. ....	59
<b>Figure 32</b> Raman spectra obtained 90 minutes after the chemical reduction contain no Raman modes associated with divalent samarium. ....	60
<b>Figure 33</b> Cyclic voltammogram of 0.01 mol % SmCl <sub>3</sub> in LiCl-KCl eutectic at 500 °C using a 250 mV/s potential sweep rate. ....	61
<b>Figure 34</b> Raman spectra of electrochemically reduced samarium in LiCl-KCl eutectic at 500 °C from a 5 mol % SmCl <sub>3</sub> melt. ....	62
<b>Figure 35</b> Proposed processing flowsheet for a commercial pyrochemical reprocessing installation equipped to reprocess LWR oxide and fast reactor metallic fuel [37]. ....	66
<b>Figure 36</b> FTIR spectra of eutectic salt components as received, 24-hour baked, and 72-hour baked. ....	69
<b>Figure 37</b> Illustration of experimental setup. ....	71
<b>Figure 38</b> Cyclic voltammograms from a molten LiCl-KCl (eutectic) and SmCl <sub>3</sub> (6.69·10 <sup>-4</sup> mol cm <sup>-3</sup> )-LiCl-KCl(eutectic) sample at 773 K and 250 mV s <sup>-1</sup> . ....	74
<b>Figure 39</b> Five overlaid CV scans from a SmCl <sub>3</sub> (5.65·10 <sup>-4</sup> mol cm <sup>-3</sup> )-LiCl-KCl(eutectic) melt at 250 mV s <sup>-1</sup> and 773 K with calculated peak cathodic current standard deviation (WE area = 0.840 cm <sup>2</sup> ). ....	75
<b>Figure 40</b> Overlaid CV scans from a SmCl <sub>3</sub> (5.65·10 <sup>-4</sup> mol cm <sup>-3</sup> )-LiCl-KCl(eutectic) melt at 250 mV s <sup>-1</sup> and 773 K acquired using the immersion step method. ....	76
<b>Figure 41</b> Peak cathodic and anodic current response plotted as a function of WE immersion from a SmCl <sub>3</sub> (5.65·10 <sup>-4</sup> mol cm <sup>-3</sup> )-LiCl-KCl(eutectic) melt at 250 mV s <sup>-1</sup> and 773 K. ....	77
<b>Figure 42</b> Overlaid CV scans from a SmCl <sub>3</sub> (6.69·10 <sup>-4</sup> mol cm <sup>-3</sup> )-LiCl-KCl(eutectic) melt at 773 K acquired across the broad range of scan rates (WE surface area = 0.782 cm <sup>2</sup> ). ....	79
<b>Figure 43</b> Peak cathodic and anodic current response plotted as a function of the square root of scan rate from a SmCl <sub>3</sub> (5.65·10 <sup>-4</sup> mol cm <sup>-3</sup> )-LiCl-KCl(eutectic) melt at and 773 K (WE surface area = 0.782 cm <sup>2</sup> ). ....	80
<b>Figure 44</b> Peak cathodic and anodic current response ratio plotted as a function of scan rate from a SmCl <sub>3</sub> (5.65·10 <sup>-4</sup> mol cm <sup>-3</sup> )-LiCl-KCl(eutectic) melt at and 773 K (WE surface area = 0.782 cm <sup>2</sup> ). ....	81
<b>Figure 45</b> Peak cathodic current density versus the square root of scan rate correlations for the broad (left) and narrow (right) scan rate regions. ....	82
<b>Figure 46</b> Peak cathodic current density plotted as a function of SmCl <sub>3</sub> concentration with (left) and without (right) the highest concentration data point. ....	83

<b>Figure 47</b> Diffusion coefficient of $\text{Sm}^{3+}$ values and their respective errors versus $\text{SmCl}_3$ concentration. ....	84
<b>Figure 48</b> Proposed pyroprocessing flowsheet published by Williamson et al. reports a variety of unit processes (electrorefiner, oxidant production, lanthanide drawdown, U/TRU drawdown) that require concrete understanding of analyte behavior before optimization can be pursued. ....	90
<b>Figure 49</b> Experimental setup employed for spectroscopic and electroanalytical investigations in molten LiCl-KCl eutectic consists of precision alignment stages for electrochemical and spectroscopic focusing, electrode alignment mounts, fiber cabling for 532 nm laser excitation, a polarized Raman probe, and a high-temperature ceramic cylindrical furnace. ....	92
<b>Figure 50</b> The XRD pattern obtained from separated, consolidated, and dried precipitate indicates the formation of SmOCl with relatively few impurities. ....	96
<b>Figure 51</b> SEM images of plate-like precipitate particles (left) and fluff-like precipitate particles (right) both illustrate the regions of interest (purple outline) where EDS chemical analysis was conducted. ....	97
<b>Figure 52</b> TEM diffraction analysis shows the 110-plane d-spacing is in agreement with the measured XRD pattern reported in Figure 50, confirming the precipitate to be SmOCl. ....	98
<b>Figure 53</b> Raman spectra obtained from the precipitate show five symmetry modes that confirm the precipitate to be SmOCl [107]. ....	99
<b>Figure 54</b> An additional anodic peak (*) manifests in a slightly more oxidative region than the traditional $\text{SmCl}_3$ redox couple at low concentrations. ....	100
<b>Figure 55</b> A comparison of CV curves obtained from a low-concentration $\text{SmCl}_3$ melt with the additional anodic peak and a molten LiCl-KCl melt containing synthesized SmOCl indicate the additional peak is due to SmOCl formation. ....	101
<b>Figure 56</b> A clear shift in the location and magnitude of the peak current response is observed in the CV acquired post-SmOCl synthesis as compared to the CV acquired before SmOCl synthesis. ....	102
<b>Figure 57</b> The lack of features in the Raman spectra acquired after the SmOCl synthesis indicate the SmOCl is either soluble at levels below the detection limits of the Raman or does not exhibit Raman active modes when solvated in the molten LiCl-KCl eutectic. .	103
<b>Figure 58</b> CV results (left) with respect to scan rate from the LiCl-KCl- $\text{SmCl}_3$ (pre-synthesis) indicate high levels of peak current vs. scan rate linearity (right), and therefore high levels of Randles-Sevcik applicability. ....	104
<b>Figure 59</b> CV results (left) with respect to scan rate from the LiCl-KCl-SmOCl (post-synthesis) indicate lower levels of peak current vs. scan rate linearity (right), and therefore lower levels of Randles-Sevcik applicability. ....	104

<b>Figure 60</b> Overlaid CV curves at various scan rates from the molten LiCl-KCl eutectic at 500 °C solvated with CeCl <sub>3</sub> , EuCl <sub>3</sub> , and SmCl <sub>3</sub> .....	108
<b>Figure 61</b> Peak anodic and cathodic current response versus square root of potential scan rate data for molten LiCl-KCl eutectic solvated with CeCl <sub>3</sub> , EuCl <sub>3</sub> , and SmCl <sub>3</sub> .....	109
<b>Figure 62</b> Comparison of individually solvated and mixed CeCl <sub>3</sub> and SmCl <sub>3</sub> Raman spectra in the molten LiCl-KCl eutectic.....	110
<b>Figure 63</b> Polarized (VV) and depolarized (HV) in situ Raman spectra of ZrCl <sub>4</sub> solvated in the molten LiCl-KCl eutectic .....	111



## Chapter 1 Introduction

### 1.1 Nuclear Security and Nonproliferation

Nuclear technology has played a central role in a variety of defense and civilian applications since the mid-20<sup>th</sup> century. Preliminary advances in the understanding of radiation and the atomic nucleus paved the way for the harvesting of energy from atomic fission. Unfortunately, the energy associated with fission was eventually developed into the most destructive weapons humankind has ever witnessed. Balancing the protection of nuclear weapons and material with the spread of peaceful nuclear technology has since been a central mission of the United Nations (UN) Security Council and its subordinate organization, the International Atomic Energy Agency (IAEA) [1-5].

The IAEA relies on a combination of political and scientific tools to ensure nation states that have ratified the Nuclear Nonproliferation Treaty (NPT) hold up their commitments in terms of peaceful use of nuclear technology and honest reporting of special nuclear material (SNM). SNM is defined as the following fissile isotopes that serve as central components in nuclear explosives:  $^{233}\text{U}$ , uranium enriched to  $^{235}\text{U}$ , and  $^{239}\text{Pu}$  [5]. Once a nation state establishes a Safeguards Agreement or an Additional Protocol with the IAEA, inspectors are provided access to civilian nuclear facilities to monitor the nuclear processes and confirm SNM buildup logs reported by the nation state's government [6]. Although defense installations are exempt from inspector access, the tracking of SNM remains an important goal of the nation state to ensure efficient SNM consolidation and prevent potential loss or theft of SNM from going undetected [7].

Nuclear material accountancy (NMA) is the backbone of the IAEA's nuclear security regime, and the agency employs a variety of process monitoring technologies to conduct NMA and ensure SNM reporting and processing is conducted in a safe and honest manner.

## 1.2 Advancements in Nuclear Technology

As the international community adapts to the effects of climate change and institutes policies to mitigate greenhouse gas (GHG) emissions, nuclear energy has the potential to play a central role in the global transition to a carbon-free energy portfolio [8, 9]. Traditionally the majority of nuclear processes, whether civilian or defense related, have relied on aqueous media to consolidate nuclear material, produce or reprocess nuclear fuel, and provide heat transfer in power generation systems; however, desire for improved economics, energy efficiency, proliferation resistance, and passive safety features have inspired a new generation of nuclear technology [10].

In 2011, the Fukushima Daiichi nuclear power plant accident in Japan provided a vivid example of the pitfalls associated with water-based nuclear systems and inspired a desire to transition to safer, more robust media for both heat transfer and fuel containment [11]. The IAEA created the Generation IV International Forum (GIF) for advanced reactor concepts and Innovative Project on Innovative Nuclear Reactors and Fuel Cycles (INPRO) in response to facilitate the research, development, and deployment of potential alternatives to light water reactors (LWRs) and aqueous reprocessing schemes for used nuclear fuel (UNF) [8]. Molten salts are a leading candidate in both the GIF and INPRO initiatives, as they have the potential to increase energy efficiency, bolster

proliferation resistance, and decrease high level nuclear waste (HLW) footprints after energy production is complete [12].

One of the greatest hurdles facing this next generation of nuclear technology remains the development of effective nuclear material accountancy (NMA) techniques for non-aqueous systems [10]. Accurate and reliable NMA is the backbone of the IAEA nuclear security regime. NMA techniques associated with aqueous systems are heavily reliant on radiation detection and signature-based safeguards to monitor nuclear material and track its movement [6]. Signature-based safeguards, laser-induced breakdown spectroscopy (LIBS), pneumatic dip-tube densitometry, and hybrid K-edge densitometry (HKED) systems are often installed to monitor aqueous nuclear power and reprocessing plants [13-15]. As these techniques were not developed for high temperature applications, they are either not applicable or experience a decrease in effectiveness when deployed in high temperature environments [16]. Although advanced methods for radiation detection, specifically neutron detection and active interrogation of nuclear material, continue to develop, the high temperature and non-aqueous nature of molten salts presents a unique set of challenges that must be addressed before large-scale deployment of these technologies can progress [15].

As more nations begin to consider nuclear power as a viable GHG-free energy technology, high temperature molten salt systems will undoubtedly emerge as potential reactor and reprocessing systems, especially in China, India, and Russia [17]. Furthermore, molten salt reprocessing technology is currently utilized as an electrolyte for the electrorefining of UNF using the pyrochemical process at Idaho National Laboratory (INL).

The domestic nuclear weapons complex at the Y-12 National Security Complex and Los Alamos National Laboratory (LANL) also utilize molten salt for the consolidation of SNM. Both of these molten salt applications will require bolstering of NMA capabilities, and chemical-based sensing methods are one promising avenue for achieving those NMA milestones.

### 1.3 Nuclear Material Accountancy in Molten Chloride Salts

Although molten salt nuclear reactors are not yet utilized for energy production anywhere in the world, chloride salt technology is considered a leading candidate in a variety of reactor designs, advanced reprocessing schemes, and the domestic nuclear weapons complex. Chloride salts have long been employed for SNM consolidation through electrochemical reduction methods at LANL and Y-12. These single-analyte streams are cleaner than those associated with civilian installations; however, their SNM concentrations will run much higher than civilian systems and decay products do begin to contaminate the streams over time [18, 19]. Chemical-based sensing methods can provide bolstered NMA capabilities if coupled with radiation detection methods and also provide insights into the chemistry of SNM solvated in these chloride media. Understanding chemistry of solvated material is important when attempting to address imperfect reductions of SNM and subsequent formation of alternative chemistries, such as oxides or oxychlorides, that can lead to SNM loss or buildup [18].

Molten salts have also been proposed as heat transfer and fuel containment media for advanced nuclear power plant designs. The reactors can be deployed as

traditional power plants, hydrogen production plants, fissile fuel production (breeder), or actinide burners [20]. The reactors range in molten salt application from fueled salt to coolant salt but tend to be more in favor of fluoride systems [20-22]. Chloride salts are less prevalent but do provide some advantages in terms of lower melting points and higher actinide solubility [23]. Monitoring solution chemistry for corrosion control, criticality, and solubility of fuel elements is possible through chemical-based sensing methods, along with improving NMA abilities at proposed reactors [24].

The focus of this dissertation is the molten LiCl-KCl eutectic system as it is the proposed electrolyte for the pyrochemical reprocessing of UNF. Lanthanide chlorides serve as surrogates for SNM and fission products (FPs) [15, 25-30]. Pyrochemical reprocessing development began at the DOE's Argonne National Laboratory (ANL) during the 1980's. The research and development of the pyrochemical reprocessing scheme was part of ANL's Integral Fast Reactor (IFR) program whose goal was to close the IFR's fuel cycle and provide a means for decreasing the United States' need for a nuclear waste repository [25].

Pyrochemical reprocessing utilizes a molten eutectic LiCl-KCl electrolyte to electrochemically separate uranium, plutonium, and other transuranic (TRU) elements from UNF [29, 31]. The process is an alternative to the traditional aqueous reprocessing scheme, Plutonium Uranium Redox Extraction (PUREX). Short-cooled fuels containing high amounts of minor actinides (MA) can be reprocessed pyrochemically in smaller facilities with less criticality concerns [32]. Furthermore, the pyrochemical process does not produce a pure plutonium stream, rather it is mixed with other TRU elements, making

the process inherently more proliferation resistant than PUREX [10, 27, 31, 33]. The highly radioactive and high temperature environment associated with pyrochemical reprocessing produces high amounts of background signal that disrupt traditional techniques such as signature-based safeguards [34-36]. Russia, France, Italy, Spain, the United Kingdom, the Czech Republic, Japan, South Korea, and India have all participated in the development of pyrochemical reprocessing [10].

A proposed pyrochemical reprocessing flowsheet for existing LWR UNF stockpiles is illustrated in Figure 1 and can be adjusted for application in a fast reactor fuel cycle with minimal adjustment [37].

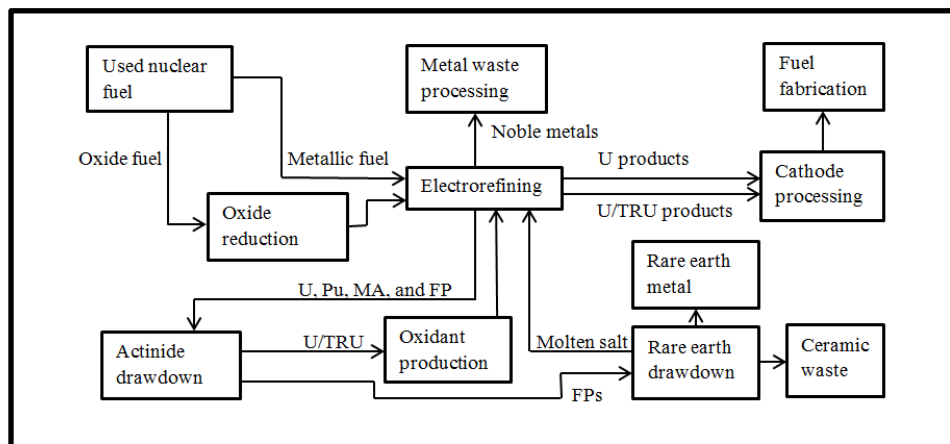


**Figure 1** A proposed pyrochemical reprocessing flowsheet for the LWR fuel cycle illustrating the many unit operations that may require NMA [37]

There are many unit operations that comprise the overall pyrochemical reprocessing scheme, and most would require accurate NMA to ensure SNM or radioactive material is not being lost or stolen. The electrolytic reduction and electrorefining steps have a potential for SNM buildup; furthermore, the actinide and lanthanide drawdown steps present a need for NMA to aid in SNM security and overall process optimization. The molten LiCl-KCl eutectic is maintained at 500 °C in the electrorefiner for bulk reductions.

Understanding the chemistry of dissolved elements will ensure reductions and oxidations steps are completed in efficient manners while minimizing loss of material to alternative reactions [34]. Chemical-based sensing methods are ideal for such an application as they achieve both NMA and the option to study solution chemistry.

#### 1.4 Electroanalytical Voltammetry in the Molten LiCl-KCl Eutectic

Electroanalytical techniques are under consideration for *in situ* process monitoring applications in the molten LiCl-KCl eutectic. Voltammetric methods for electroanalytical measurement of dissolved content are ideal for molten salt systems containing nuclear material as the high temperature and highly radioactive nature of the environment do not affect the electroanalytical components [38]. Furthermore, electroanalytical methods are non-destructive, eliminating the need for sample collection, analysis, and subsequent destruction. Destructive analysis is not only more time consuming, but it also produces more HLW. Electroanalytical measurements correlate current response to the concentration of the dissolved species if the diffusion behavior of the analyte is well understood [39]. The applied potential (volts vs. reference electrode) associated with a dissolved analyte's electric current response is analyte-specific, allowing for mixed solution monitoring [38, 39]. Building a consolidated and accurate diffusion coefficient library would allow electroanalytical techniques to produce reliable and repeatable data for NMA.

There are many electroanalytical techniques that can be employed to build this diffusion coefficient library. Our research group employs cyclic voltammetry (CV), square

wave voltammetry (SWV), and normal pulse voltammetry (NPV). Each technique has application-specific advantages. SWV is the most limited in application as the current response measurements are inaccurate at dissolved analyte concentrations at or above 0.5 wt. % dissolved analyte [40]. However, SWV does elucidate the electron transfer characteristics of electrochemical reactions, which becomes vital in evaluating the applicability of empirical relationships for diffusion coefficient determination [39-41].

NPV capabilities are less developed than CV; however, NPV has produced large strides forward in terms of uncertainty mitigation and mixed-analyte solution monitoring [42-46]. Optimization of NPV continues in both the community and our lab; however, the focus of this dissertation is the application of CV for *in situ*, real-time process monitoring in the molten LiCl-KCl eutectic and subsequent coupling with additional chemical-based sensing methods. Although diffusion coefficient values for identical systems are known to vary across different electroanalytical methods, diffusion coefficient comparisons with the literature were not limited to CV. This comparison method is accepted in the literature, and uncertainty mitigation is a focus of this dissertation [38, 43, 47-52].

CV is a three-electrode electrochemical method that relies on a cyclic potential sweep to scan a voltage range for analyte-specific redox reactions. Current response can be correlated to analyte concentration if the diffusion behavior of the analyte is well understood [39]. The three diffusion mechanisms present in the molten LiCl-KCl eutectic electrochemical system are mass transfer, migration, and convection. The Randles-Sevcik equation can be applied to CV data assuming all diffusion is mass transfer limited, linear in nature, and the redox reaction of interest is reversible; however, it is suggested that



higher concentrations may lead to larger migration contribution [39, 45, 52, 53]. If a multi-electron transfer to metallic form is being investigated, the deposits are assumed to exhibit unit activity [38].

The Randles-Sevcik relationship as it relates to reversible electron transfer reactions is detailed in Equation 1.

$$i_p = 0.4463 \cdot n \cdot F \cdot A \cdot C_i \cdot \left(\frac{n \cdot F}{R \cdot T}\right)^{1/2} \cdot \nu^{1/2} \cdot D^{1/2} \quad (1)$$

Here  $i_p$  is the peak current response,  $n$  is the number of electrons transferred during the redox reaction,  $F$  is Faraday's constant,  $A$  is the surface area of the working electrode (WE),  $C_i$  is the bulk concentration of the dissolved analyte of interest,  $R$  is the ideal gas constant,  $T$  is temperature,  $\nu$  is the potential scan rate, and  $D$  is the diffusion coefficient of the analyte of interest [39, 53]. The Randles-Sevcik equation can be reorganized to solve for diffusion coefficient as a function of peak current response, temperature, WE surface area, potential scan rate, and bulk analyte concentration. It is important to note the many variables present in the Randles-Sevcik equation that can affect peak current response and subsequent diffusion coefficient determinations. It is therefore of the utmost importance to accurately maintain temperature and WE surface area. Furthermore, the solution chemistry must remain undisturbed during CV analysis. Tylka *et al.* developed a method for accurate WE surface area measurement that correlates peak current response to the immersion level of the electrode assembly allowing for the WE surface area to be linearly interpolated [38]. Tylka *et al.* also report an experimental sequence that produces repeatable CV results and ensure solution chemistry remains

undisturbed between CV scans [39, 52]. This experimental sequence is reported in Table 1 and was modified slightly for the electroanalytical studies presented in this dissertation.

Sequence Step	Description
1	Working electrode cleaning through application of an oxidative potential
2	Hold at working electrode at potential where no reactions occur
3	Hold working electrode at open circuit potential (OCP)
4	Stir the solution at potential where not reaction occurs

**Table 1** An experimental electroanalytical sequence developed by Tylka *et al.* employed for accurate and repeatable CV acquisition

Samarium and cerium were analyzed as a fission product and SNM surrogate, respectively using CV. Fission products must be removed from the recycled fuel product due to their negative neutronic effects, and cerium is often employed as a surrogate for SNM [5, 38, 52]. As indicated in Equation 1, there are a multitude of variables that can affect diffusion coefficient values and repeatability of data. Furthermore, reported diffusion coefficients in the literature often vary with respect to the electroanalytical technique employed for analysis, making the consolidation of diffusion coefficient libraries difficult [38, 50]. The nuclear industry's uncertainty requirements are extremely stringent, making uncertainty mitigation a large focus of current research initiatives in the literature [54].

Cerium has only one stable, trivalent ionic state when solvated in the molten LiCl-KCl eutectic and undergoes a three-electron transfer reaction in the eutectic to form a metallic deposit on the WE [50, 55-58]. Samarium exists in a stable divalent and trivalent

ionic state when solvated in the molten LiCl-KCl eutectic. The reduction of samarium to metallic form occurs in a further cathodic region in relation to the  $\text{Li}^+/\text{Li}^0$  couple [47, 49, 50, 56, 59-61]. Although some lanthanides spontaneously reduce to their divalent state, samarium's tendency to do so is much less prevalent [60, 62]. The electrochemical reaction for cerium and samarium are reported in Equations 2 and 3, respectively.



Table 2 provides a range of diffusion coefficient values for analyte concentrations below 5 wt. % reported in the recent literature for samarium and cerium ions dissolved in the molten LiCl-KCl eutectic at environmental conditions and electroanalytical methods similar to the studies presented in this dissertation. Data presented in this dissertation will be directly compared to the literature results presented in Table 2; however, temperature range, WE electrode material, WE surface area uncertainty, and variation in peak current all vary or go unreported in the literature and may make direct comparisons less reliable.

Literature Source	$D_{\text{Ce}^{3+}} (\cdot 10^5 \text{ cm}^2/\text{s})$	$D_{\text{Sm}^{3+}} (\cdot 10^5 \text{ cm}^2/\text{s})$
Iizuka [58]	0.73 – 2.72	-
Marsden <i>et al.</i> [57]	0.92 – 2.08	-
Cordoba <i>et al.</i> [47]	-	0.98 – 1.30
Castrillejo <i>et al.</i> [49]	-	0.77 – 1.44
Yamada <i>et al.</i> [59]	-	0.13 – 0.45

**Table 2** Diffusion coefficients from the literature obtained measured in environmental conditions similar to this study for trivalent cerium and trivalent samarium at concentrations below 5 wt. % [47, 49, 57-59]

The literature is much more abundant at low concentrations of dissolved analyte, typically under 5.0 wt. %. Higher concentrations of dissolved analyte and multi-analyte solutions

are expected to have an effect on diffusion behavior of these analytes and the applicability of the Randles-Sevcik relationship [39, 50].

### 1.5 Raman Spectroscopy in the Molten LiCl-KCl Eutectic

Raman spectroscopy, in the present context, offers information regarding the coordination chemistry and speciation of dissolved content. Both of these characteristics can aid in better understanding the diffusion behavior of dissolved analytes. Acquisition of a Raman spectrum relies on the measurement of scattered light from a sample excited by an incident monochromatic radiation. Raman scattering is inelastic in nature and much less prevalent than elastic, or Rayleigh, scattering. The change in the incident radiation's energy is reported in the form of a Raman shift ( $\text{cm}^{-1}$ ) in the wavelength of the emitted light. This shift can be further explained as a shift in vibrational frequency associated with a specific bond in the sample and the bond's form of excitation: stretching, bending, etc. The vibrational frequency associated with a bond is specific to that bond's form of bending or stretching, and also the atoms or ions joined at the bond of interest [63]. Along with Rayleigh and Raman scattering, a sample may also exhibit fluorescence. Fluorescence is defined as a sample's excitation to an elevated electronic state, followed by a characteristic emission of photons as the sample returns to its electronic ground state. This photon emission is traditionally preceded by a radiation-less decay from the excited electronic state to a vibrational state within that excited electronic state [63]. Raman scattering may also be segregated into an anti-Stokes or Stokes designation. Anti-Stokes scattering (decrease in wavelength) can play a slightly larger role in sample

characteristics in high temperature environments. Figure 2 provides an illustration of Raman scattering, Rayleigh scattering, and fluorescence.

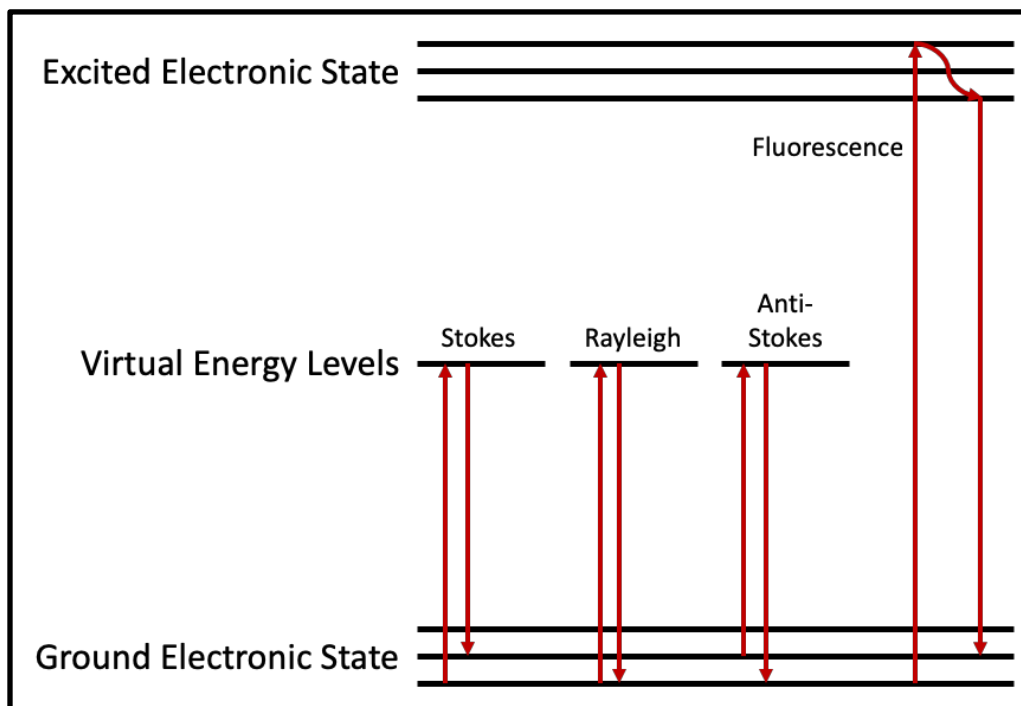


**Figure 2** A Jablonski diagram illustrating the differences between Raman scattering, Rayleigh scattering and sample fluorescence as they relate to energy states modified from Harris *et al.* [64]

Stokes scattering (increase in wavelength) is more prevalent as the sample begins in a ground state; however, there are small anti-Stokes contributions from the sample being initially excited to an elevated electronic state within the ground vibrational state [63].

Polarized Raman spectroscopy offers insights into the symmetry of sample molecules, which is valuable when studying the coordination chemistry of analytes dissolved in molten salt [63]. Polarized (VV) Raman modes indicate a symmetric vibration is occurring, whereas depolarized (HV) Raman modes indicate an asymmetric vibration is occurring. Polarizing Raman aids in the assignment of normal vibration modes when analyzing an acquired spectrum. Normal vibration modes exhibit a characteristic

vibrational frequency, or Raman shift, dependent on the bond of interest's atomic makeup and the nature of the bond's excitation [63]. A non-linear molecule will produce  $3N-6$  normal vibration modes, where  $N$  denotes the number of atoms constituting that molecule [63-65]. Symmetry group theory dictates the analysis of Raman spectra by elucidating which normal modes are associated with Raman active modes, and more specifically those which are symmetric or asymmetric in nature [64]. Unfortunately, this theory is developed for isolated molecules. Although molten salt environments do not adhere to these isolated characteristics, the literature has established the applicability of symmetry group theory when studying molten salt with Raman spectroscopy [66-70].

There are an established set of selection rules that facilitate the analysis of Raman spectra and assignment of normal vibration modes to specific features on the acquired spectra. Symmetric vibrations that do not deform the molecule and the presence of highly polarizable atoms produce intense Raman features [63]. The incident radiation associated with the laser excitation source of a Raman system produces an electric field,  $E$ . This electric field is modified by the positive and negatively charged ions that make up the molecule of interest, producing a dipole moment,  $\mu$ . Three-dimensional matrix recombination of symmetry table elements,  $E$  vectors, and  $\mu$  tensor vectors establish which normal vibration modes are Raman active [63]. A symmetric vibration with respect to the central nucleus of a molecule will be Raman active. Lanthanides dissolved in the molten LiCl-KCl eutectic are known to form complexes that exhibit an octahedral ( $O_h$ ) symmetry [71, 72].

Lanthanide chlorides in the trivalent state, when dissolved in the molten LiCl-KCl eutectic are known to form  $[\text{LnCl}_6]^{3-}$  complexes due to the excess  $\text{Cl}^-$  ions present in solution [71-73]. The  $\text{Li}^+$  ions in solution, due to their high polarizing power, affect the Raman shift of normal vibration modes as well [71]. Figure 3 provides an illustration of normal vibration modes associated with an  $O_h$  point group symmetry. The  $A_{1g}$ ,  $E_g$ , and  $T_{2g}$  modes associated with  $O_h$  symmetry are Raman active [63].

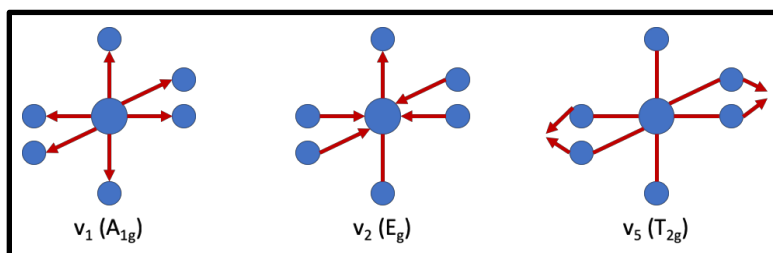


**Figure 3** Point group  $O_h$  Raman active modes of vibration for a molecule similar to an  $[\text{LnCl}_6]^{3-}$  complex –  $v_1$ ,  $v_2$ , and  $v_5$  modes Raman active, modified from Ferraro [63]

The  $A_{1g}$  and  $E_g$  normal vibration modes are symmetric stretches of the Ln-Cl bond. The  $F_{2g}$  normal vibration mode results from the angular deformation of the Ln-Cl bond [63].

Application of Raman spectroscopy in the molten LiCl-KCl is limited in the literature, and the majority of the literature relies on microscope-based systems to obtain data. This method of analysis is destructive in nature and requires a sample be sealed in quartz before analysis on a heated microscope stage. Fiber-based Raman systems equipped with probes offer nondestructive analysis of molten salt samples and could offer real-time data acquisition in the pyrochemical reprocessing of UNF or the nuclear weapons complex. Furthermore, in both processes, metallic elements will be present, making it vital to study the speciation and coordination of these dissolved elements when metallic elements are present. Recently, research from our group successfully used a

Raman fiber probe to study the dissolution of metallic lithium in the molten LiCl-Li<sub>2</sub>O-Li system [74]. To our knowledge, speciation studies have only been reported for cerium and neodymium in the literature using Raman spectroscopy [73].

## 1.6 Summary

This dissertation reports the design, construction, and testing of an electroanalytical system coupled with a fiber-based Raman unit. The system was designed to address gaps in the existing literature as it relates to uncertainty mitigation in electroanalytical studies, high temperature fiber-based Raman spectroscopy, and coupled spectroelectrochemical (SPEC) system for chemical-based NMA. After construction, the system was first calibrated using low concentrations CV analysis and nitrate salt Raman analysis. Preliminary CV studies were conducted using a quasi-reference electrode and traditional reference electrode on melts containing low concentrations of dissolved samarium. Cerium was also analyzed using CV to ensure the system performs equally well for multi-electron transfer reactions involving metallic deposits. These preliminary results are presented in Chapter 3.

Chapters 4, 5, and 6 are three manuscripts that used the SPEC system to study high concentration samarium CV, samarium valence state speciation, and samarium oxychloride formation, respectively. The high concentration samarium CV manuscript investigates the uncertainty associated with studying the analyte at high concentrations and suggests methods for mitigating that uncertainty to maintain CVs reliability as an NMA technique in high temperature molten salt (Chapter 4). The valence state,



complexation, and speciation of samarium were investigated using the SPEC system in the speciation manuscript, producing what we believe to be the first Raman spectra reported for divalent samarium in the molten LiCl-KCl eutectic (Chapter 5). The SPEC system was then used to investigate the nature of samarium oxychloride formation in situ for NMA and evaluate the nuclear material management implications of this alternative chemistry as they relate to unit operations associated with the pyrochemical reprocessing of UNF (Chapter 6).

Chapter 7 reports preliminary results from the SPEC system's deployment in multi-analyte scenarios. CV and Raman spectroscopy were evaluated for NMA deployment individually and from a synergistic perspective. Chapter 8 presents a brief discussion of this dissertation's results that are not addressed in the manuscript chapters, including an evaluation of the SPEC system and suggestions for SPEC system deployment for NMA in the nuclear industries currently using or considering high temperature molten salt. This dissertation concludes with suggestions for further development of the SPEC system in Chapter 9.

## Chapter 2 Experimental

### 2.1 Spectroelectrochemical Apparatus

A combined spectroscopy and electrochemical (SPEC) apparatus was engineered for *in situ* detection of lanthanides solvated in a molten chloride salt at 773 K under inert atmosphere. Independent electrochemical and Raman spectroscopy systems previously built by our group formed the initial design basis of the combined system [74, 75]. The coupled system was iteratively constructed over an extended period of time [76-79]. The fiber-based 532 nm, 300 mW Raman spectroscopy system with built-in polarizing capability consists of a Horiba iHR320 Imaging Spectrometer equipped with a Sincerity Charge-Coupled Device (CCD) Deep Cooled Camera for high resolution data acquisition over 150 nm to 1500 nm spectral range. The Raman apparatus was also equipped with an Oxxius LCX-532 low-noise DPSS laser aperture and an Oxxius LaserBoxx Controller to adjust laser power outside of the glovebox. The Raman spectroscopy system was constructed on a counterweighted Newport Model 410-RC mobile platform for positioning over the melt crucible and rough focusing of the Raman laser. The Raman laser outlet probe was assembled on a breadboard plate attached to the head of the mobile platform. A micron resolution motorized stage (Zaber X-LSM200B-KX13A) was integrated to mount the Raman laser outlet probe from the breadboard over the melt for fine laser focusing. A suite of adaptable varying magnification objective lenses was employed to adjust the focal length from the Raman laser outlet probe in order to optimize the signal of the divalent and trivalent species in the melt. The fiber cable servicing the laser from

the spectrometer to the outlet probe in the glovebox was passed through an aluminum flange (Kurt J. Lesker KF40-150-LFA) and hermetically sealed with a resin under vacuum to protect the integrity of the glovebox atmosphere while permitting users to control the laser external to glovebox. To the best of our knowledge, this Raman system is one of only a few fiber-based systems with the polarizing capability to filter  $T_{2g}$  Raman modes with the focusing and insulating systems integrated for *in situ* SPEC study of high temperature molten salt. Optically polished quartz discs were used as consumable to protect the laser outlet probe from attack by volatile melt components. The ceramic insulation cap on top of the furnace (Watlow VC403A06A-G009F) was specially designed in Autodesk Inventor Professional 2016 to minimize thermal gradients within the melt while allowing a point of entry for the Raman laser and electrodes for simultaneous spectroscopy and electrochemical study. Signal dampening from thermal interference was mitigated by implementing a custom insulation fitting at the laser aperture. The electrode guides on the insulation cap were machined in line with the electrode mounting plate at the end of a high-resolution motorized stage (Zaber X-LSM200B-KX13A) affixed to the back wall of the glovebox for repeatable SPEC analysis required for reliable *in situ* process monitoring operations. Autodesk Inventor Professional 2016 was also utilized to design a powder coated aluminum glovebox window cover to attenuate diffracted laser beams during operation and inhibit contaminate light from entering the glovebox. Laser attenuating windows on the glovebox window cover were installed on a hinge to allow operators to align the SPEC apparatus before experiments were conducted. In order to accommodate all of the individual electronics used to engineer the SPEC apparatus a power supply

(Letour S-500-12, DC Output = 12 V, AC Input = 110/220 V) was installed inside the glovebox. A schematic of the SPEC setup is shown in Figure 4.

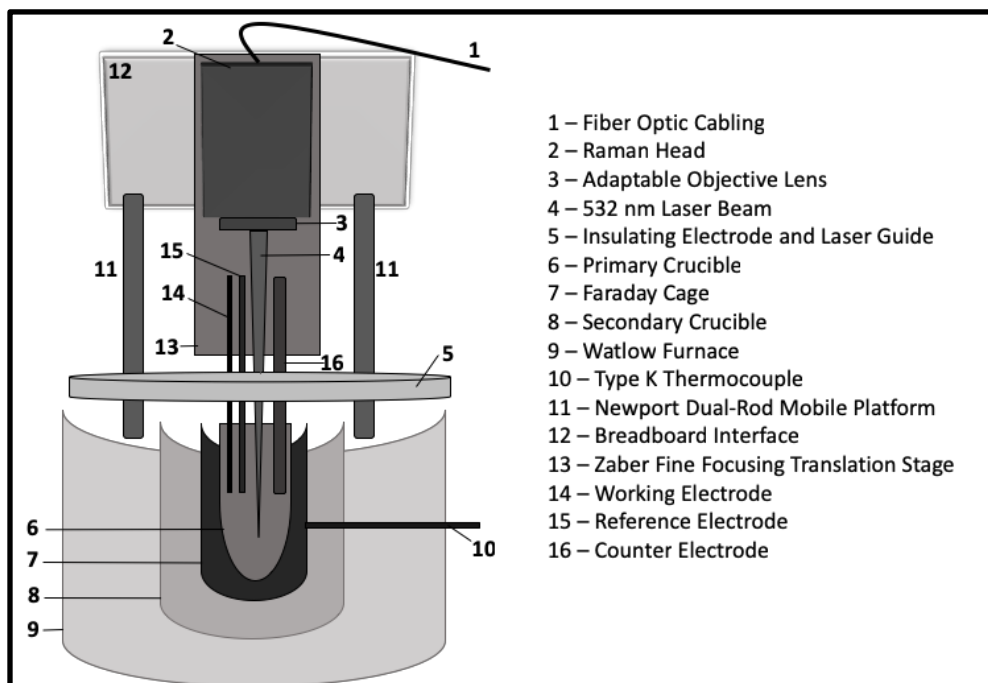


**Figure 4** Spectroelectrochemical system constructed and tested for simultaneous voltammetric and spectroscopic studies in the molten LiCl-KCl eutectic

The Faraday cage was nested in a secondary stainless-steel crucible which also served as the point of contact for K type thermocouple providing feedback through a custom LabView National Instruments program to regulate melt temperature. The crucibles were placed in a clamshell furnace (Watlow VC403A06A-G009F) maintained within  $\pm 2$  K of the setpoint temperature control controlled by a custom LabView program. A K type thermocouple was used to record the working temperature of the melt. All salts were handled inside UHP argon (Airgas 99.99%) atmosphere glovebox (Vacuum Atmospheres Co. VAC Controlled Atmospheres Systems) with moisture and oxygen content maintained below 1 ppm. The reference electrode consisted of a silver wire (1 mm diameter) in contact with a 5 mol% silver chloride solution in the LiCl-KCl molten eutectic, contained

in a Pyrex<sup>TM</sup> tube (1  $\mu\text{m}$  thickness tip). The working and counter electrodes were tungsten rods 1/16" and 1/8" diameters, respectively. A motorized stage (Zaber X-LSM200B-KX13A) with integrated controller was used to remotely insert and withdraw the electrodes from the melt with  $\pm 0.1$  mm precision [74]. All electrochemical experiments were performed at 773 K using a Gamry Ref3000 potentiostat controlled by a computer running Gamry Framework software. Gamry Echem Analyst software was used to analyze electrochemical data.

## 2.2 Chemicals and Materials

Nitrate salts stable in open atmosphere were employed to calibrate the Raman spectroscopy system. A  $\text{KNO}_3$  (Sigma-Aldrich 99.99 % pure) and  $\text{NaNO}_3$  (Sigma-Aldrich 99.99 % pure) eutectic was used for calibrations.  $\text{LiCl}$  (Sigma-Aldrich 99.9 % pure) and  $\text{KCl}$  (Sigma-Aldrich 99.9 % pure) were individually baked under vacuum to minimize moisture impurities prior to preparation of a eutectic matrix composed of 46 wt.%/54 wt.%  $\text{LiCl}$ - $\text{KCl}$ , respectively. The eutectic mixture was fused under argon atmosphere and trivalent samarium solutions were prepared by solvating anhydrous  $\text{SmCl}_3$  (Sigma-Aldrich 99.99 % pure),  $\text{CeCl}_3$  (Sigma-Aldrich 99.99 % pure), or  $\text{EuCl}_3$  (Sigma-Aldrich 99.99 % pure). Samarium metal (Alfa Aesar 99.9 % pure) was used in chemical reduction experiments to convert trivalent samarium ions into divalent species. The eutectic mixture was added to alumina, graphite, nickel, or tantalum crucibles fitted with an in-house constructed faraday cage made of stainless steel. Alumina crucibles were primarily employed for electroanalytical studies before coupling the system with the Raman probe.

### 2.3 Solid State Characterization

The total concentration of the samarium in the melt was determined by inductively coupled plasma optical emission spectroscopy (ICP-OES) analysis of a complexed melt solution. A Perkin Elmer Optima 8000 ICP-OES was employed for this analysis, and all solution standards were purchased from SCP Scientific. Measured concentrations obtained from the ICP-OES were consistently less than the theoretical concentration based on the initial mass of lanthanide chloride solvated in the molten LiCl-KCl eutectic. Precipitate was collected and analyzed using a variety of solid-state characterization methods. A Thermo Scientific DXR Raman microscope equipped with a 10 mW, 532 nm wavelength laser was employed for solid-state Raman analysis of the precipitate. X-ray diffraction patterns were obtained from the collected precipitates using a Rigaku Smartlab X-ray diffractometer. Diffraction patterns were analyzed using a PDXL software package. A Hitachi S-4700 field emission scanning electron microscope (SEM) equipped with energy dispersive x-ray spectroscopy (EDS) was employed to investigate precipitate morphology and elemental makeup, respectively. Transmission electron microscopy (TEM) analysis was carried out using a JEOL-JEM 2100F Analytical TEM.

## Chapter 3 System Development and Calibration

### 3.1 Raman Calibration

Due to nitrate salt stability in open atmosphere and their relatively lower melting points compared to chlorides, nitrate salts were employed to calibrate the fiber-based Raman system. The sample prepared for analysis consisted of a 60 wt. %  $\text{NaNO}_3$  and 40 wt. %  $\text{KNO}_3$  eutectic salt mixture. This ratio was chosen because, not only did it offer the lowest possible melting temperature, but also our group has had experience with it [80]. Raman spectra were obtained from the molten salt mixture at approximately 250 °C.

The most comprehensive article available from the literature was one published in 1961 by Janz *et al.* This study was completed in a sealed quartz tube that was subsequently heated to melting temperature and analyzed via Raman through the quartz. It is also worth noting that the laser source employed by Janz *et al.* used a 435 nm wavelength, while the HORIBA system tested used an excitation laser of 532 nm wavelength. The article provides Raman modes for  $\text{NaNO}_3$ ,  $\text{KNO}_3$  and a 50/50 wt. % eutectic of the two salts. Raman modes are reported for both the individual salts in solid and molten form, while the eutectic salt's Raman modes are only from the molten salt. The system tested at HORIBA had an output laser power of approximately 100 mW at the sample. Output power from the laser source is 150 mW; however, the fiber cables coupling the probe to the spectrometer will attenuate the laser power. Table 3 and Table 4 summarize the expected Raman modes and intensities reported by Janz *et al.* [66].

<b>Raman Mode Reported by Janz <i>et al.</i></b>				
<b>SOLID SALTS</b>				
<b>NaNO<sub>3</sub></b>	1069 cm <sup>-1</sup>	1391 cm <sup>-1</sup>	728 cm <sup>-1</sup>	-
<b>KNO<sub>3</sub></b>	1050 cm <sup>-1</sup>	1343, 1361 cm <sup>-1</sup>	714 cm <sup>-1</sup>	-
<b>MOLTEN SALTS</b>				
<b>NaNO<sub>3</sub></b>	1053 cm <sup>-1</sup>	1398 cm <sup>-1</sup>	722 cm <sup>-1</sup>	-
<b>KNO<sub>3</sub></b>	1048 cm <sup>-1</sup>	1383 cm <sup>-1</sup>	718 cm <sup>-1</sup>	-
<b>50/50 Eutectic</b>	1050 cm <sup>-1</sup>	1655 cm <sup>-1</sup>	1296-1452 cm <sup>-1</sup>	718 cm <sup>-1</sup>

**Table 3** Expected Raman mode values from the literature are reported for solid state, molten, and eutectic mixtures of NaNO<sub>3</sub> and KNO<sub>3</sub> [66].

<b>Eutectic NaNO<sub>3</sub>/KNO<sub>3</sub> Raman Modes and Intensities</b>	
<b>Raman Mode</b>	<b>Intensity</b>
1050 cm <sup>-1</sup>	10
1655 cm <sup>-1</sup>	1
1296-1452 cm <sup>-1</sup>	1
718 cm <sup>-1</sup>	2

**Table 4** Raman modes and associated intensities for molten eutectic NaNO<sub>3</sub>/KNO<sub>3</sub> were reported by Janz *et al.* [66].

The Raman modes are from the NO<sub>3</sub><sup>-</sup> polyatomic ion associated with both nitrate salts, and the presence of different cations at different concentrations causes subtle shifts in these modes [66].

Figure 5 reports Raman spectra obtained from the NaNO<sub>3</sub>/KNO<sub>3</sub> molten eutectic using the HORIBA fiber-based Raman system. The system features a 'de-noise' function, whose effects were also investigated. This data smoothing feature is algorithm-based in the analysis program and not a physical function of the spectrometer.



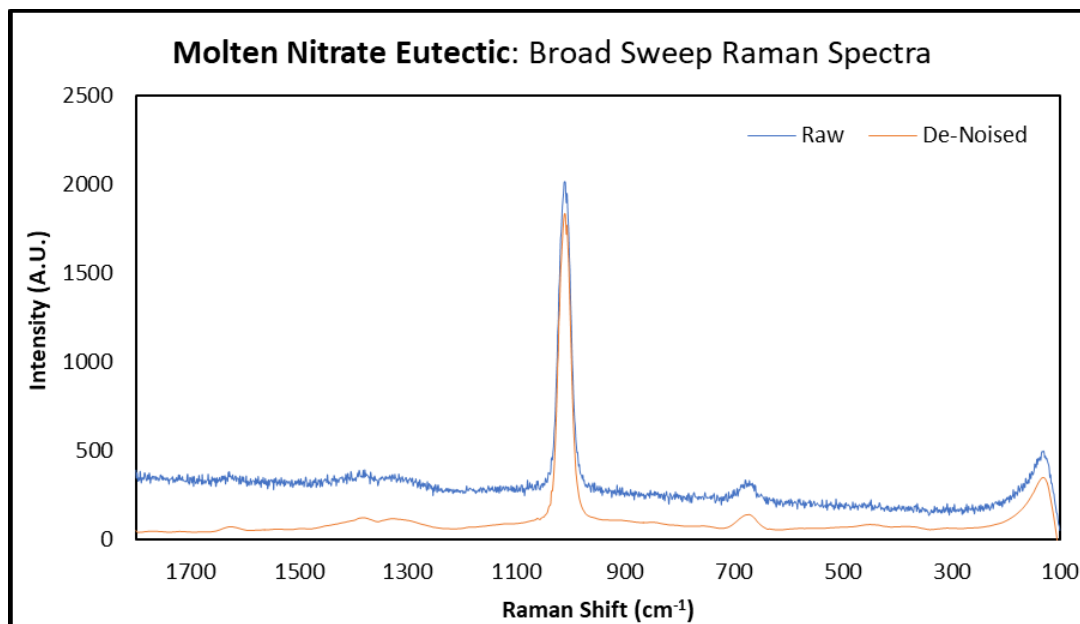


**Figure 5** Broad sweep results indicated the presence of Raman modes and were compared with the available literature.

The results of the verification using nitrates are reported in Table 5 and compared to the results published by Janz *et al* [66]. The results were relatively consistent with one another.

<b>HORIBA Data vs. Literature Values for Molten NaNO<sub>3</sub>/KNO<sub>3</sub> Eutectic</b>	
<b>Literature Value</b>	<b>Values Obtained using HORIBA System</b>
1050 cm <sup>-1</sup>	1010 cm <sup>-1</sup>
1655 cm <sup>-1</sup>	1631 cm <sup>-1</sup>
1296-1452 cm <sup>-1</sup>	1260-1466 cm <sup>-1</sup>
718 cm <sup>-1</sup>	679 cm <sup>-1</sup>

**Table 5** Results obtained using the fiber system were compared to the literature values published by Janz *et al.* [66].

### 3.2 Preliminary Chloride Salt Raman

The environment associated with the study of analytes solvated in the molten LiCl-KCl eutectic is more extreme than that associated with the nitrate salt verification study. First, the experiments must be conducted in an argon atmosphere glove box due to chloride salts' sensitivities to oxygen and moisture. Second, the temperature associated

with the LiCl-KCl studies is twice as hot when compared to nitrate salt investigations. Third, the effects of focal length and salt vapors were more pronounced when installing the Raman system for LiCl-KCl studies. Figure 6 illustrates the increase in spectral quality observed when decreasing the working distance of the Raman probe.

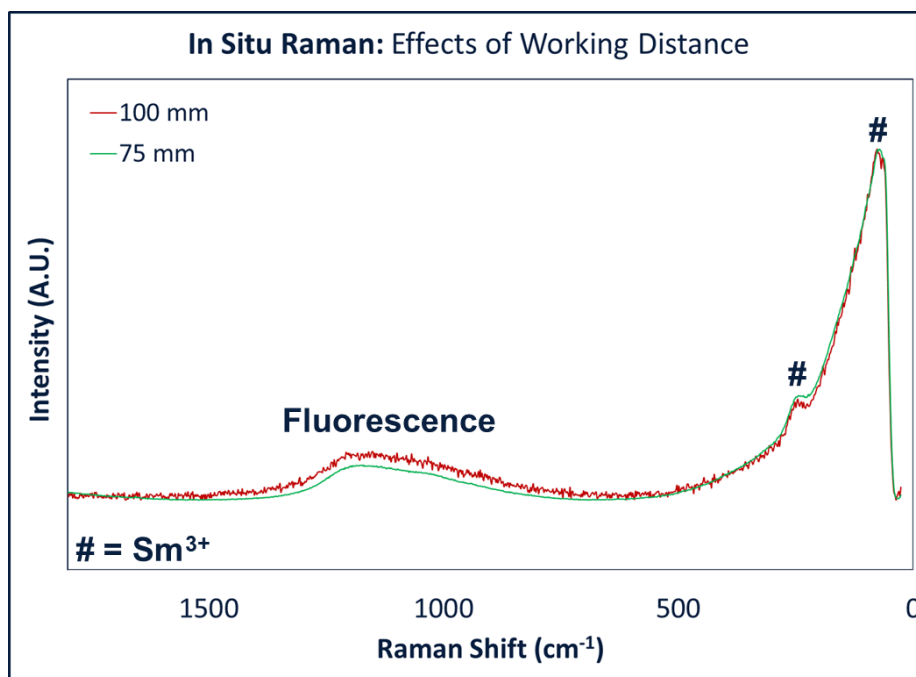


**Figure 6** Working distance of the fiber-based Raman had a pronounced effect on spectral quality in terms of signal-to-noise ratio.

Lowering the focal length of the installed objective lens decreased the working distance, improving spectral quality in terms of signal-to-noise ratio. Custom cooling in the form of Peltier coolers was installed on the fiber probe to allow for the unit to be positioned closer to the molten LiCl-KCl samples.

Vapors associated with the molten salt also play a role in spectral quality. In order to protect the objective lenses, quartz discs were installed above the molten salt samples. The effects of quartz disc installation are illustrated in Figure 7.

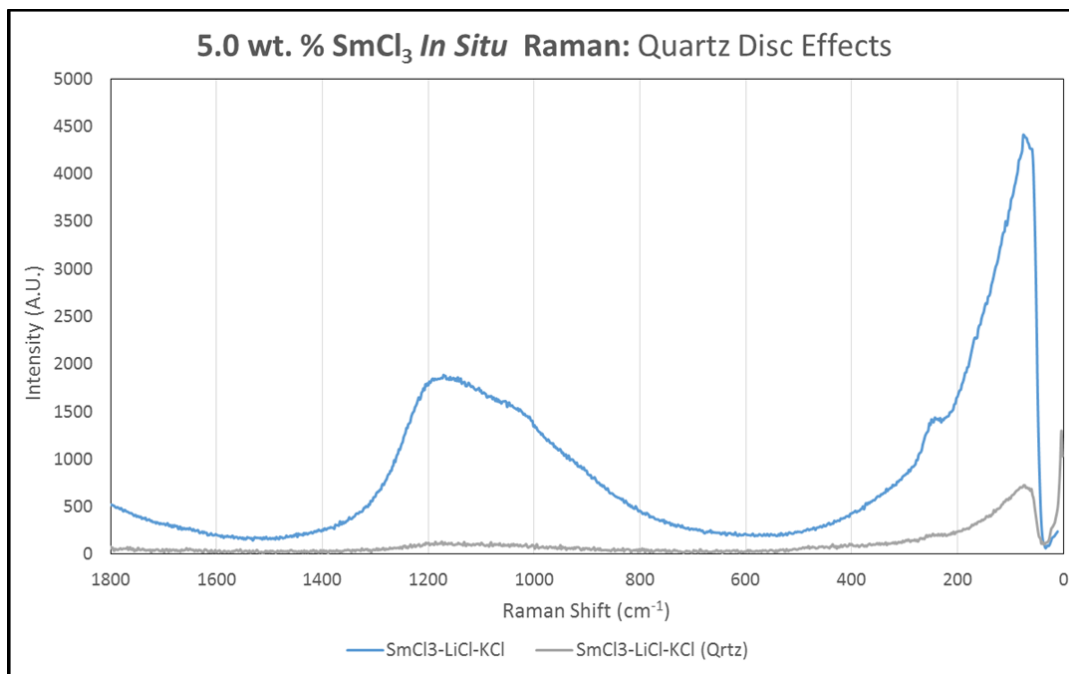


**Figure 7** The installation of quartz discs between the Raman objective and molten salt sample significantly decreased signal magnitude.

A drastic decrease in magnitude of signal was observed upon installation of the quartz disc (1/16" thick). The decision was made instead to treat objective lenses installed on the Raman probe as consumables to ensure no Raman modes would go undetected in subsequent studies.

### 3.3 Preliminary CV Investigations

The initial CV investigations conducted were completed using existing infrastructure available in the laboratory from previous molten salt projects [75]. Work commenced with the location of the Sm<sup>3+</sup>|Sm<sup>2+</sup> redox couple inside the LiCl-KCl electrochemical window and continued with repeatability studies. A quasi-reference silver wire reference electrode was initially employed, followed by the implementation of traditional reference electrode obtained from Argonne National Laboratory (ANL).

Tungsten rods were employed as both the working and counter electrodes because of their relative stability in molten chloride systems. Initial results indicated our salt supplies contained both impurities and moisture. The first study aimed to correlate measured peak current values with concentration of  $\text{SmCl}_3$  in the  $\text{LiCl-KCl}$  eutectic. The Randles-Sevcik relationship states these two values should be directly proportional. The cleaning procedure described in Table 1 was not implemented for the first study. Figure 8 is a collection of CV curves obtained at five different  $\text{SmCl}_3$  concentrations followed by a plot detailing the measured peak current vs. concentration results from the preliminary study. All other parameters (electrode surface area, scan rate and temperature) remained constant during this study. Impurity or moisture levels in the salts may have caused the low levels of repeatability and poor peak current vs. concentration correlation produced by the initial investigations.

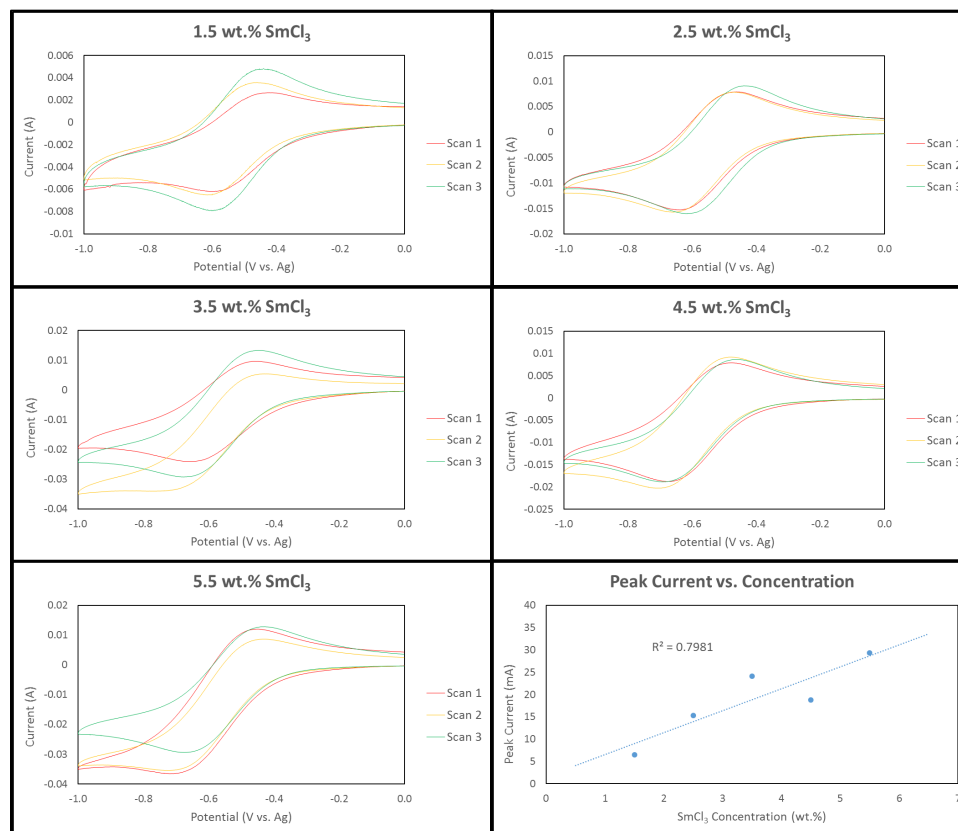


**Figure 8** Preliminary investigations produced a collection of CVs obtained at varying  $\text{SmCl}_3$  concentrations and peak current vs. concentration results. Repeatability and the theoretically linear relationship between peak current and scan rate were evaluated.

The slight drift in potential illustrated by the difference in peak locations relative to the x-axis indicated the quasi-reference electrode was not remaining entirely stable in the system. Figure 9 is an example of the improved repeatability in CV curves after integrating the procedure outlined in Table 1 with the same quasi-reference electrode. Across all of the preliminary studies, the first CV acquired was consistently different than the subsequent repeat curves. This discrepancy was attributed to the conditioning of the new WE electrode surface exposed to the high temperature molten salt environment.

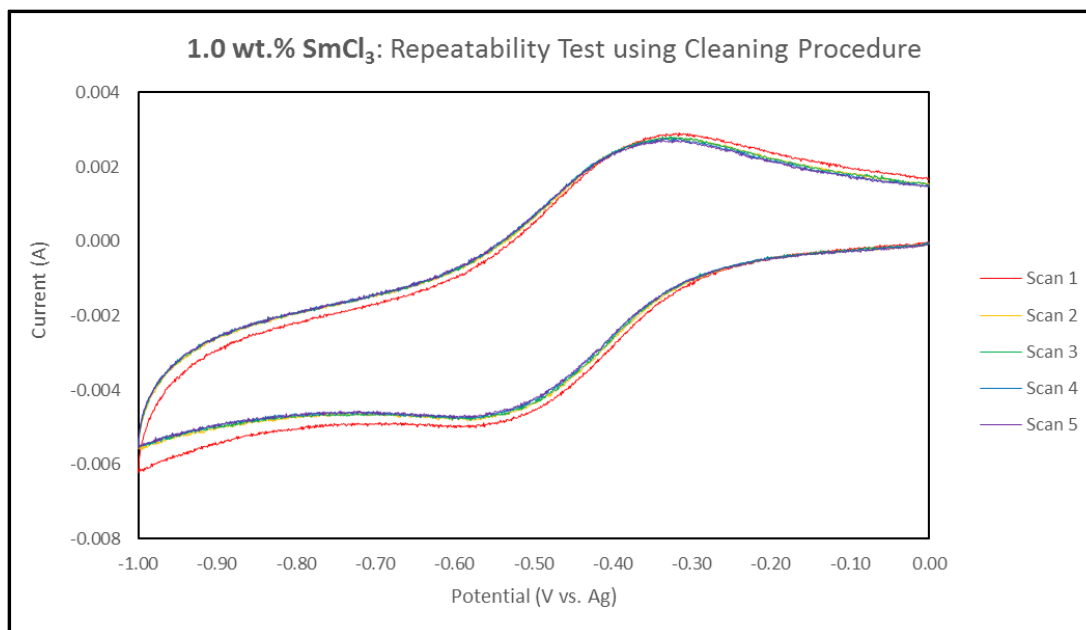


**Figure 9** The preliminary repeat study after implementation of the adjusted experimental procedure increased repeatability of CV scans.

After relative repeatability in peak current response was achieved through consistent CV acquisitions, the next development experiments focused on WE surface area determination.

Determining the electroactive surface area of the working electrode exposed to the molten salt melt can be difficult to achieve in an accurate and precise manner. There are a variety of methods employed by the community to measure this area. A common, but crude method susceptible to large amounts of error is a simple measurement of length regarding the solidified salt layer on the working electrode after an experiment is complete. Due to salt creep up the working electrode and surface tension effects, the calculated area from this method is often only a rough estimate. A second method was tested during the preliminary CV investigations. By stepping the electrodes in a controlled fashion using a micro-resolution translation stage, a back-calculation can be performed

to determine the amount of working electrode immersed in the melt. Figure 10 illustrates the high amount of error associated with peak current values that was observed during initial attempts at using this procedure as seen with the error bars associated with peak current values obtained at various translation stage immersion height settings.

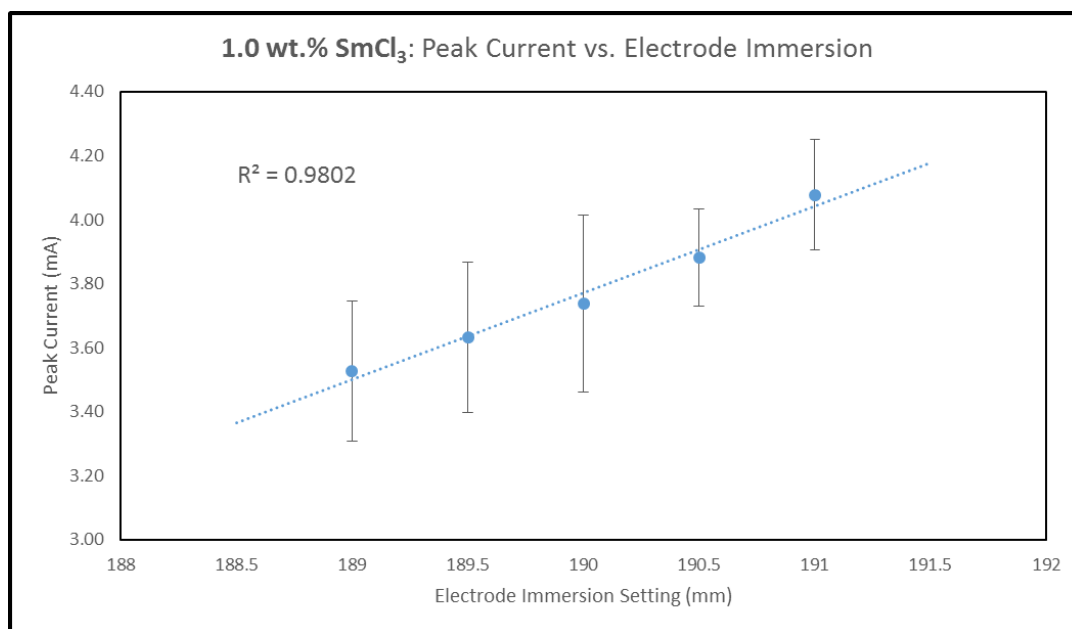


**Figure 10** Preliminary attempt at immersion experiment for determining working electrode surface area produced the expected linear correlation but large amounts of error in current response.

Although the linearity was fairly clear, the error bars indicated a high level of error when obtaining multiple CVs at the same height setting.

All studies up to this point were conducted using a potentiostat outside an inert atmosphere glove box connected to BNC (Bayonet Neill-Concelman) cables extending the cell cable leads into the glove box. Two concerns arose regarding the use of extension wiring to connect a potentiostat to electrodes inside a glove box. First, using extension wires inherently creates some un-compensated-for resistance ( $iR$ ) in the electrochemical cell. Since the peak current values are the measurement of interest, some sort of  $iR$

compensation must be taken into account regarding the extension wires. Second, the current sensing leads are susceptible to electrical noise if they are not shielded properly; therefore, any extension wiring being employed must be properly shielded to prevent any electrical frequency noise from affecting CV scans.

In order to determine whether peak current values can be affected by the employment of extension wiring, a traditional aqueous CV experiment using ferricyanide as the electroactive species in a potassium nitrate solution electrolyte was conducted with and without extension wires. The electrodes used were a fixed area platinum working electrode, coiled platinum wire counter electrode and standard calomel reference electrode (SCE). CVs obtained using a direct connection exhibited much less electrical noise and produced a slightly higher peak current value. It was briefly considered to place a potentiostat inside the glove box; however, salt vapors and the presence of lithium metal would most likely cause damage to the apparatus. Instead, when building a new, automated system for dedicated electrochemical work, longer potentiostat cell cables were fitted into vacuum fittings using a high-density resin. The fitted cables could then be run directly into the glove box through a K flange and eliminate the need for extension wiring. Figure 11 illustrates the slight differences that can manifest when incorporating extension wiring into an electrochemical system, with regards to both peak current and levels of electrical noise.



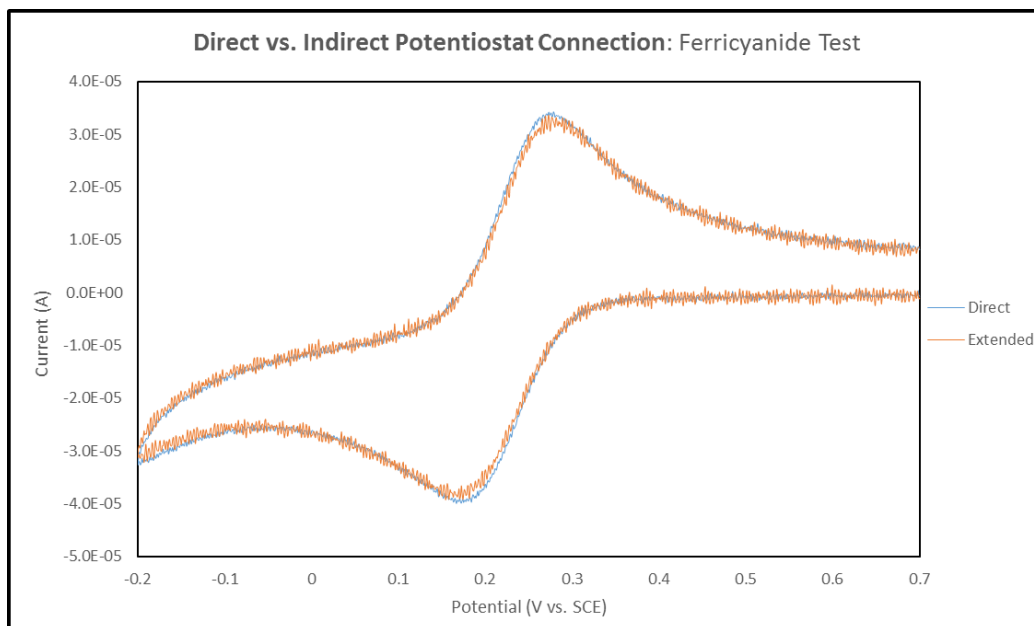


**Figure 11** CVs taken with a direct and indirect connection to cell leads using an aqueous electrochemical system inspired a drift away from extension cable use.

From these studies, design and fabrication began on a new, dedicated electrochemical setup for continuation of these studies.

### 3.4 Automated System Quasi-Reference CV Study

A newly constructed electroanalytical system was employed to conduct a repeat study of  $\text{SmCl}_3$  solvated in the molten  $\text{LiCl-KCl}$  eutectic at  $500\text{ }^\circ\text{C}$ . Melts containing 1.0, 2.0, 3.0, 4.0 and 5.0 wt. %  $\text{SmCl}_3$  were prepared and analyzed according to expected correlations between peak current and scan rate, along with peak current and concentration stated in the Randles-Sevcik relationship. All samples were maintained at  $500\text{ }^\circ\text{C}$  during testing. The redox peaks were much more pronounced, allowing for clear interpretation of peak current values; however, small amounts of electrical noise were still observed in the form of sinusoidal frequency noise. The noise is difficult to see in most CV scans; however, the noise could potentially affect peak current values and needed

further investigation. Figure 12, Figure 13, Figure 14, Figure 15, and Figure 16 are compiled CV results from the 1.0, 2.0, 3.0, 4.0 and 5.0 wt. %  $\text{SmCl}_3$  samples, respectively. Each of these figures contain five plots of CVs taken at various scan rates and one plot detailing the peak cathodic current vs. square root of scan rate relationship dictated by the Randles-Sevcik equation.

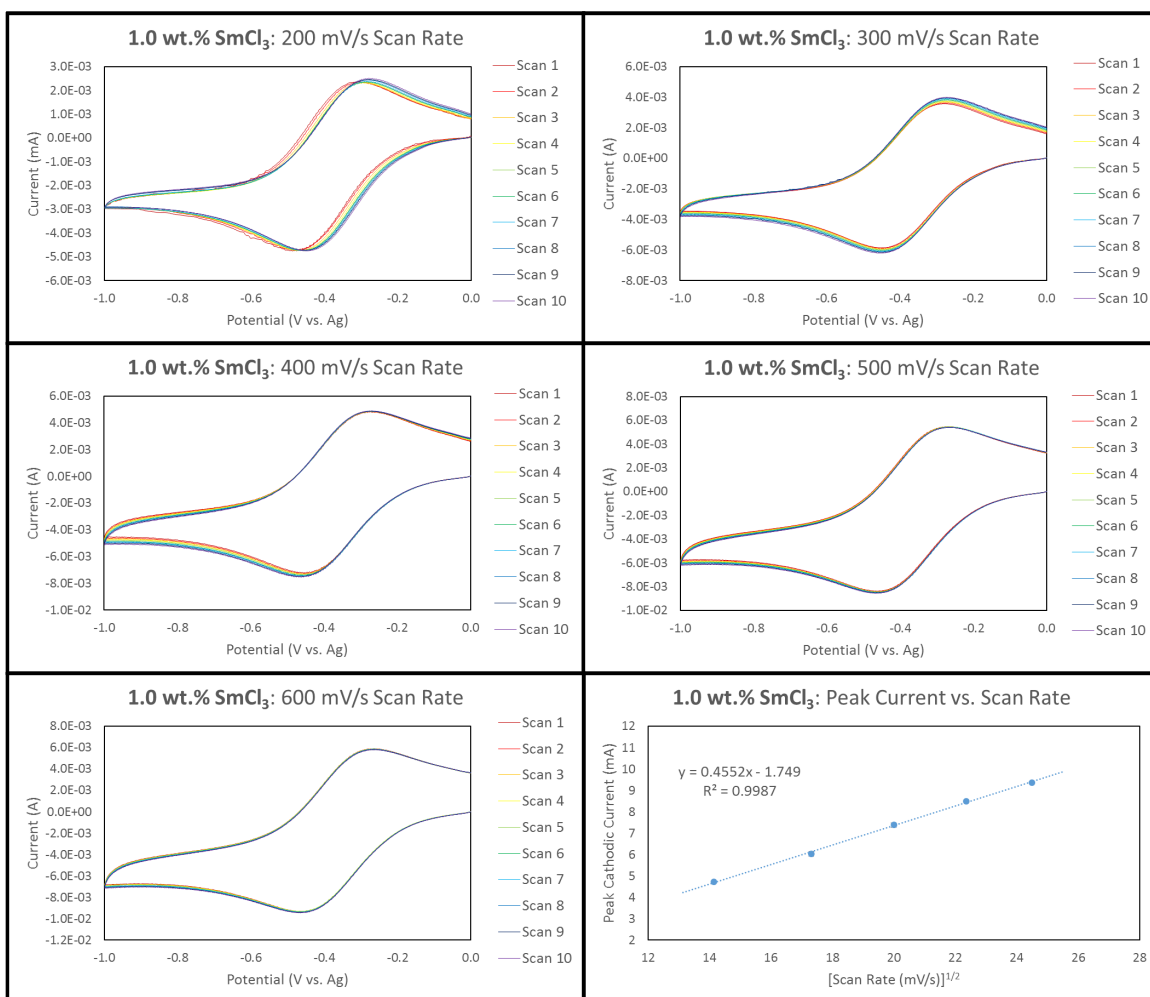


**Figure 12** Cyclic voltammetry of 1.0 wt. %  $\text{SmCl}_3$  solvated in the molten LiCl-KCl eutectic at 500 °C and analyzed according to the Randles-Sevcik equation.

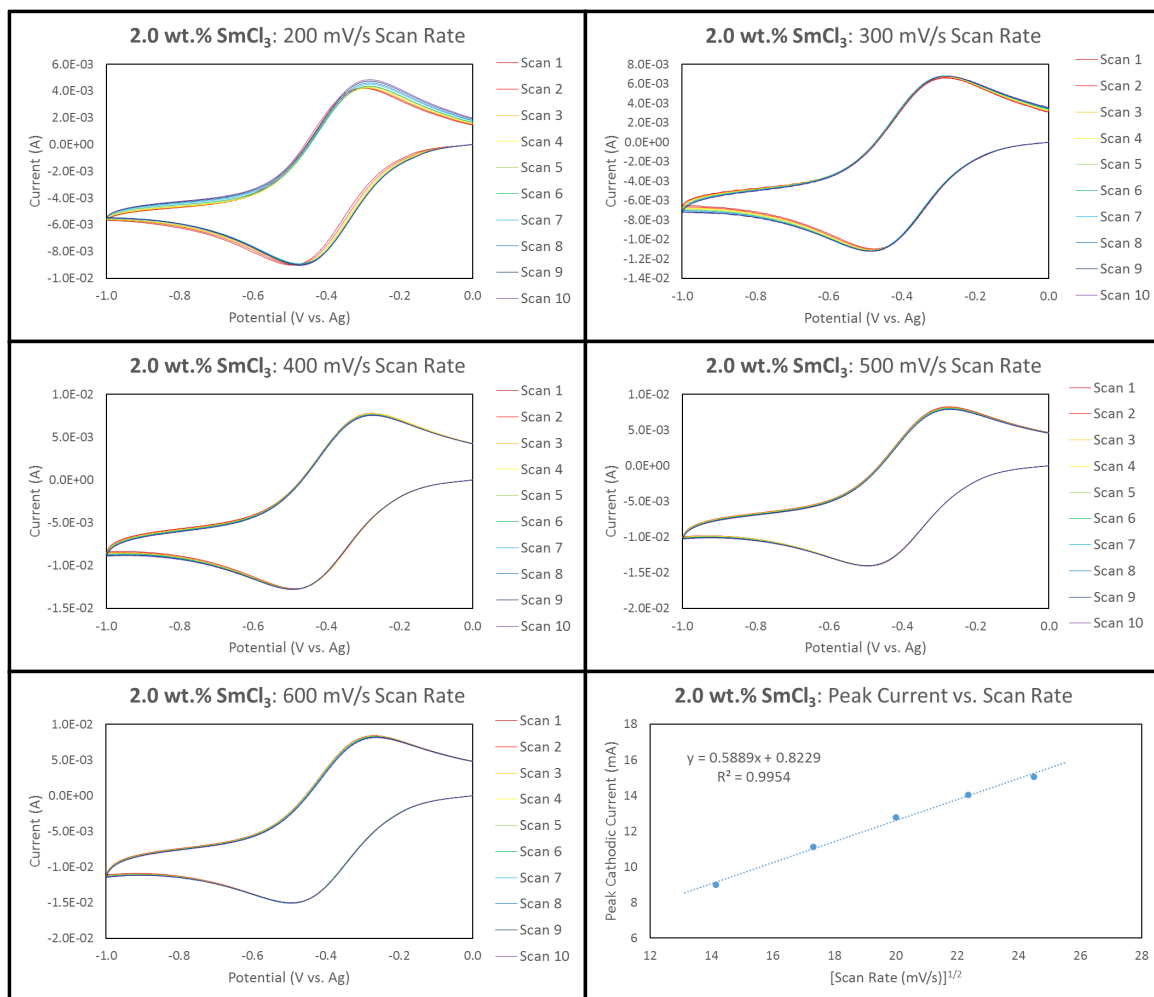


**Figure 13** Cyclic voltammetry of 2.0 wt. %  $\text{SmCl}_3$  solvated in the molten  $\text{LiCl-KCl}$  eutectic at  $500^\circ\text{C}$  and analyzed according to the Randles-Sevcik equation.

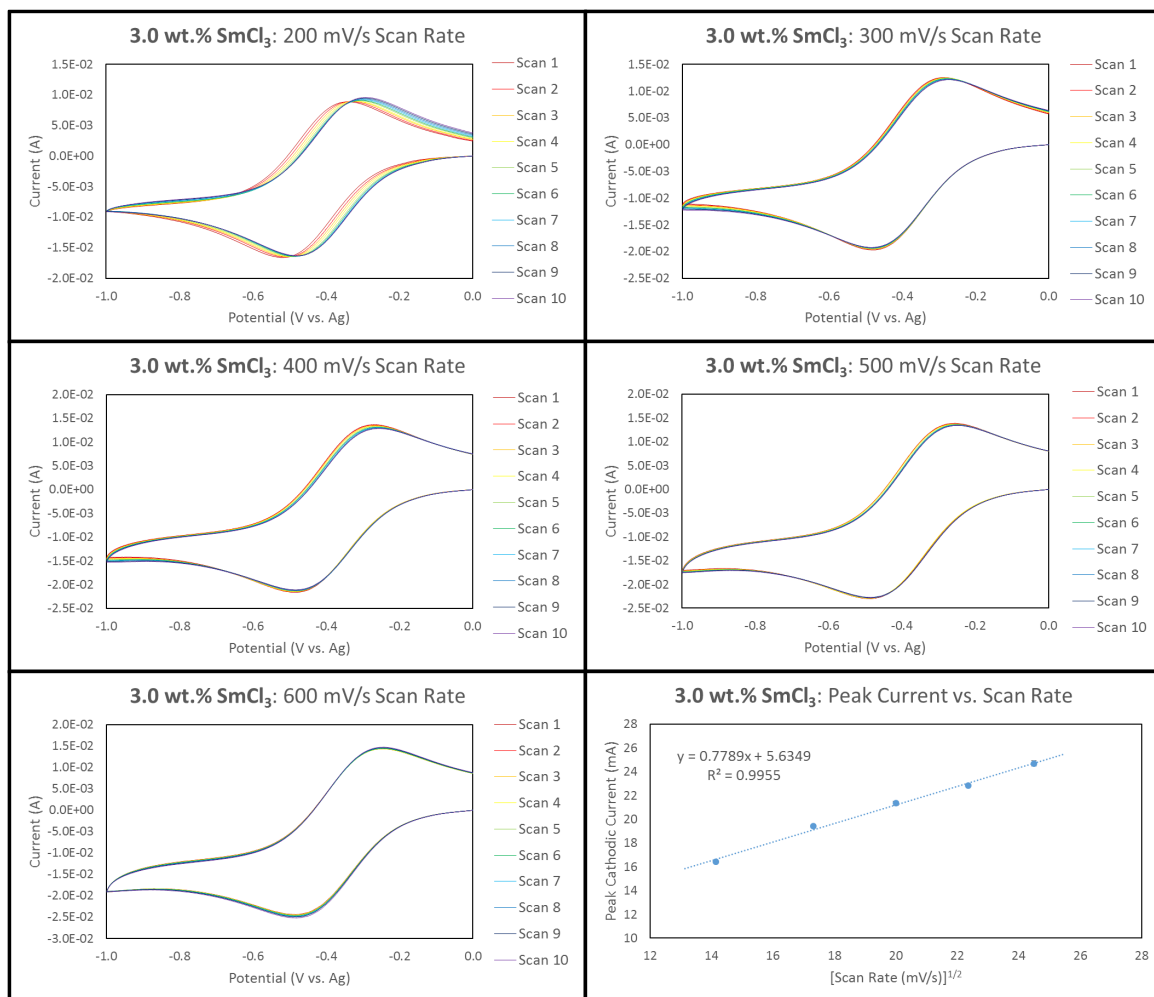


**Figure 14** Cyclic voltammetry of 3.0 wt. %  $\text{SmCl}_3$  solvated in the molten  $\text{LiCl-KCl}$  eutectic at  $500^\circ\text{C}$  and analyzed according to the Randles-Sevcik equation.

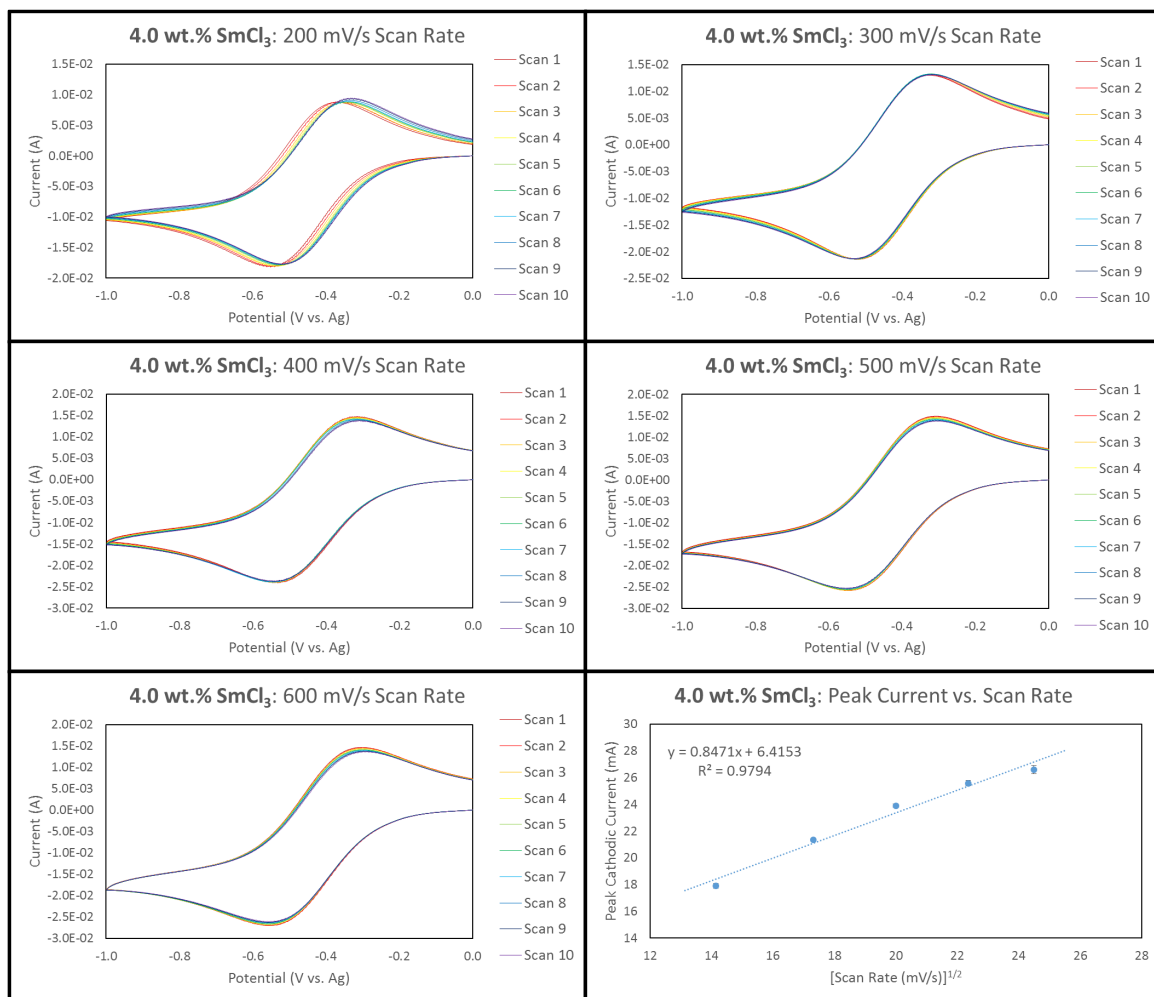


**Figure 15** Cyclic voltammetry of 4.0 wt. %  $\text{SmCl}_3$  solvated in the molten  $\text{LiCl-KCl}$  eutectic at  $500^\circ\text{C}$  and analyzed according to the Randles-Sevcik equation.

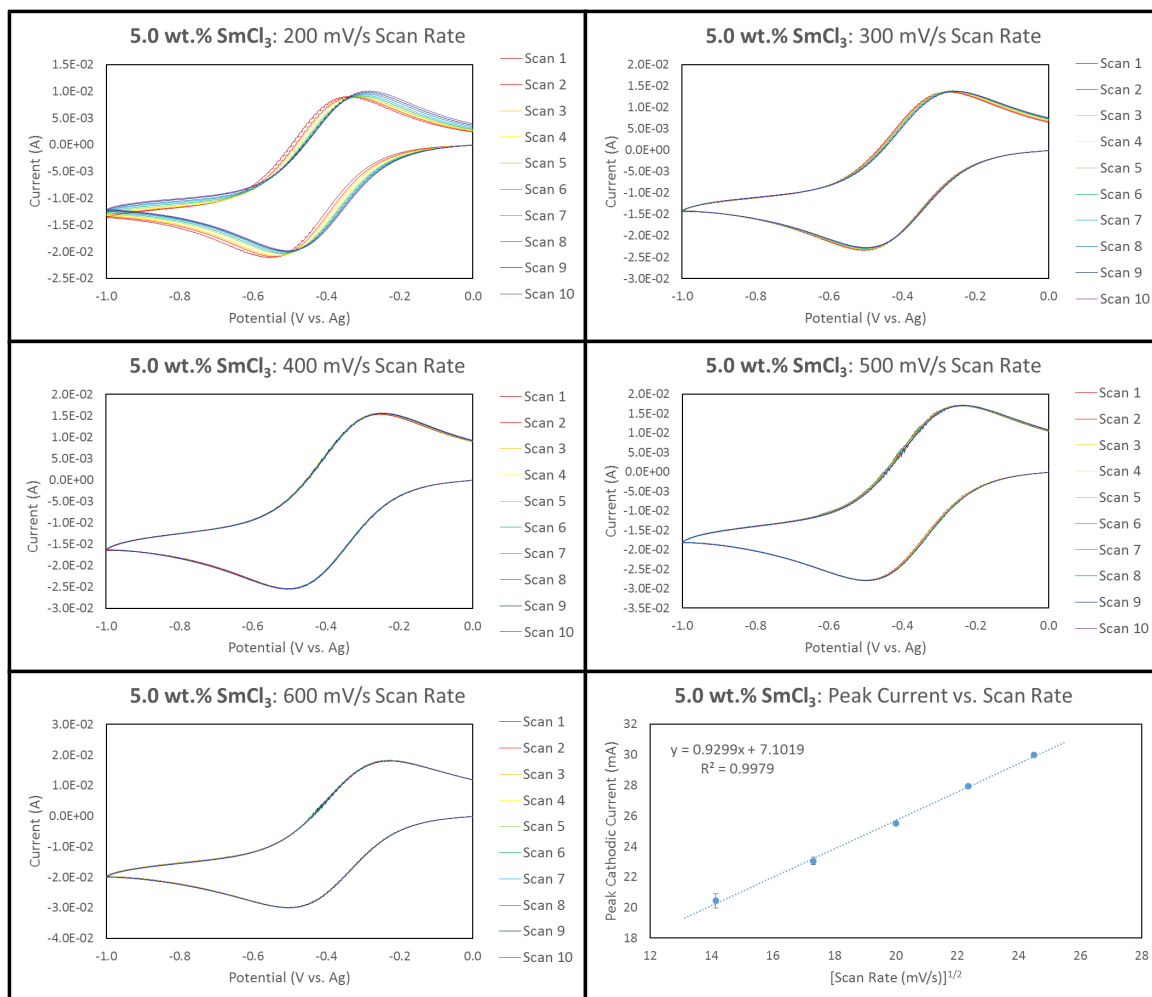


**Figure 16** Cyclic voltammetry of 5.0 wt. %  $\text{SmCl}_3$  solvated in the molten  $\text{LiCl-KCl}$  eutectic at  $500^\circ\text{C}$  and analyzed according to the Randles-Sevcik equation.

CV curves in the 1-5 wt. %  $\text{SmCl}_3$  quasi-reference study, obtained using the high purity  $\text{SmCl}_3$  were observed to have more defined redox peaks and minimal amounts of electrical frequency noise. Furthermore, each peak current vs. scan rate correlation, except one conducted at 4.0 wt. %, produced an  $R^2$  value greater than 0.99 with regards to linear fit. Some results indicated slight potential drift, most likely caused by the quasi-reference electrode's instability. The peak current vs. concentration relationship was also analyzed at the scan rates of interest. This correlation was less clear than that produced

by the peak current vs. scan rate results. Figure 17 is the summary of peak current vs. concentration results at 200, 300, 400, 500 and 600 mV/s scan rates.

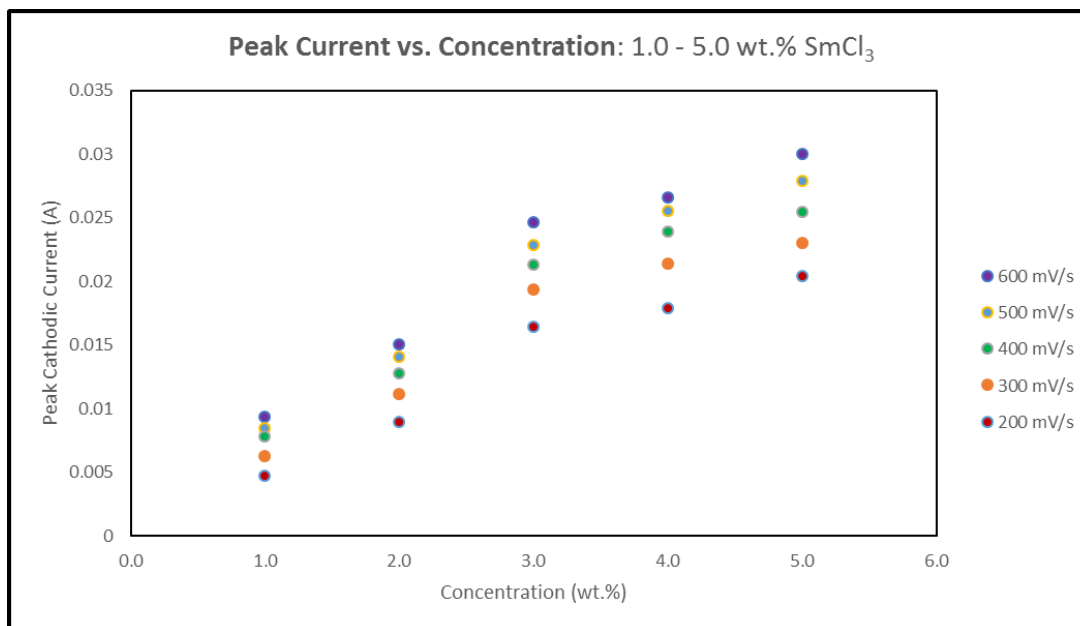


**Figure 17** Peak current varied in a relatively linear fashion with respect to concentration as a result of the quasi-reference study.

These experimental and data analysis protocols were used to determine diffusion coefficients for  $\text{Sm}^{3+}$  in the molten eutectic LiCl-KCl and compared to the recently published literature in the Chapter 4 manuscript.

### 3.5 Ag|AgCl Reference Electrode Implementation for CV

A silver-silver chloride (Ag|AgCl) reference electrode designed at ANL by Tylka *et al.* was obtained and integrated into the electroanalytical system [38]. Traditional reference electrodes were constructed at 5 mol% AgCl in the LiCl-KCl eutectic and the previous, quasi-reference study was once again repeated using the Ag|AgCl reference. Although the reference electrode was new, the same size WE and counter electrode tungsten electrodes were employed. Peak current vs. scan rate experiments were

conducted at 1.0, 3.0, 5.0 and 7.0 wt. %  $\text{SmCl}_3$ . The scan rate experiments were each conducted at scan rates up to 500 mV/s in 25 mV/s increments to provide better resolution on the peak current vs. scan rate plots. The goal of this study, and continuing studies, has been to begin testing the limits of the Randles-Sevcik applicability in the molten chloride system of interest. Furthermore, immersion stepping was employed to determine working electrode surface area as part of these studies as well. Figure 18, Figure 19, Figure 20, and Figure 21 summarize the peak current vs. scan rate and immersion study experiments at 1.0, 3.0, 5.0 and 7.0 wt. %  $\text{SmCl}_3$ , respectively.

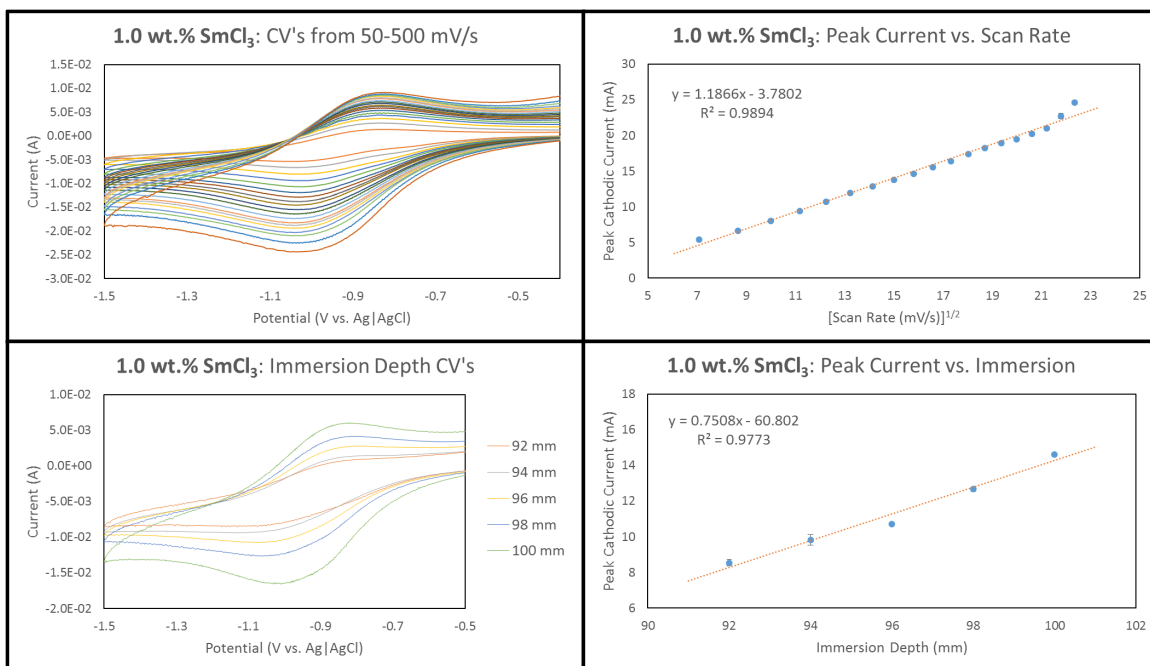


**Figure 18** Cyclic voltammetry of 1.0 wt. %  $\text{SmCl}_3$  in molten LiCl-KCl eutectic maintained at a temperature of 500 °C produced relatively linear trends with respect to scan rate and immersion depth of the WE.



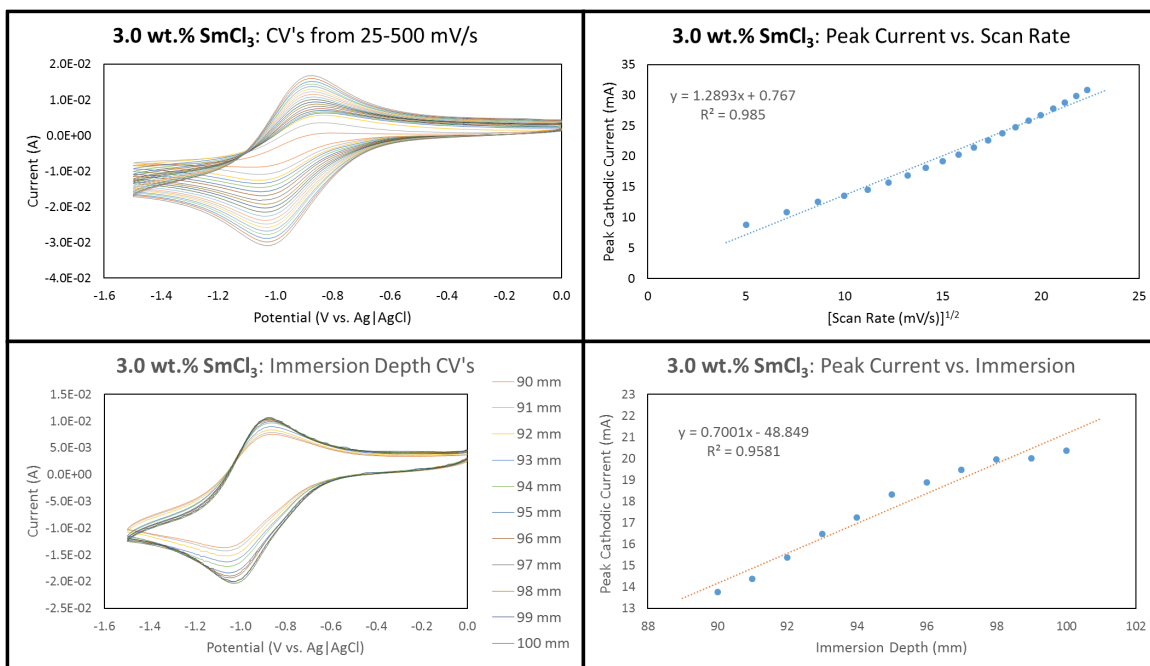


**Figure 19** Cyclic voltammetry of 3.0 wt. % SmCl<sub>3</sub> in molten LiCl-KCl eutectic maintained at a temperature of 500 °C produced relatively linear trends with respect to scan rate and immersion depth of the WE.

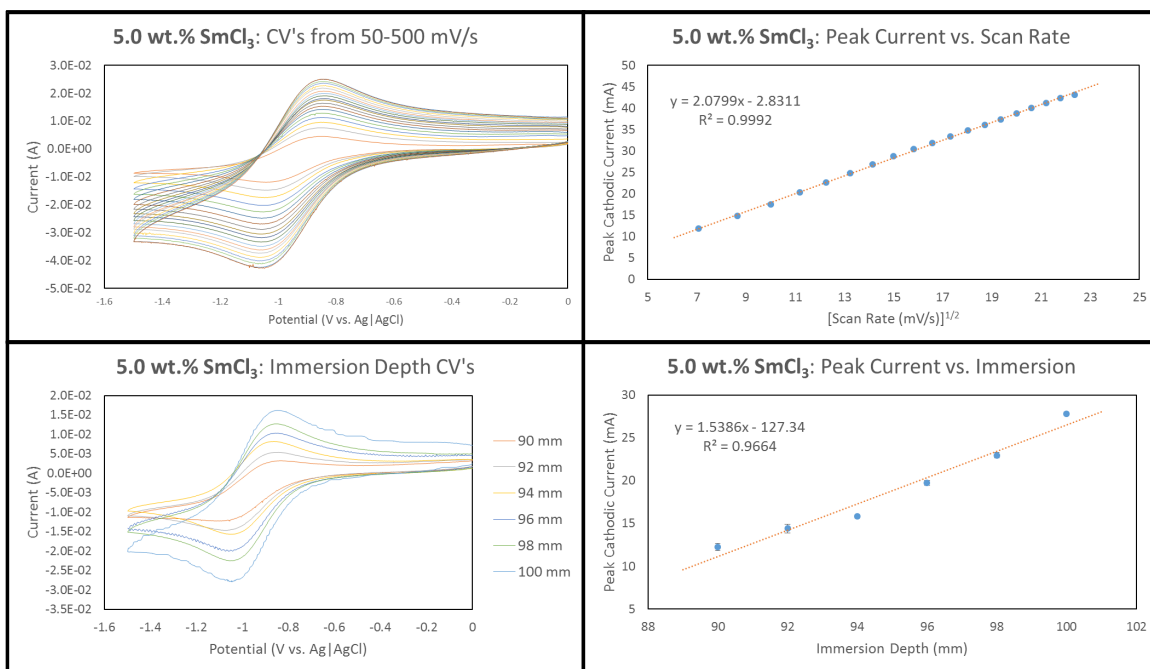


**Figure 20** Cyclic voltammetry of 5.0 wt. % SmCl<sub>3</sub> in molten LiCl-KCl eutectic maintained at a temperature of 500 °C produced relatively linear trends with respect to scan rate and immersion depth of the WE.

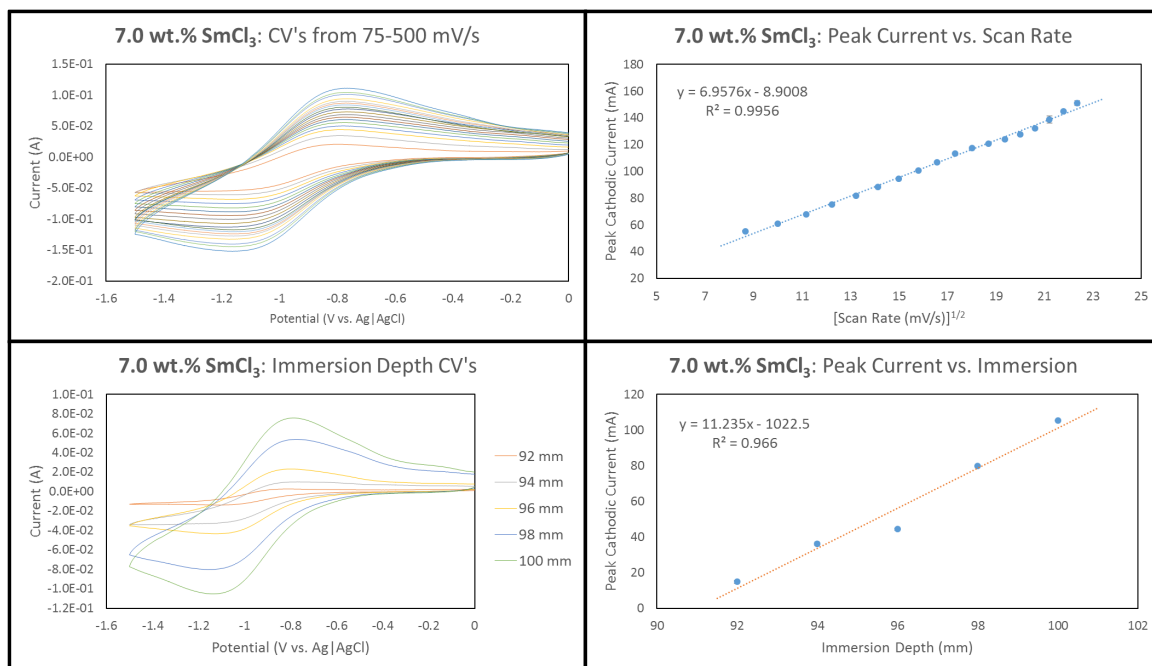


**Figure 21** Cyclic voltammetry of 7.0 wt. %  $\text{SmCl}_3$  in molten LiCl-KCl eutectic maintained at a temperature of 500 °C produced relatively linear trends with respect to scan rate and immersion depth of the WE.

The peak current vs. concentration relationship was also investigated as part of this study.

Peak current vs. concentration data was analyzed at all scan rates between 25 and 500 mV/s, and the relationship remained consistent across all scan rates.

Figure 22 illustrates the peak current vs. concentration correlation at five different scan rates, with and without the 7.0 wt. %  $\text{SmCl}_3$  data set. The experiments at 7.0 wt. %  $\text{SmCl}_3$  were much higher in peak current than expected. This increase may be due to applicability limits of the Randles-Sevcik equation or the manifestation of additional diffusion mechanisms such as migration.

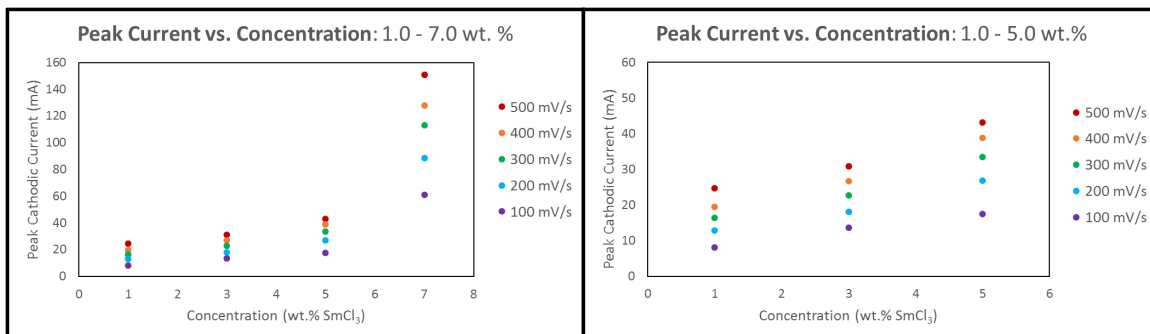


**Figure 22** Peak current concentration results with (left) and without (right) the 7.0 wt. % data set suggested limits in the Randle-Sevcik's applicability or the manifestation of migration at higher analyte concentration.

Immersion study results were utilized to back-calculate the working electrode surface area instead of using the dip measurement method.

### 3.6 Low Concentration Cerium CV Study

All experimental procedures were identical to the samarium studies with respect to reference electrode preparation, salt baking and the amount of time each melt was molten before commencing data collection (5 hours). Separate electrode sets were employed for the samarium and cerium studies in order to prevent cross contamination of melt samples. Figure 23 provides CVs taken from 25 to 500 mV/s scan rates from a 1.0 wt. % CeCl<sub>3</sub> melt. The scan rate resolution and cleanliness of the CVs is comparable to that obtained from samarium. The cerium CVs confirmed the system's capabilities with multi-electron transfer systems, rather than single electron transfer systems associated with samarium.

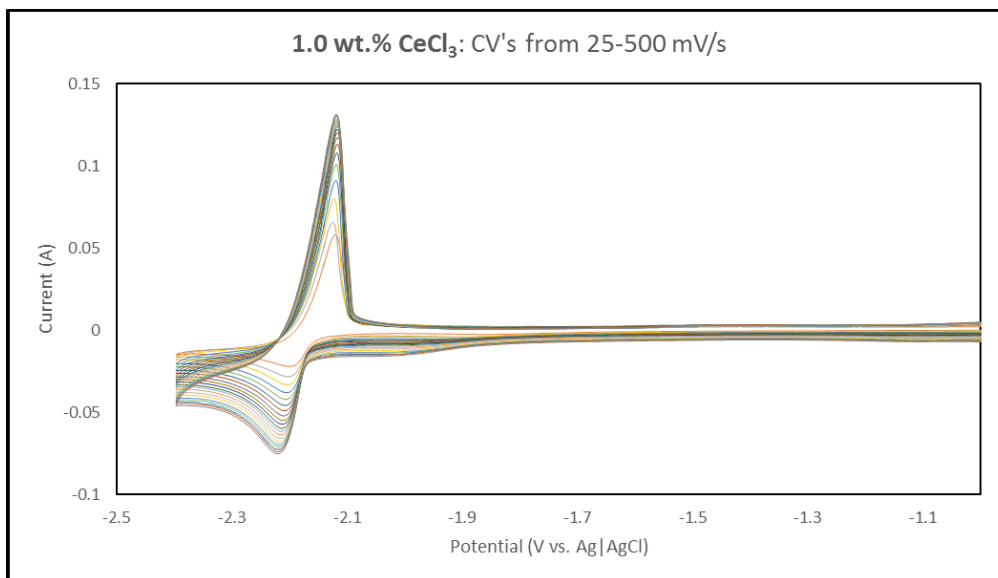


**Figure 23** CVs obtained from 1.0 wt. %  $\text{CeCl}_3$  melt at various scan rates were clean and exhibited relatively consistent spacing.

The peak current versus scan rate relationship also manifested as expected with a clearly linear relationships between the two characteristics. Figure 24 illustrates this peak current versus scan rate data obtained from the 1.0 wt. %  $\text{CeCl}_3$  melt.

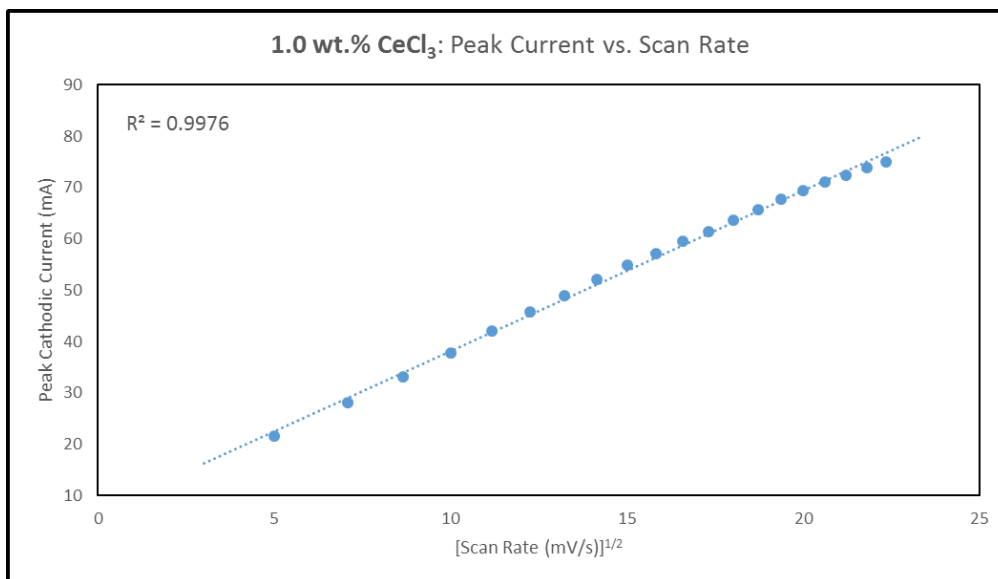


**Figure 24** Peak current versus scan rate data from preliminary 1.0 wt. %  $\text{CeCl}_3$  sample exhibited a linear correlation as expected.

Unfortunately, the formation of unexplained redox peaks was also observed as part of the cerium studies. The source of these impurities, as with the samarium studies, is thought to be associated with the formation of an oxychloride. Figure 25 illustrates the unexplained redox peaks detected during a repeat 1.0 wt. %  $\text{CeCl}_3$  experiment.

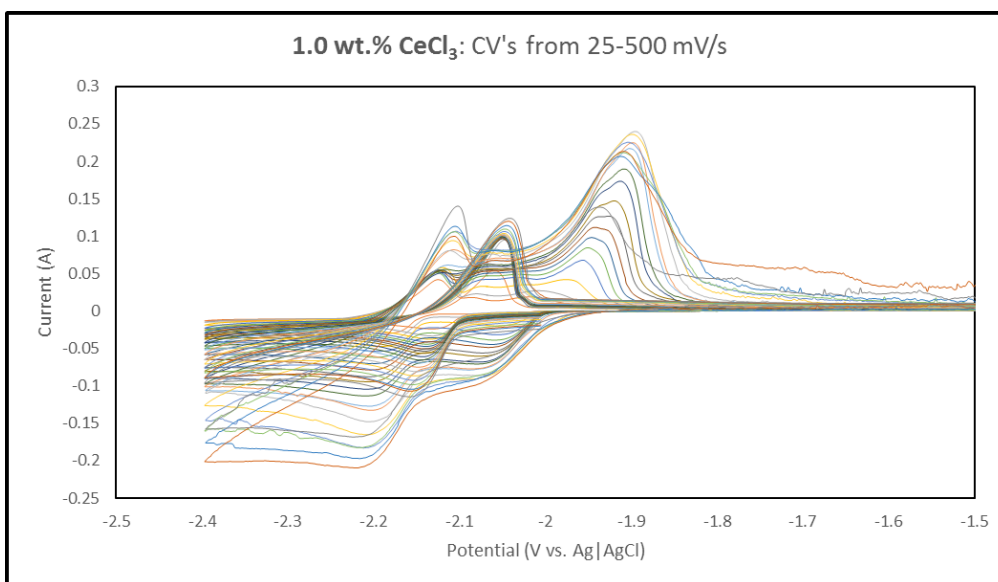


**Figure 25** CVs obtained from a repeat 1.0 wt. %  $\text{CeCl}_3$  experiment indicated the presence of unexplained redox peaks not associated with typical  $\text{CeCl}_3$  data

The impurity peaks continued to manifest at other concentrations of  $\text{CeCl}_3$  as shown by the results from a 2.0 wt. %  $\text{CeCl}_3$  study illustrated in Figure 26. Investigations into the source of these redox peaks requires further investigation. The clean data obtained from the low concentration experiments was utilized to confirm system performance for a 3-electron transfer reaction by comparing diffusion coefficients for cerium with the literature.

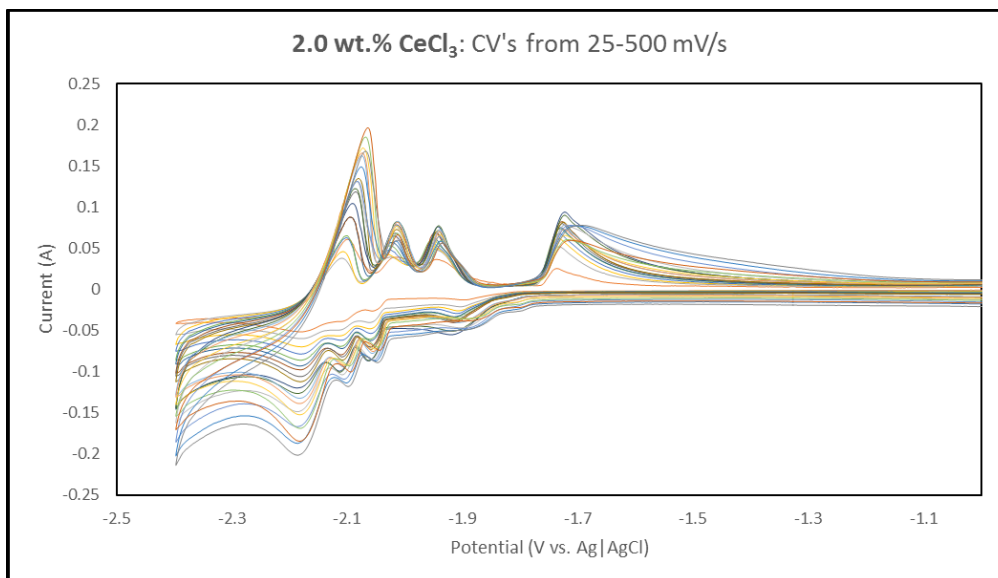


**Figure 26** CVs obtained from a 2.0 wt. %  $\text{CeCl}_3$  melt indicated the presence of unexplained redox peaks as well.

Diffusion coefficient results from the cerium CV investigations are reported in Table 6 and compared with the recently published literature.

Literature Source	$D_{\text{Ce}^{3+}} (\cdot 10^5 \text{ cm}^2/\text{s})$
Iizuka [58]	0.73 – 2.72
Marsden <i>et al.</i> [57]	0.92 – 2.08
<b>This Study</b>	<b>1.82 – 2.16</b>

**Table 6** Diffusion coefficient results for trivalent cerium from this study were compared with the recent literature.

The range in diffusion coefficient values was consistent with the literature in terms of both reported value and variation.

## Chapter 4 *In Situ* Raman Spectroscopy of Samarium Ions in Molten LiCl-KCl Eutectic

### 4.1 Introduction

Molten salt systems are being investigated as heat transfer or flow media for renewable and nuclear energy systems. Chloride salts have long been considered as reactor cooling and fuel containment media in the nuclear energy industry.<sup>[12, 33]</sup> LiCl-KCl eutectic salt is the electrochemical media for the reprocessing of used nuclear fuel (UNF) through pyrochemical methods.<sup>[26, 28-30, 32, 38, 54]</sup> An understanding of chloride salt chemistry may offer insight into the corrosion behavior of proposed structural materials, and process optimization as it pertains to reprocessing and nuclear material accountancy (NMA) in salt systems containing special nuclear material (SNM). Furthermore, *in situ* techniques for the analysis and monitoring of salt content offer a path toward commercialization for many of these advanced reactor and reprocessing concepts.<sup>[38]</sup> Raman spectroscopy is one such analytical technique that provides information regarding molten salt content, dissolved analyte coordination and speciation.<sup>[66, 67, 73]</sup>

Raman spectroscopy for the analysis of lanthanide trichloride ( $\text{LnCl}_3$ ) chemistry in molten LiCl-KCl eutectic is typically conducted using microscopes equipped with high temperature stages. Molten salt samples are traditionally prepared in inert atmosphere by sealing quartz sample tubes with the salt of interest inside before being transferred to a Raman microscope for analysis in open atmosphere.<sup>[66, 67, 70, 71, 73, 81, 82]</sup> Chloride systems,

such as the LiCl-KCl eutectic, are extremely hygroscopic; therefore, if a system can be deployed that does not require the removal of salt samples from a bulk electrochemical processing cell, spectral analysis can offer real-time information during operations. Reproducing spectral quality and resolution using fiber-based *in situ* Raman probes has been explored in a very limited capacity.<sup>[73]</sup> Our group designed and built an *in situ* Raman spectroscopy system to study molten salts and successfully employed it to study the nature of Li in LiCl-Li<sub>2</sub>O.<sup>[74, 83]</sup> The design reported in this manuscript is based off the previous design but with several improvements such as laser power and polarizability. Previous research conducted by our group, using the *in situ* Raman system reported here, has produced high quality Raman spectra from nitrate salts in open atmosphere.<sup>[84]</sup> Rodriguez-Betancourt *et al.* have deployed both a fiber-based and microscope system to study cerium and neodymium in LiCl-KCl eutectic salt. Samarium is another common lanthanide found in UNF that exhibits negative neutronic effects and must be removed from UNF before the usable uranium and plutonium can be recycled for energy production.<sup>[27]</sup>

LnCl<sub>3</sub> salts coordinate to form LnCl<sub>6</sub><sup>3-</sup> complexes when dissolved in alkali chloride melts. The octahedral (O<sub>h</sub>) symmetry of these complexes is well understood and relatively consistent across the lanthanide elements.<sup>[68, 70, 71]</sup> This coordination behavior has been further established using X-ray absorption fine structure (XAFS) analysis, along with computational simulations.<sup>[85, 86]</sup> The location of vibration modes associated with this symmetry varies as a function of Li<sup>+</sup> ion concentration due to its polarizing power caused by its large ionic radius, LnCl<sub>3</sub> concentration, and sample temperature.<sup>[68, 71, 87]</sup> Spectral



comparison and consistency across the literature is therefore difficult to achieve due to the number of variables associated with vibration mode location. Coordination of divalent lanthanide species in LiCl-KCl eutectic is far less understood. Raman spectroscopy data is extremely limited in terms of divalent spectra, with only cerium and neodymium having been reported to our knowledge.<sup>[73]</sup> Ultraviolet-visible (UV-vis) absorption spectroscopy has been employed to study the formation of divalent samarium in LiCl-KCl eutectic. Unfortunately, trivalent samarium is not detectable using UV-vis spectroscopy.<sup>[62]</sup> If Raman spectroscopy is able to detect both trivalent and divalent samarium, it could consolidate *in situ* methods for analysis of molten salt composition and allow for a better understanding of speciation behavior for a variety of lanthanides. Speciation can be studied in a targeted manner by employing both electrochemical and chemical methods.<sup>[62, 73]</sup> Electroanalytical methods have been employed by our group in the past to study valence states of samarium in the LiCl-KCl eutectic, and voltammetric techniques were utilized to identify reducing potentials for electrochemical reductions.<sup>[88-90]</sup> This study provides a comprehensive examination of samarium ion behavior in the LiCl-KCl eutectic under consideration for the pyrochemical reprocessing of UNF using a fiber-based Raman spectroscopy system coupled with electroanalytical capabilities designed for high temperature molten salt environments.

## 4.2 Experimental

### Spectroelectrochemical Apparatus

A combined spectroscopy and electrochemical (SPEC) apparatus was custom-designed and built for *in situ* detection of lanthanides solvated in a molten chloride salt at 500 °C under inert atmosphere. A schematic of the setup is shown in Figure 27. A 532 nm laser was utilized as the excitation source. A ceramic insulation cap on top of the furnace was specially designed to minimize thermal gradients within the melt while providing a point of entry for the Raman laser and electrodes for simultaneous spectroscopic and electrochemical studies. The electrode guides on the insulation cap were machined in line with an electrode mounting plate at the end of a motorized stage which helps make the experiments repeatable by ensuring electrodes are immersed in a consistent and perpendicular orientation. A three-electrode setup consisting of a tungsten plate working electrode, graphite counter and silver wire quasi-reference was employed for electrochemical reduction experiments. Cyclic voltammetry (CV) was conducted to identify a reducing potential for Sm<sup>2+</sup> formation. The reducing potential was held for 2 hours concurrently with Raman spectra acquisition.

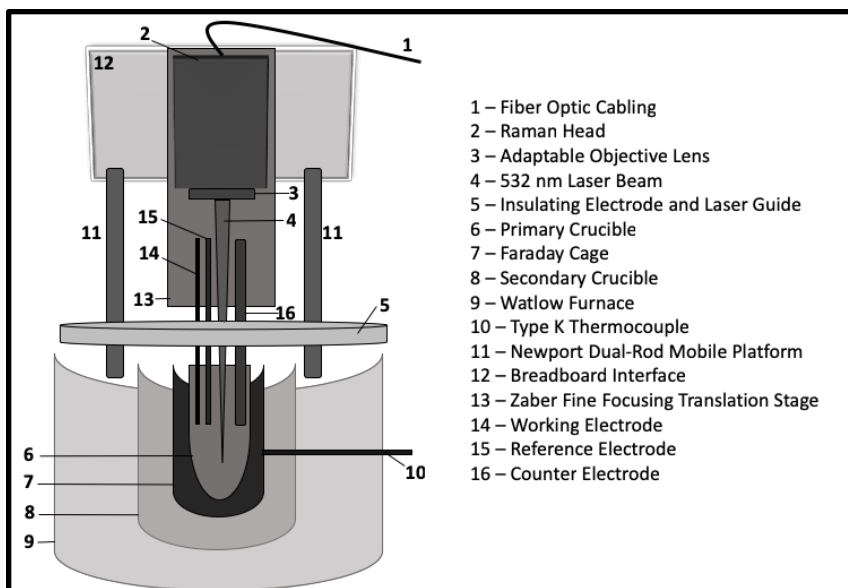


**Figure 27** SPEC setup employed for dual Raman spectroscopy and electrochemical studies.

### Chemicals and Materials

LiCl (Alfa Aesar 99% pure) and KCl (Alfa Aesar 99% pure) were individually baked under vacuum to minimize moisture impurities prior to preparation of a eutectic matrix composed of 46 wt. %, 54 wt. % LiCl and KCl, respectively. The eutectic mixture was added to a 55 mL tantalum crucible inside a stainless-steel faraday cage nested in a secondary stainless-steel crucible. This secondary vessel also served as the point of contact for a K-type thermocouple providing feedback to the furnace through a custom LabView National Instruments program. The crucibles were placed in a furnace maintained within  $\pm 2$  °C of the temperature setpoint. All salts were handled inside an ultra-high purity argon (Airgas 99.99%) atmosphere glovebox (Vacuum Atmospheres Co. VAC Controlled Atmospheres Systems) with moisture and oxygen content maintained below 1 ppm. The eutectic mixture was fused under argon atmosphere and trivalent samarium solutions were prepared by directly introducing anhydrous  $\text{SmCl}_3$  (Alfa Aesar 99.9% pure). Samarium

metal (Alfa Aesar 99.9% pure) was used in chemical reduction experiments to convert trivalent samarium ions into divalent species. All electrochemical experiments were performed at 500 °C using a Gamry Ref3000 potentiostat controlled using the Gamry Framework software. Gamry Echem Analyst software was used to analyze electrochemical data.

### 4.3 Results and Discussion

#### Trivalent Samarium

Rayleigh scattering contributions were removed using a differential operation previously reported in the literature.<sup>[69, 71]</sup> A spectrum of LiCl-KCl eutectic without any SmCl<sub>3</sub> dissolved was also obtained to subtract from all subsequent spectral acquisitions. The Rayleigh-reduced Raman intensity,  $R(\omega)$ , was calculated using Equation 4. Removing Raleigh-induced scattering effects allows for temperature and asymmetry effects to be studied in detail.<sup>[69]</sup>

$$R(\omega) = \frac{I(\omega) \cdot \omega}{(\omega_0 - \omega)^4 [n(\omega) + 1]} \quad (4)$$

$I(\omega)$  is the Raman intensity at wavenumber  $\omega$ , and  $\omega_0$  is the incident excitation laser frequency. The Boltzmann thermal population component is  $[n(\omega) + 1]$  and is further defined in Equation 5.

$$n(\omega) + 1 = \frac{1}{\exp\left(\frac{h\omega c}{kT}\right) - 1} + 1 \quad (5)$$

Here  $h$  is Planck's constant,  $c$  is the velocity of light,  $k$  is the Boltzmann constant, and  $T$  is the temperature of the molten salt sample. Isotropic (ISO) and anisotropic (ANISO)

scattering intensities were calculated from the reduced Raman intensities using Equations 6 and 7, respectively.<sup>[69, 71]</sup>

$$I_{ISO} = I_{VV}(\omega) - \frac{4}{3}I_{HV}(\omega) \quad (6)$$

$$I_{ANISO} = I_{HV}(\omega) \quad (7)$$

Here subscripts VV and HV refer to polarized and depolarized spectra, respectively. Concentration of  $\text{SmCl}_3$  was maintained at or below 5 mol % percent in order to maintain the  $O_h$  symmetry associated with the  $\text{SmCl}_6^{3-}$  complex.<sup>[71]</sup> Figure 28 illustrates a polarized and depolarized Raman spectra collected from a 5 mol %  $\text{SmCl}_3$  in LiCl-KCl sample.

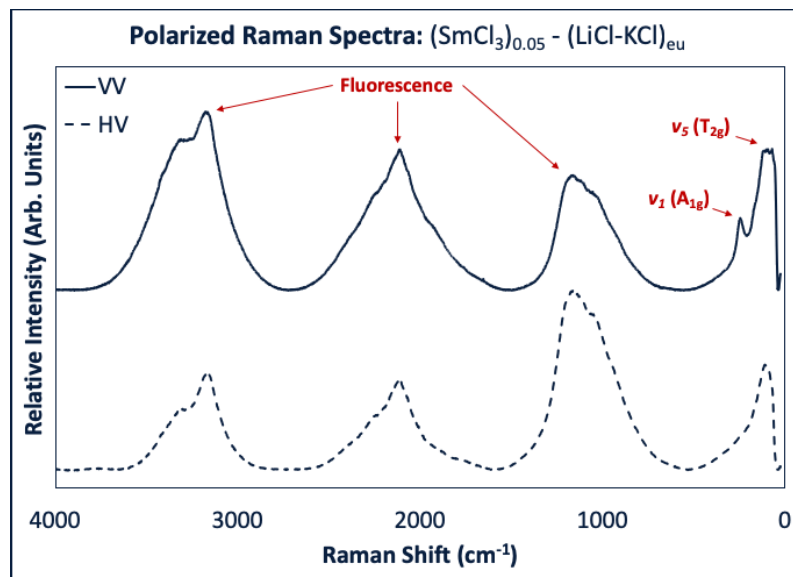


**Figure 28** Raman polarized (VV) and depolarized (HV) spectra of 5 mol % trivalent samarium in LiCl-KCl eutectic.

Although the octahedral complex  $\text{SmCl}_6^{3-}$  has three distinct active Raman modes, only two are detectable. The  $\nu_1 (A_{1g})$  vibration mode located at 235-270  $\text{cm}^{-1}$  is assigned as the symmetric stretching of the  $\text{Sm}^{3+}\text{-Cl}^-$  bond. This vibration mode is removed when depolarized spectra are collected. The  $\nu_5 (F_{2g})$  vibration mode located at 60-85  $\text{cm}^{-1}$  is assigned as degenerative bending of the same  $\text{Sm}^{3+}\text{-Cl}^-$  bond. The location of this peak

differs slightly with previously reported literature using microscope systems; however, this may be attributed to a variation in  $\text{Li}^+$  concentration,  $\text{LnCl}_3$  concentration and sample temperature, which are known to cause such slight differences.<sup>[70, 71]</sup> Signal depression caused by the notch filter cuts off the  $\nu_5$  ( $F_{2g}$ ) peak. Theoretically, an octahedral species will have an asymmetric stretching vibration, or  $\nu_2$  ( $E_g$ ), mode; however, this vibration may be too weak for detection.<sup>[71]</sup> Broad peaks located in the shift region greater than  $600\text{ cm}^{-1}$  have been previously reported as sample fluorescence.<sup>[73]</sup> Equations 4-7 and spectral normalization were applied to raw Raman data in order to investigate the isotropic and anisotropic components of the trivalent samarium spectra. Figure 29 shows the reduced isotropic and anisotropic Raman spectra of the  $\text{SmCl}_6^{3-}$  octahedral complex.

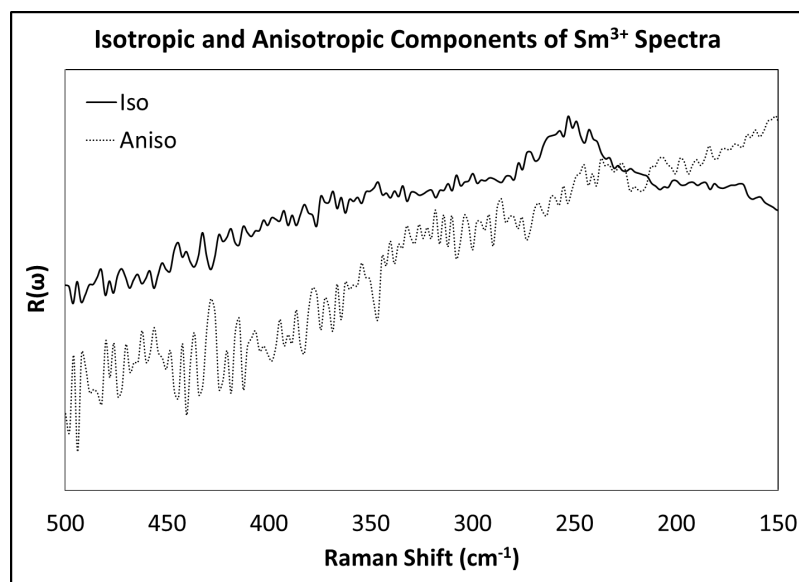


**Figure 29** Reduced Raman spectra of isotropic and anisotropic components associated with trivalent samarium in LiCl-KCl eutectic at  $500\text{ }^\circ\text{C}$ .

The spectra reported in Figure 29 exhibited noise levels that affected the prominence of the expected Raman mode. This noise may be attributed to laser attenuation and

reflection associated with deploying a fiber probe. Nevertheless, the  $\nu_1 (A_{1g})$  was observed in the reduced isotropic Raman spectrum around  $250 \text{ cm}^{-1}$  as expected.<sup>[71]</sup>

### Chemical Reduction

After solvation of  $\text{SmCl}_3$ , the trivalent samarium ions were reduced chemically with addition of samarium metal ( $\text{Sm}^0$ ) powder. Equation 8 details the proposed chemical reaction that occurs in the molten salt upon addition of  $\text{Sm}^0$  metal.



$\text{SmCl}_3$  at 0.01 mol % in LiCl-KCl eutectic was reduced using an equimolar amount of  $\text{Sm}^0$ . Vapors, which may be lithium or sodium, were observed emanating from the melt and are indicative of reducing conditions.<sup>[91]</sup> Figure 30 shows polarized and depolarized Raman spectra obtained 30 minutes after the addition of  $\text{Sm}^0$  powder.

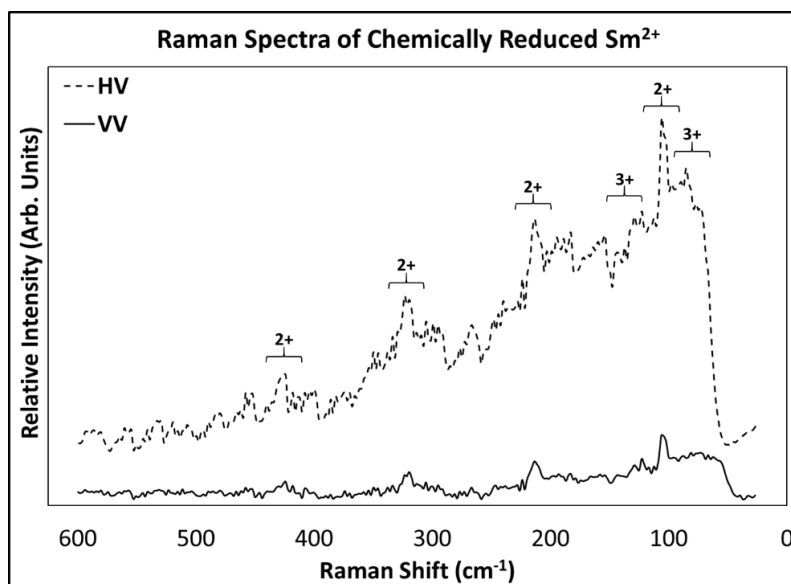


**Figure 30** Polarized (VV) and depolarized (HV) Raman spectra of 0.01 mol %  $\text{SmCl}_3$  in LiCl-KCl eutectic 30 minutes after the addition of an equimolar amount of  $\text{Sm}^0$  at  $500 \text{ }^\circ\text{C}$ .

Polarization of Raman spectra affected neither the location nor the peak intensity ratios attributed to divalent samarium ions. As reported in the literature, the melt transitions

from transparent to a dark orange color upon reduction of trivalent samarium to a divalent state.<sup>[62]</sup> The vibration modes associated with trivalent samarium are slightly visible in Figure 30 and labelled with a 3+ designation, indicating the chemical reduction may not be 100 % efficient. Nevertheless, new vibration modes manifest upon the addition of Sm<sup>0</sup> and are labelled with a 2+ designation, as no clear metal colloidal suspensions were observed. Table 7 summarizes the location of these new vibration modes and compares them to that of the previously published divalent neodymium literature.<sup>[73]</sup>

Vibration Mode	Nd <sup>2+</sup> (Betancourt-Rodriguez <i>et al.</i> )	Sm <sup>2+</sup> (This Study)
v <sub>2</sub>	115 cm <sup>-1</sup>	104 – 121 cm <sup>-1</sup>
v <sub>3</sub>	175 cm <sup>-1</sup>	214 cm <sup>-1</sup>
v <sub>4</sub>	340 cm <sup>-1</sup>	320 cm <sup>-1</sup>
v <sub>5</sub>	450 cm <sup>-1</sup>	425 cm <sup>-1</sup>

**Table 7** Comparison of previously published Nd<sup>2+</sup> vibration modes and Sm<sup>2+</sup> modes reported in this study

It is important to note that the difference in lanthanide species of interest, Li<sup>+</sup> ion concentration and temperature of the melt matrix can all shift the expected vibration modes to some degree.<sup>[70, 71]</sup> Furthermore, the change in melt color associated with samarium reduction created a much less transparent melt. The fiber-based laser beam is distorted and reflected much more as a result of decreased transparency, creating larger amounts of signal noise. It was found to be beneficial to lower focal distance when conducting fiber-based Raman spectroscopy; however, temperature-induced heating of the probe dampens signal greatly and has the potential to damage internal optics.

The chemical nature of divalent lanthanide species and their coordination behavior in LiCl-KCl is not well understood, making the assignment of vibration modes in



terms of stretching, bending and degeneracy difficult. Nevertheless, the octahedral,  $O_h$ , vibration modes are no longer the dominant modes present after chemical reduction, suggesting a change in chemistry. The spectra offer some insight into electron localization and jump rate. Betancourt-Rodriguez *et al.* hypothesize a fast electron jump rate will allow for re-equilibration of trivalent and divalent species through intervalence charge transfer, and a lack of change in the half widths of vibration bands as the reduction progresses may also indicate the complexes forming are re-equilibrating spontaneously.<sup>[73]</sup> Further optimization of the system may allow for half-width monitoring in the future. It is unclear whether the chemical reduction of  $\text{Sm}^{3+}$  to  $\text{Sm}^{2+}$  goes to completion; however, if this re-equilibration is occurring, it may explain the presence of trivalent vibration modes under reducing conditions. It should be noted that samarium reduces to metallic form at a more negative potential than the  $\text{Li}^+$  ions associated with the eutectic.<sup>[47]</sup> Therefore,  $\text{Sm}^0$  will not be thermodynamically stable in the system and most likely will spontaneously reduce  $\text{Li}^+$  or  $\text{Na}^+$  impurities in solution. Figure 31 shows the formation and disappearance of divalent samarium Raman modes over the course of 60 minutes, in 10-minute intervals, after the addition of an equimolar amount of samarium metal. The disappearance of divalent modes suggests the divalent samarium is indeed re-equilibrating into some other ionic form. The exact nature of this re-equilibration is not established; however, some literature suggests the divalent samarium disproportionates into its trivalent state and  $\text{Sm}^0$ .<sup>[60, 62]</sup> However, since we observe the experimental formation of  $\text{Sm}^{2+}$  upon the addition of  $\text{Sm}^0$ , we do not believe that the reverse reaction is spontaneous as suggested in the literature. Since  $\text{Sm}^{2+}$  is unstable and

highly reactive, we hypothesize that it undergoes oxidation to  $\text{Sm}^{3+}$  and reduces ( $\text{Li}^+/\text{Na}^+$ ) that led to the vapors observed in this chemical reduction experiment. The spectra shown in Figure 31 and Figure 32 may support this hypothesis.

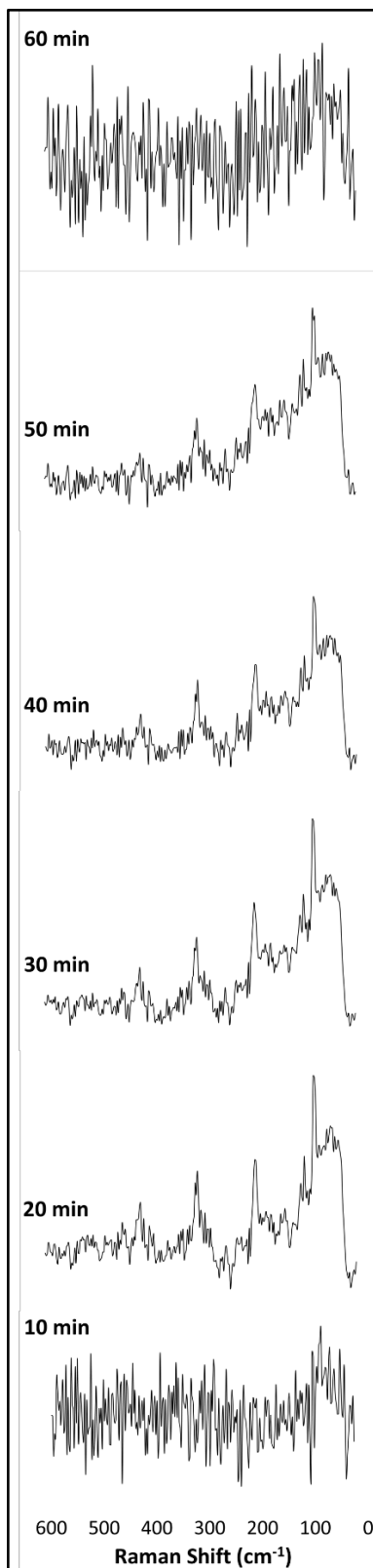


**Figure 31** Raman spectra obtained during the chemical reduction of trivalent samarium by equimolar samarium metal addition for 60 minutes from 0.01 mol % SmCl<sub>3</sub> in LiCl-KCl eutectic salt at 500 °C.

It is noted that although the Raman spectra shown in Figure 31 suggest divalent samarium is no longer present after 60 minutes, the melt does not return to its original transparency. Instead, the melt color remains dark orange in nature and solidifies into a dark brown ingot. This could be due to the presence of some  $\text{Sm}^{2+}$ , but the concentration of which is below that which can be detected by this system. Spectra collected 90 minutes after the addition of samarium metal are shown in Figure 32 and do not contain divalent Raman modes.

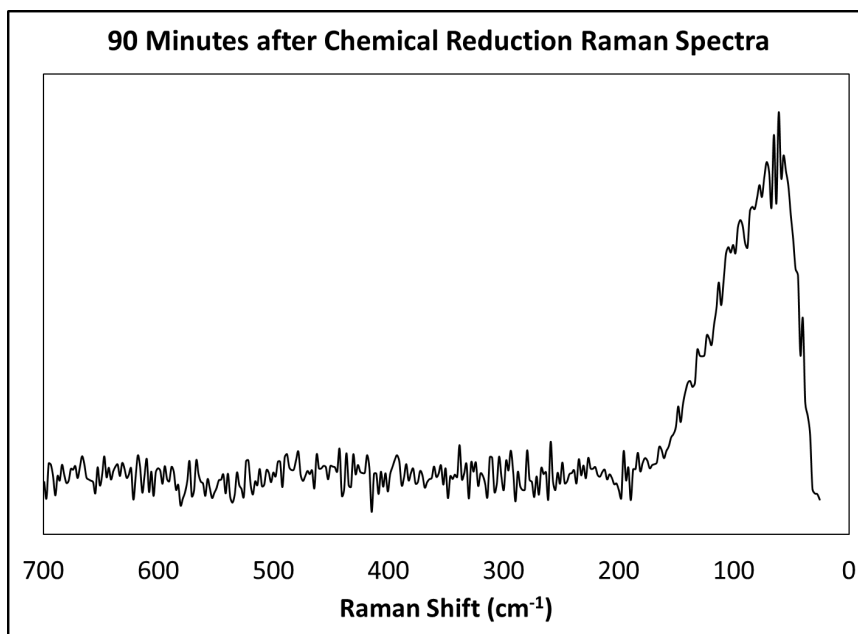


**Figure 32** Raman spectra obtained 90 minutes after the chemical reduction contain no Raman modes associated with divalent samarium.

The spectra shown in Figure 32 are more similar to the initial trivalent spectra shown in Figure 28. This similarity in spectra, along with the melt's maintained dark orange appearance, suggest the divalent samarium ions oxidize while reducing  $\text{Li}^+/\text{Na}^+$  ion to their metallic counterparts. Presence of  $\text{Li}^0$  in the molten salt is known to darken the salt as reported by the literature.<sup>[83, 91]</sup>

### Electrochemical Reduction

Cyclic voltammetry studies indicate the reduction of  $\text{Sm}^{3+}$  occurs around  $-0.70$  V vs. Ag. A reducing potential of  $-1.25$  V vs. Ag was selected to electrochemically produce  $\text{Sm}^{2+}$ . Raman spectra were acquired after the reducing potential was held for 2 hours. The Raman laser was positioned near the working electrode where reduction was occurring in order to selectively detect the formation of divalent samarium ions. Figure 33 provides a CV acquired from a  $0.01$  mol %  $\text{SmCl}_3$  melt at  $500$  °C with a  $250$  mV/s potential sweep rate.

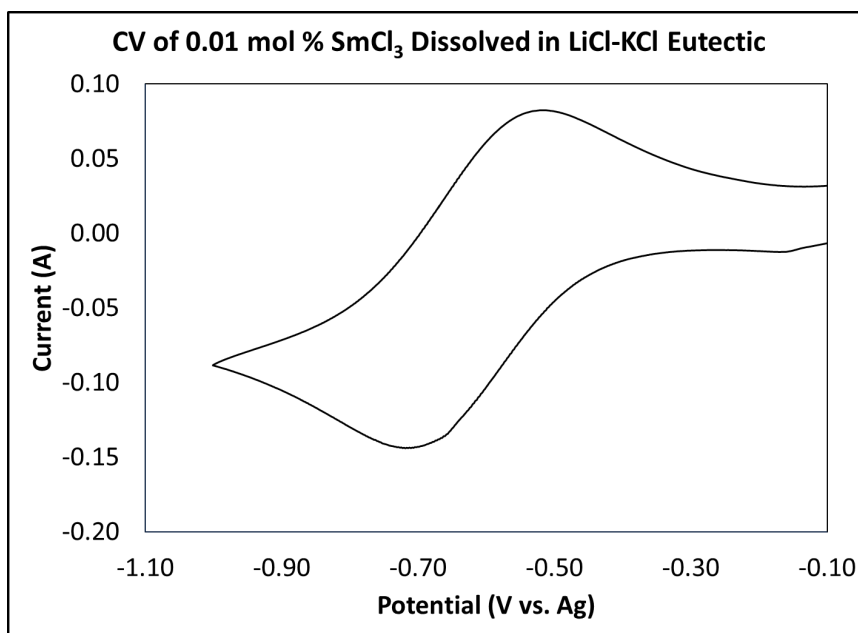


**Figure 33** Cyclic voltammogram of  $0.01$  mol %  $\text{SmCl}_3$  in LiCl-KCl eutectic at  $500$  °C using a  $250$  mV/s potential sweep rate.

The melt color transitions from transparent to a dark orange color as observed during the chemical reduction process; however, divalent samarium vibration modes do not manifest noticeably when compared to the Raman spectra obtained from the chemical reduction experiments. Furthermore, sodium vapors seen during chemical reduction

experiments, which are indicative of reducing conditions, are not visible during the electrochemical reduction process. Sodium is a common impurity in LiCl and KCl salts. It is hypothesized that some samarium is reduced to  $\text{Sm}^{2+}$  during the electrochemical reduction, but the overwhelming samarium content is in its trivalent state both due to an incomplete reduction at the working electrode and the divalent state's propensity to disproportionate back to a trivalent state. Figure 34 provides the Raman spectra acquired after the 2-hour reduction.

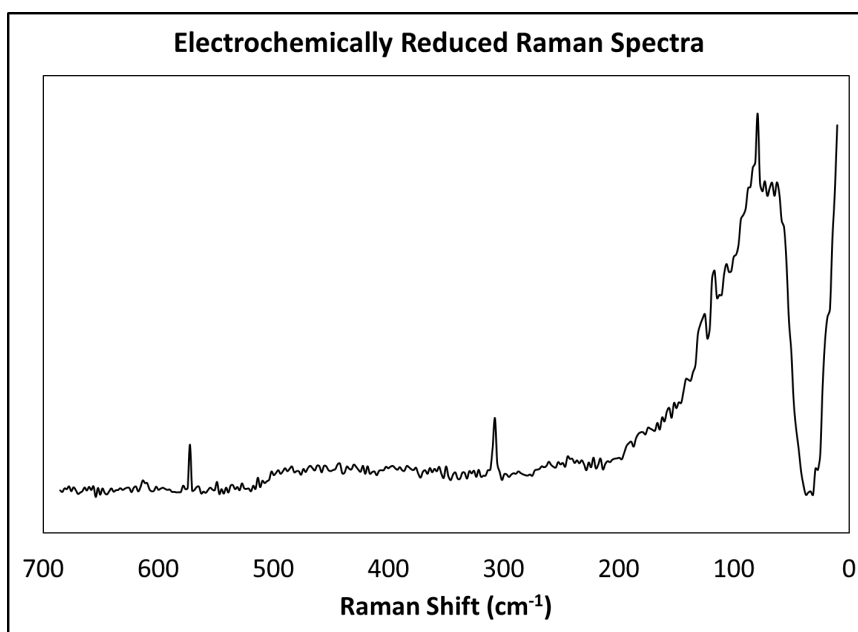


**Figure 34** Raman spectra of electrochemically reduced samarium in LiCl-KCl eutectic at 500 °C from a 5 mol %  $\text{SmCl}_3$  melt

The Raman spectra reported in Figure 34 is indicative of a reduction in trivalent samarium's associated vibration modes; however, the unidentified peaks do not indicate the presence of divalent samarium when compared to the chemical reduction studies or the neodymium literature. Although UV-vis spectroscopy studies clearly suggest a presence of divalent samarium after electrochemical reduction, this is most likely due to

trivalent samarium's inactive nature in terms of UV-vis spectroscopy.<sup>[62]</sup> Table 8 summarizes the location of the electrochemically reduced vibration modes in comparison with the neodymium literature and chemical reduction spectra from this study.

Vibration Mode	Nd <sup>2+</sup> (Betancourt-Rodriguez <i>et al.</i> )	Chemical Reduction	Electrochemical Reduction
$\nu_2$	115 cm <sup>-1</sup>	104 – 121 cm <sup>-1</sup>	80 cm <sup>-1</sup>
$\nu_3$	175 cm <sup>-1</sup>	214 cm <sup>-1</sup>	115 – 125 cm <sup>-1</sup>
$\nu_4$	340 cm <sup>-1</sup>	320 cm <sup>-1</sup>	308 cm <sup>-1</sup>
$\nu_5$	450 cm <sup>-1</sup>	425 cm <sup>-1</sup>	572 cm <sup>-1</sup>

**Table 8** Comparison of neodymium vibration modes from the literature, chemically reduced divalent samarium modes and electrochemically reduced divalent samarium modes

It is unclear whether the peaks detected during electrochemical reduction of samarium are indeed divalent vibration modes or an indication of some other phenomenon. Lower concentration electrochemical reductions did not produce discernable Raman spectra, further indicating an inefficient reduction process.

#### 4.4 Conclusions

A fiber-based Raman spectroscopy system for high temperature molten salt was employed for the study of samarium ion chemistry in molten LiCl-KCl eutectic. The trivalent complex symmetry and spectra were indicative of octahedral SmCl<sub>6</sub><sup>3-</sup> complexes. Chemical reduction experiments produced spectra similar to those reported for divalent neodymium in the literature. To our knowledge, this is the first Raman spectrum of divalent samarium in molten LiCl-KCl eutectic. The divalent vibration modes disappeared one hour after their initial manifestation, suggesting divalent samarium undergoes oxidation to Sm<sup>3+</sup> and reduces Li<sup>+</sup>/Na<sup>+</sup> ions. Electrochemical reduction experiments produced Raman spectra dissimilar to the chemically reduced spectra. This discrepancy is

likely due to the slow nature of electrochemical reduction compared to instantaneous chemical reduction.



## Chapter 5 Cyclic Voltammetry of Samarium Ions in the Molten LiCl-KCl Eutectic for Diffusion Coefficient Analysis

### 5.1 Introduction

Molten salt media have been developed for a variety of electrochemical processing schemes including used nuclear fuel (UNF) reprocessing, plutonium refining, rare-earth metal recycling, and the electrolysis of lithium, magnesium, and titanium [27, 46, 92, 93]. The pyrochemical reprocessing scheme relies on the molten LiCl-KCl eutectic electrolyte to electrochemically separate uranium, plutonium, and other transuranic (TRU) elements from UNF [29, 54]. After being anodically solvated into the molten eutectic, uranium is consolidated on a solid stainless steel cathode, while plutonium and TRU elements are co-deposited on a liquid cadmium cathode [27]. The pyrochemical reprocessing scheme is an alternative to the traditional plutonium uranium redox extraction (PUREX) method and offers some valuable advantages. A pyrochemical facility would be more compact in terms of space requirements and produce an impure and more proliferation-resistant plutonium product [42]. The pyrochemical process is also compatible with the fast reactor fuel cycle, utilizes simple waste processing operations, and exhibits lower criticality risks than the PUREX method [29]. Several nations are pursuing pyrochemical reprocessing development including France, India, Japan, Russia, South Korea, and the United States [94, 95]. Figure 35 provides a proposed flowsheet for

a commercial pyrochemical reprocessing installation outfitted to reprocess existing light water reactor (LWR) fuel stockpiles and fast reactor fuel [37].

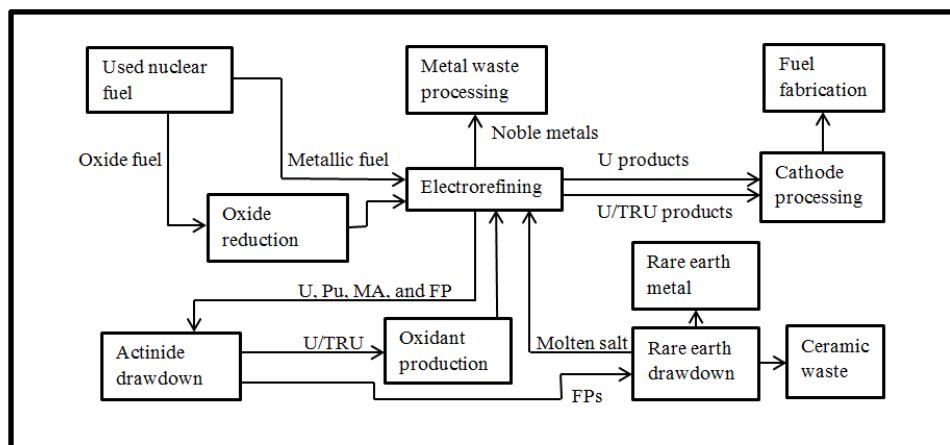


**Figure 35** Proposed processing flowsheet for a commercial pyrochemical reprocessing installation equipped to reprocess LWR oxide and fast reactor metallic fuel [37].

Figure 35 illustrates the disconnected nature of unit operations associated with the pyrochemical process. Product and waste materials exiting each unit operation are handled as separate packages and transferred between unit operations in such a manner that could pose nuclear material holdup and accountancy problems [94]. Furthermore, the electrorefining operation is subject to constantly shifting actinide and lanthanide concentrations that require real-time and nondestructive monitoring to ensure optimized process control and accurate safeguards measurements [42].

Since there is no commercial pyrochemical reprocessing facility in a non-weapons nation state subject to the International Atomic Energy Agency's (IAEA) safeguards agreement, there is a need for the development of real-time and nondestructive nuclear material accountancy (NMA) approaches before any such facility can be constructed [96]. Although Idaho National Laboratory (INL) currently operates an electrorefiner for the consolidation of breeder reactor fuel, NMA methods are heavily reliant on destructive

analyses which are both time consuming and offer no real-time data for process optimization or control [54]. Traditional safeguarding approaches using radiation detection and spectroscopic methods fall short in efficacy due to the high-temperature and extreme nature of the molten salt environment [16]. Electroanalytical methods are ideal for NMA in these systems as they are resistant to high radiation fields, compatible with remote handling and inert gas environments, and make available valuable information regarding electrochemical or kinetic behavior of dissolved analytes that can be used to optimize the unit operations [37, 42, 94].

Cyclic voltammetry (CV) is one electroanalytical technique that has been employed in the molten LiCl-KCl eutectic to investigate the electrochemical, diffusion, and kinetic behavior of solvated actinide and lanthanide chlorides [38, 44-49, 52, 61]. Actinide chloride data is more abundant, as actinides pose greater proliferation risk and are the main analytes of interest in the electrorefiner. The effects of concentration on electroanalytical measurements are a focus of current studies and the high concentration regime (> 3 wt. %) is generally less understood [42, 46, 52, 97]. Low concentration lanthanide data is available and preliminary studies of  $\text{NdCl}_3$  have explored concentrations up to 9 wt. % [26, 98]. Samarium electroanalytical data is primarily available for the low concentration regime [47, 49, 59, 61]. Understanding lanthanide electrochemical behavior is vital, as these species have negative neutronic effects on nuclear fuel and must therefore be effectively monitored and removed throughout the pyrochemical reprocessing scheme.

In this work, the effect of high concentration  $\text{SmCl}_3$  solvated in the molten  $\text{LiCl-KCl}$  eutectic at 773 K was investigated using CV. A method developed for actinide systems was adjusted and employed to produce repeatable current response and determine the working electrode (WE) surface area. The electrochemical reversibility characteristics were investigated through scan rate correlation and peak current ratio analysis across a high concentration range [38, 52]. The concentration regime of interest was approximately 5 to 17 wt. %  $\text{SmCl}_3$ . Based on the results, diffusion coefficients were calculated across the concentration range and compared with the literature. Additionally, cylindrical and migration diffusion effects were investigated. By conducting these analyses at high concentrations of  $\text{SmCl}_3$ , this work will help elucidate the implications of conducting CV in high concentration process conditions and develop a path forward to further mitigating uncertainties associated with this concentration region.

## 5.2 Experimental

### Chemicals and Materials

The eutectic salt was prepared by baking the individual eutectic components,  $\text{LiCl}$  (Alfa Aesar 99.9 % pure) and  $\text{KCl}$  (Alfa Aesar 99.9 % pure), for extended periods of time to ensure moisture impurities were minimized. The eutectic salt components were each baked under vacuum for over 72 hours as Fourier-transform infrared spectroscopy (FTIR) analysis suggested the presence of moisture in the salt up until the 72-hour time point. Figure 36 shows the FTIR spectra obtained from as received, 24-hour baked, and 72-hour baked salts. The spectral features associated with moisture contamination are mitigated

only after 72 hours of baking; however, residual moisture impurities are assumed to still be present and result in some oxychloride or oxide formation during experiments [49]. Once baked, the eutectic components were then mixed at a 59:41 (LiCl:KCl) mole ratio.

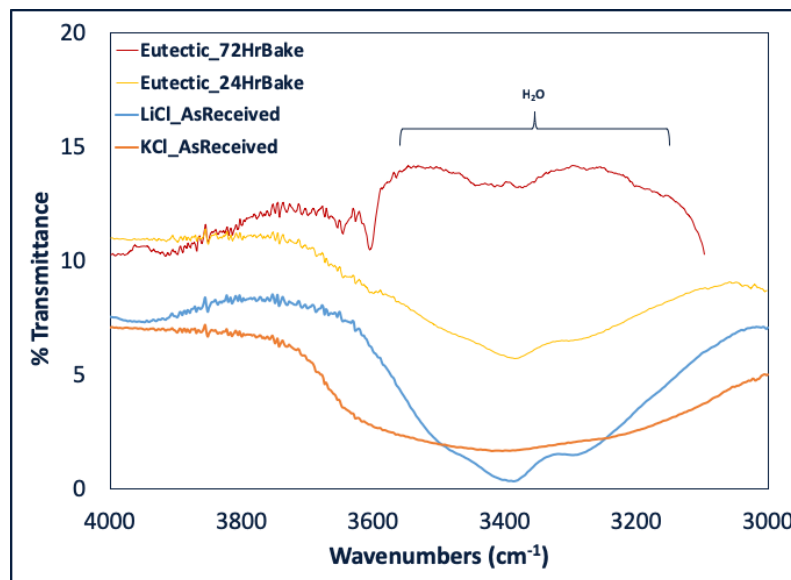


**Figure 36** FTIR spectra of eutectic salt components as received, 24-hour baked, and 72-hour baked.

$\text{SmCl}_3$  (Alfa Aesar 99.99 % pure) was solvated in the molten LiCl-KCl eutectic at various concentrations and agitated using an alumina rod (McMaster-Carr, 1/16" diameter) before the electrodes were immersed in the molten salt solutions. Tungsten rods were employed as the working electrode (WE, ESPI metals 99.95 % pure, 1/16" diameter) and counter electrode (CE, ESPI metals 99.95 % pure, 1/8" diameter). A highly-stable Ag|AgCl reference electrode (RE) consisted of silver wire (ESPI metals 99.95 % pure, 1/16" diameter) immersed in 5 mol % AgCl (Alfa Aesar 99.99 % pure) LiCl-KCl solution. The reference electrode was encased in a Pyrex tube with a thinned bottom wall to provide ionic contact with the sample melts. This reference design was obtained from Tylka *et al.* [38, 52]. The working electrode (WE), counter electrode (CE), and reference electrode

(RE) were gently polished with SiC pads and rinsed with anhydrous methanol (99.9 % pure Alfa Aesar) between experiments to prevent cross contamination of samples. All molten salt solutions were contained inside alumina crucibles (GraphiteStore) that were fired at 1273 K, along with the alumina agitation rods, to remove any contaminants and organic binders.

### Experimental Apparatus

All experiments were conducted in an argon atmosphere glovebox with moisture and oxygen levels maintained below 1 ppm. Chemicals and materials were stored in this atmosphere to mitigate the formation of moisture and oxygen induced impurities. AgCl was stored in a dark bottle to prevent light-induced chemical degradation. A Gamry REF3000AE potentiostat was employed for electroanalytical measurements. The potentiostat cabling was fed directly into the glove box to prevent any extension wire induced resistance. The molten salt samples contained in alumina crucibles were placed inside a stainless-steel Faraday cage to prevent electrical frequency noise created by the furnace from affecting electroanalytical measurements. The alumina crucible and Faraday cage were placed inside a Watlow ceramic tube furnace with  $\pm 1$  K temperature control. The electrodes were mounted onto a micron-resolution translation stage for accurate and repeatable positioning in the molten salt melt. The electrodes were aligned in a perpendicular fashion with respect to the melt using alumina tubing, stainless-steel alignment plates, and alignment holes drilled into the ceramic furnace cap. The electrode translation stage and furnace were remotely operated using National Instruments

LabVIEW software. Figure 37 illustrates the experimental setup employed for the electroanalytical investigations.

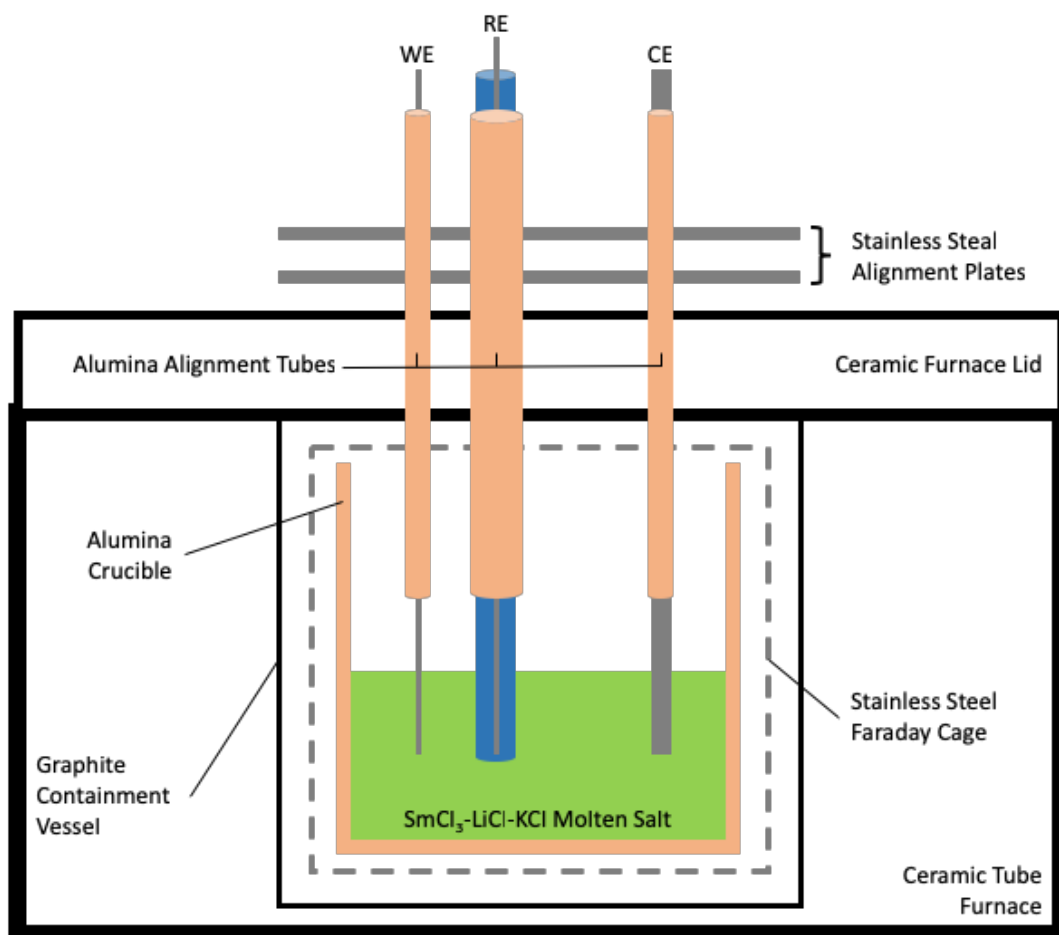


Figure 37 Illustration of experimental setup.

### Electroanalytical Measurement Methodology

After temperature calibration, component bakes, melting of the components, and agitation of the molten salt solutions, the electrodes were immersed and allowed to equilibrate for an extended period of time. Specifically, enough time must be allotted for the melting of the RE solution and establishment of ionic contact with the melt. Open circuit potential (OCP) measurements were taken for up to 7 hours to confirm the

establishment of this ionic contact. After the RE was equilibrated, the WE was anodically polarized and left to establish a clean surface, free of any passivating films [46]. In order to obtain repeatable CV curves and current response, an electroanalytical sequence previously published by Tylka *et al.* for  $\text{UCl}_3$  studies was adjusted and applied to the  $\text{SmCl}_3$  system [38, 52]. This adjusted sequence can be found in Table 9.

Sequence Step	Description	Duration (seconds)
1	CV acquisition	1 – 5
2	Hold at Open Circuit Potential (OCP)	15-30
3	Hold at oxidative potential to ensure all reduced species return to original valence state and the WE surface is restored	45 – 60
4	Hold at OCP	30-60

**Table 9** Electroanalytical sequence obtained from Tylka *et al.* and adjusted for  $\text{SmCl}_3$  analysis

The Randles-Sevcik relationship for soluble-soluble electrochemical couples was used to analyze the CV data in terms of electrochemical reversibility and calculating the diffusion coefficients. Equation 9 reports the Randles-Sevcik relationship used for CV analysis [39].

$$i_p = 0.4463 \cdot n \cdot F \cdot A \cdot C_i \cdot \left(\frac{n \cdot F}{R \cdot T}\right)^{1/2} \cdot \nu^{1/2} \cdot D^{1/2} \quad (9)$$

Here,  $i_p$  is the peak current response in A,  $n$  is the number of electrons being transferred in the electrochemical couple of interest,  $F$  is the Faraday constant in  $\text{C mol}^{-1}$ ,  $A$  is the WE surface area in  $\text{cm}^2$ ,  $C_i$  is analyte concentration in  $\text{mol cm}^{-3}$ ,  $R$  is the ideal gas constant in  $\text{J mol}^{-1} \text{K}^{-1}$ ,  $\nu$  is the potential scan rate in  $\text{V s}^{-1}$ , and  $D$  is the analyte diffusion coefficient in  $\text{cm}^2/\text{s}$ . The concentration of dissolved analyte was measured through inductively coupled plasma optical emission spectroscopy (ICP-OES) analysis of molten salt samples complexed with deprotonated ethylenediaminetetraacetic acid (EDTA) solution. The peak



cathodic current was analyzed for use in diffusion coefficient determination as it is associated with the diffusion of dissolved  $\text{Sm}^{3+}$  species. A broad range of scan rate values were analyzed with respect to peak current to establish an electrochemically reversible region for diffusion coefficient analysis. Furthermore, cathodic to anodic peak current ratio analysis helped narrow the scan rate region of interest. The WE surface area was determined using an adjusted differential method previously reported in the literature [38, 52]. Instead of calculating differential current response, the WE was stepped out of the molten salt solution at regular intervals (giving regular steps in surface area) using the high resolution translation stage. The anodic and cathodic peak current responses were then linearly analyzed with respect to immersion and used to back-calculate a WE surface area and associated uncertainty.

### 5.3 Results and Discussion

#### Electrochemical Characteristics of $\text{SmCl}_3$

The CV curves displayed in Figure 38 were obtained from 1) a melt containing only the molten LiCl-KCl eutectic and 2) another melt with  $\text{SmCl}_3$  solvated in the molten LiCl-KCl eutectic at a concentration of  $6.69 \cdot 10^{-4} \text{ mol cm}^{-3}$ . The observed standard reduction potential of the  $\text{Sm}^{3+}/\text{Sm}^{2+}$  electrochemical reaction (give the potential) is consistent with the literature [47, 49, 61].

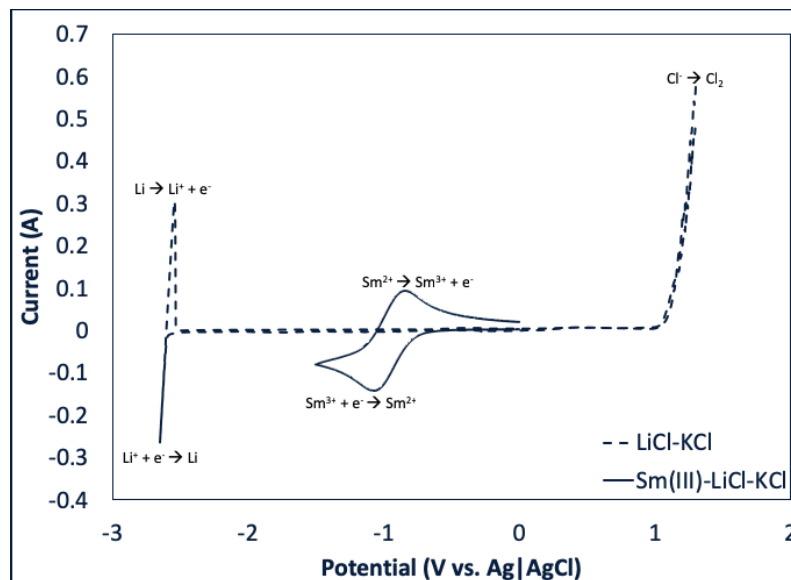


**Figure 38** Cyclic voltammograms from a molten LiCl-KCl (eutectic) and  $\text{SmCl}_3(6.69 \cdot 10^{-4} \text{ mol cm}^{-3})$ -LiCl-KCl(eutectic) sample at 773 K and  $250 \text{ mV s}^{-1}$ .

These literature studies have attributed the cathodic and anodic peaks near  $-0.90 \text{ V}$  vs. Ag|AgCl to the reduction of  $\text{Sm}^{3+}$  to  $\text{Sm}^{2+}$  and the oxidation of  $\text{Sm}^{2+}$  to  $\text{Sm}^{3+}$ , respectively. The relatively symmetric nature of the samarium features is a consequence of the  $\text{Sm}^{3+}/\text{Sm}^{2+}$  electrochemical couple being a soluble-soluble valence state transition and its electrochemical reversibility. The sharp features at the limits of the electrochemical window are attributed to the breakdown of the LiCl-KCl eutectic. The cathodic and anodic features near  $-2.65 \text{ V}$  vs. Ag|AgCl are attributed to the reduction of  $\text{Li}^+$  to metallic Li and the oxidation of metallic Li to  $\text{Li}^+$ , respectively. The feature observed at approximately  $1.05 \text{ V}$  vs. Ag|AgCl is the oxidation of  $\text{Cl}^-$  and resulting evolution of chloride gas. These features (characterized to be the breakdown of the molten LiCl-KCl eutectic) are also in agreement with the literature [26].

#### Repeatability, Immersion, and ICP-OES Results

The repeatability of CV curves and associated current response measurements was established using the electroanalytical sequence detailed in Table 9. Five repeat CV scans from a melt at  $250 \text{ mV s}^{-1}$  and  $773 \text{ K}$  containing  $5.65 \cdot 10^{-4} \text{ mol cm}^{-3} \text{ SmCl}_3$  are overlaid in Figure 39.

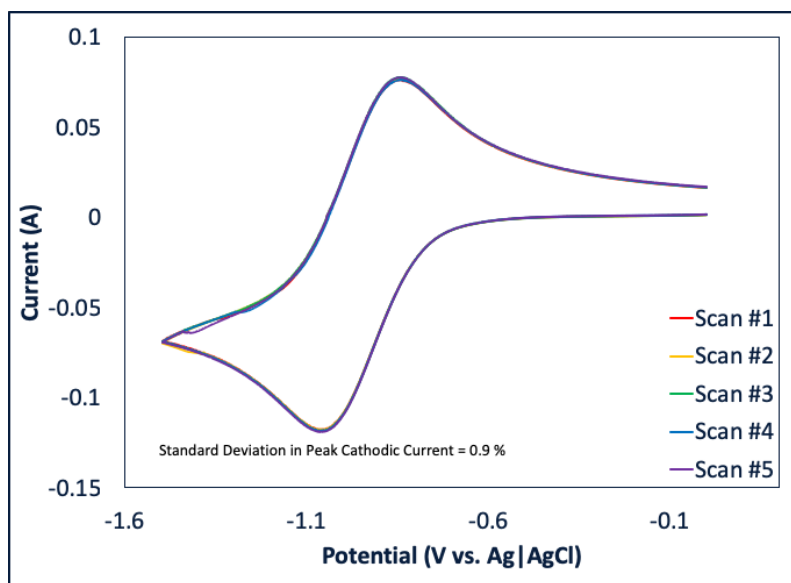


**Figure 39** Five overlaid CV scans from a  $\text{SmCl}_3(5.65 \cdot 10^{-4} \text{ mol cm}^{-3})\text{-LiCl-KCl}$ (eutectic) melt at  $250 \text{ mV s}^{-1}$  and  $773 \text{ K}$  with calculated peak cathodic current standard deviation (WE area =  $0.840 \text{ cm}^2$ ).

Using the proposed electroanalytical CV acquisition sequence, the standard deviation of current response across all scan rates and concentrations tested was generally under 1 %. CV curves acquired using the immersion step method from a melt containing  $5.65 \cdot 10^{-4} \text{ mol cm}^{-3} \text{ SmCl}_3$  at  $773 \text{ K}$  and  $250 \text{ mV s}^{-1}$  are overlaid in Figure 40.

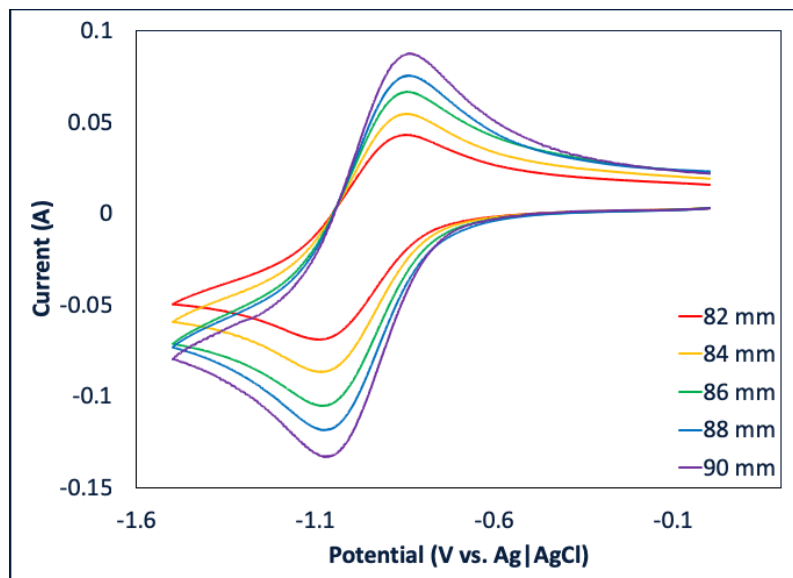


**Figure 40** Overlaid CV scans from a  $\text{SmCl}_3(5.65 \cdot 10^{-4} \text{ mol cm}^{-3})$ -LiCl-KCl(eutectic) melt at  $250 \text{ mV s}^{-1}$  and  $773 \text{ K}$  acquired using the immersion step method.

The shape of the CV curves displayed in Figure 40 remains consistent across the different immersion depths, and the curves appear to space consistently as the WE is stepped out of the melt in 2 mm increments. Figure 41 illustrates this linear spacing of the CV curves with respect to peak cathodic and anodic current responses plotted as a function of WE electrode immersion depth.

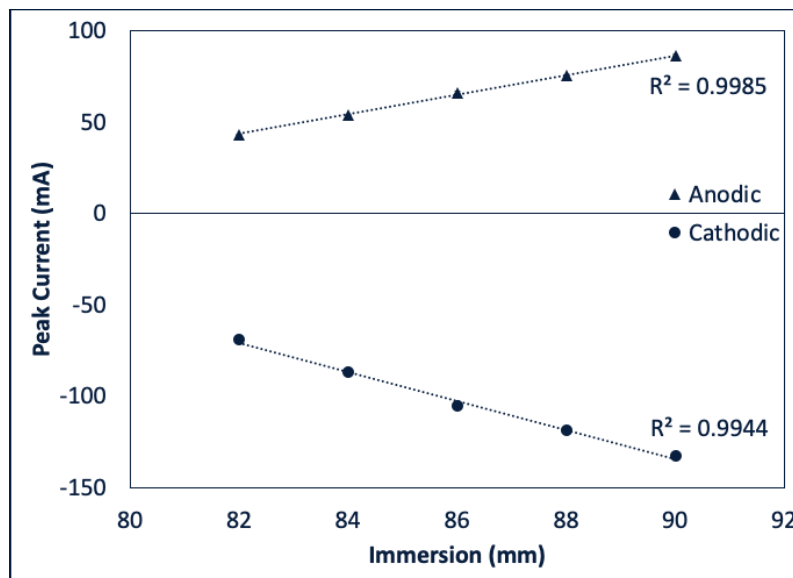


**Figure 41** Peak cathodic and anodic current response plotted as a function of WE immersion from a  $\text{SmCl}_3(5.65 \cdot 10^{-4} \text{ mol cm}^{-3})$ -LiCl-KCl(eutectic) melt at  $250 \text{ mV s}^{-1}$  and  $773 \text{ K}$ .

The immersion step method for determining WE surface area produced and linear current response data that could then be used to back calculate a surface area value and associated range of error. Both the anodic and cathodic peak current correlations were used to back calculate this surface area value. Table 10 summarizes the molten salt samples analyzed in this work, their measured concentrations using ICP-OES, and the WE surface area values determined for each sample using the immersion step method.

Sample Number	Concentration of SmCl <sub>3</sub> Wt. %	Concentration of SmCl <sub>3</sub> (mol/cm <sup>3</sup> )	Electrode Area (cm <sup>2</sup> )
1	4.66	$3.08 \cdot 10^{-4}$	$0.636 \pm 0.025$
2	6.30	$4.21 \cdot 10^{-4}$	$0.858 \pm 0.049$
3	8.39	$5.65 \cdot 10^{-4}$	$0.840 \pm 0.032$
4	9.73	$6.69 \cdot 10^{-4}$	$0.782 \pm 0.001$
5	11.9	$8.19 \cdot 10^{-4}$	$0.865 \pm 0.039$
6	13.5	$9.45 \cdot 10^{-4}$	$0.760 \pm 0.018$
7	16.3	$11.5 \cdot 10^{-4}$	$0.691 \pm 0.039$

**Table 10** Summary of the molten SmCl<sub>3</sub>-LiCl-KCl samples analyzed in this work, their respective SmCl<sub>3</sub> concentrations measured using ICP-OES, and WE surface area values determined using the immersion step method.

The peak current responses with respect to scan rate and immersion measurements were very repeatable; however, accounting for anodic and cathodic current response in immersion tests creates a level of uncertainty associated with the measurement of WE surface area that will consequentially affect peak current density versus concentration correlations and diffusion coefficient calculations. This uncertainty is likely the result of molten salt surface tension effects which have been previously reported to produce similar error in the literature [38, 46, 52].

#### Scan Rate Results

A broad range of scan rates were tested and analyzed with respect to peak current response and peak current ratio. The results of these two analyses helped establish an electrochemically reversible scan rate range that also produced the most repeatable CV curves. A broad range of 25 to 500 mV s<sup>-1</sup> scan rate values were tested for all samples. CV curves obtained from a melt solvated with  $6.69 \cdot 10^{-4}$  mol cm<sup>-3</sup> SmCl<sub>3</sub> at 773 K across the broad scan rate range are overlaid in Figure 42.

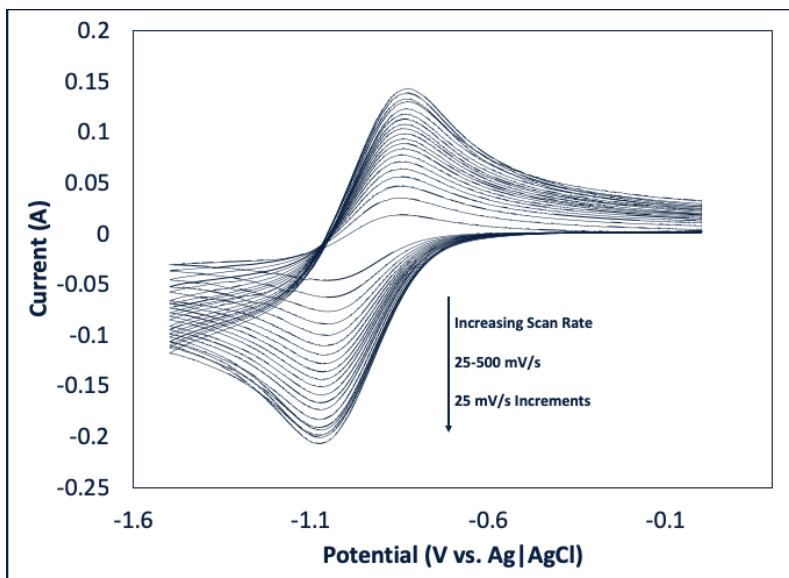


**Figure 42** Overlaid CV scans from a  $\text{SmCl}_3$  ( $6.69 \cdot 10^{-4} \text{ mol cm}^{-3}$ )-LiCl-KCl(eutectic) melt at 773 K acquired across the broad range of scan rates (WE surface area =  $0.782 \text{ cm}^2$ ).

The magnitude of peak cathodic and anodic current response is observed to increase as a function of increasing scan rate in Figure 42, consistent with the Randles-Sevcik relationship for soluble-soluble electrochemical couples. The CV curves also exhibit a small level of peak broadening across the scan rate range. This broadening can be attributed to a variety of phenomena such as increased resistance between the WE and CE, diffusion layer growth on the WE, or an increased effect of charge transfer kinetics on the reactions occurring at the WE surface [46, 97]. It is difficult to attribute the observed broadening to just one phenomenon as they are interrelated. Diffusion layer growth or surface effects on the WE can affect the uncompensated resistance. Charge transfer kinetics corrections are dependent on uncompensated solution resistance and the activity of the dissolved analyte. Fick's second law assumes the analyte activity is equivalent to its concentration; however, this assumption may lose applicability at higher concentrations [46, 96].

Both the anodic and cathodic peak current responses exhibit relative linearity with respect to the square root of the potential scan rate, as dictated by the Randles-Sevcik relationship. Figure 43 displays the peak current versus square root of scan rate correlation for both anodic and cathodic peak current values from a  $6.69 \cdot 10^{-4} \text{ mol cm}^{-3}$   $\text{SmCl}_3$  melt at 773 K.

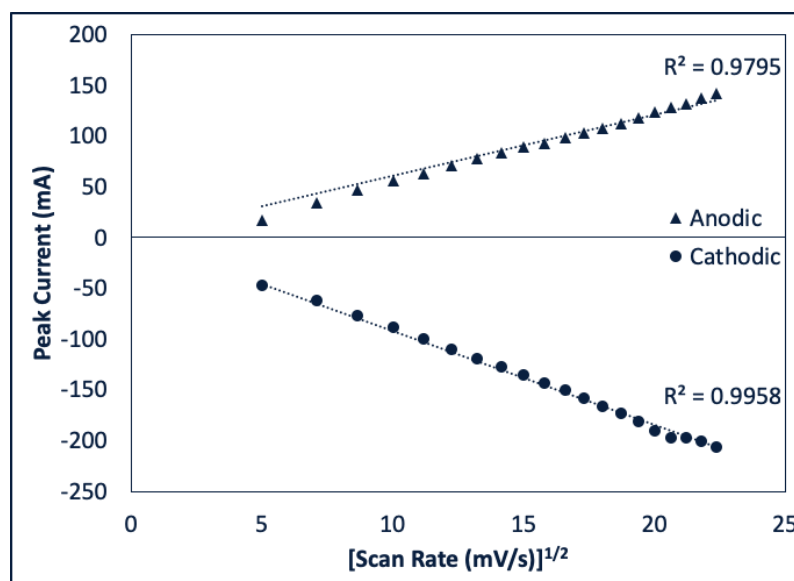


**Figure 43** Peak cathodic and anodic current response plotted as a function of the square root of scan rate from a  $\text{SmCl}_3(5.65 \cdot 10^{-4} \text{ mol cm}^{-3})\text{-LiCl-KCl(eutectic)}$  melt at and 773 K (WE surface area =  $0.782 \text{ cm}^2$ ).

The cathodic peak current response exhibits a more linear response to the square root of scan rate, as indicated by the 0.9958  $R^2$  value (versus 0.9795 for anodic) in Figure 43. This difference in linearity, along with the plotted peak current ratios as a function of scan rate in Figure 43, suggests the system is not fully reversible but rather quasi-reversible [42]. This quasi-reversibility further validates the need for the oxidative step in the electroanalytical sequence reported in Table 9, as all of the reduced species are most likely not being oxidized back to their original valence states.



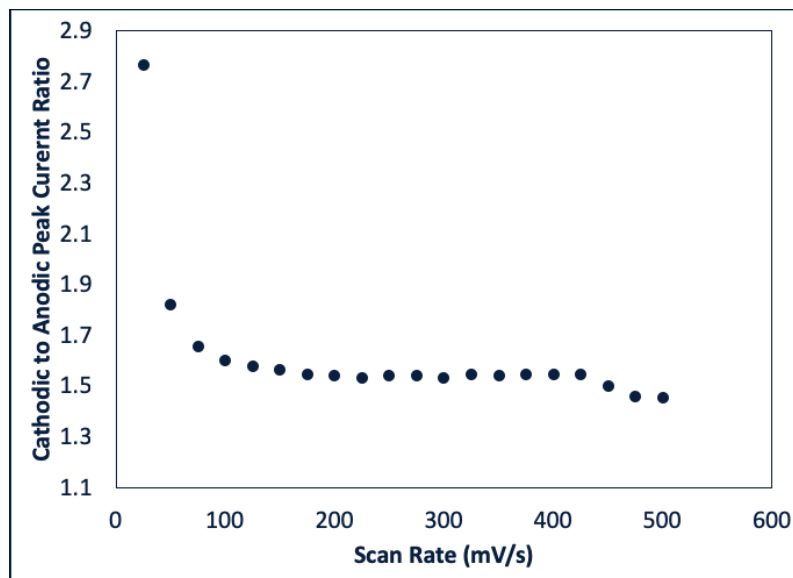


**Figure 44** Peak cathodic and anodic current response ratio plotted as a function of scan rate from a  $\text{SmCl}_3(5.65 \cdot 10^{-4} \text{ mol cm}^{-3})$ -LiCl-KCl(eutectic) melt at and 773 K (WE surface area =  $0.782 \text{ cm}^2$ ).

The peak current ratio (cathodic to anodic) levels off at approximately 1.5 in Figure 44, and this trend was consistent across all analyzed samples. This ratio suggests that approximately 66% of the reduced  $\text{Sm}^{2+}$  is oxidized back to  $\text{Sm}^{3+}$  during the CV's reverse sweep. Generally, low scan rates are used for diffusion coefficient and concentration analysis to ensure reversibility of kinetics; however, faster scan rates minimize surface effects on the WE which may explain the large peak current ratios in the low scan rate region [38, 52, 96, 97]. Furthermore, it can prove difficult in elucidating a clear peak current in the lower scan rate regions as the peaks do not manifest as sharply.

The broad range Randles-Sevick scan rate correlation, peak current ratio analysis, and the effects of charge transfer kinetics were all taken into account when establishing a narrower scan rate region for concentration and diffusion coefficient analysis. The 200 –  $300 \text{ mV s}^{-1}$  was selected for the continuing analyses. This region is consistent with results available in the literature regarding high concentration soluble-insoluble electrochemical

couples [96]. The broad and narrow peak cathodic current density versus square root of scan rate correlation results are displayed in Figure 45.

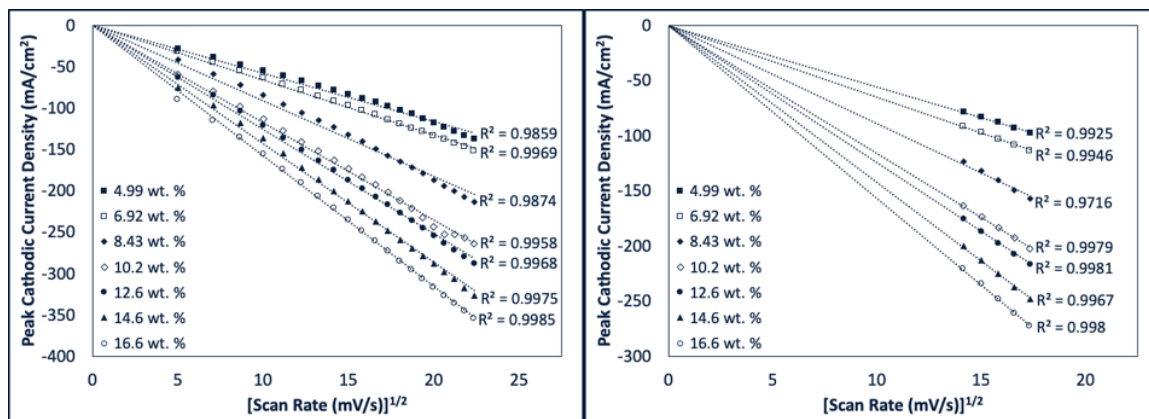


**Figure 45** Peak cathodic current density versus the square root of scan rate correlations for the broad (left) and narrow (right) scan rate regions.

Narrowing the scan rate region slightly increased the level of peak current versus the square root of scan rate linearity for some concentrations, while leaving some relatively unaffected. The system is assumed to be relatively reversible in this narrow region, and this reversibility does not seem to be affected by increasing concentration when considering the R<sup>2</sup> values reported in Figure 45.

#### Concentration and Diffusion Coefficient Results

The peak cathodic current density versus concentration correlation was analyzed for linearity. Figure 46 reports the results of this analysis with and without the highest concentration data point.

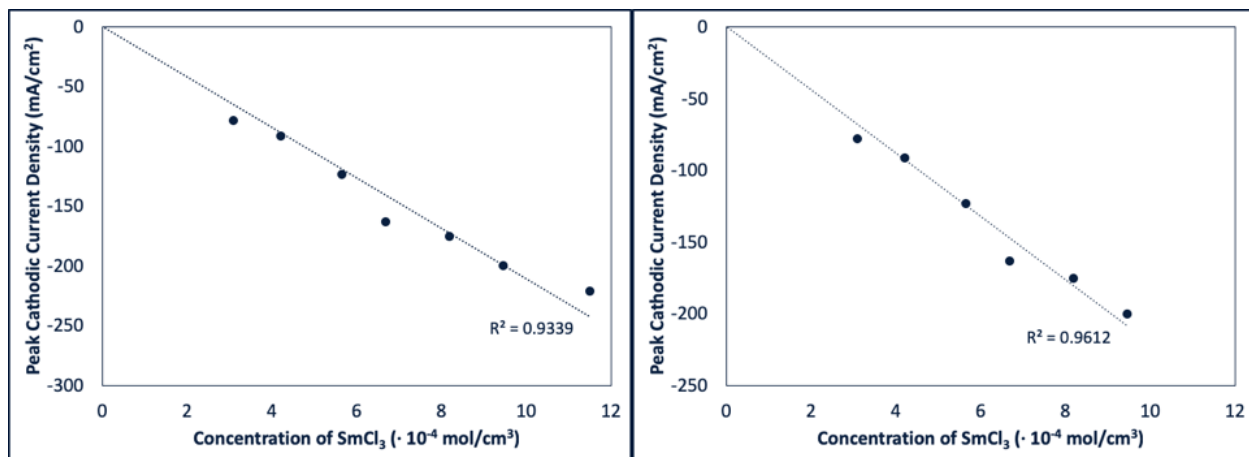


**Figure 46** Peak cathodic current density plotted as a function of SmCl<sub>3</sub> concentration with (left) and without (right) the highest concentration data point.

Both correlation results reported in Figure 46 are less linear than would be expected according to the Randles-Sevcik relationship. Removing the highest concentration data point noticeably increases linearity as illustrated by the R<sup>2</sup> values in Figure 46. WE surface area and peak current error, cylindrical diffusion effects, migration effects, charge transfer kinetics effects, uncompensated resistance, approaching the solubility limit, or concentration dependence of the diffusion coefficient all provide potential explanations for the lower levels of linearity in Figure 46. The error associated with repeat peak current response and WE surface area discussed in the repeatability results were taken into account when reporting the peak cathodic current density as a function of SmCl<sub>3</sub> concentration and Sm<sup>3+</sup> diffusion coefficient results. Diffusion coefficient values were calculated at 200 mV s<sup>-1</sup> as it is the lowest scan rate in the narrowed region of interest. This minimum scan rate was chosen to maximize the reversibility of kinetics [38, 52, 97]. The diffusion coefficient results and their associated error values are reported in Table 11 and were found to be in agreement with the available samarium literature [47, 49, 59].

Sample Number	Concentration of SmCl <sub>3</sub> Wt. %	Concentration of SmCl <sub>3</sub> ( $\cdot 10^{-4}$ mol/cm <sup>3</sup> )	Diffusion Coefficient of SmCl <sub>3</sub> ( $\cdot 10^{-5}$ cm <sup>2</sup> /s)
Cordoba et al. [20]	0.77 – 2.02	0.49 – 1.3	0.98 – 1.30
Castrillejo et al. [18]	1.54 – 1.87	0.99 – 1.2	0.77 – 1.44
Yamada et al. [24]	0.24	0.15	1.80
1	4.66	3.08	1.16 ± 0.14
2	6.30	4.21	0.859 ± 0.14
3	8.39	5.65	0.860 ± 0.10
4	9.73	6.69	1.07 ± 0.01
5	11.9	8.19	0.830 ± 0.12
6	13.5	9.45	0.806 ± 0.07
7	16.3	11.5	0.672 ± 0.12

**Table 11** Diffusion coefficient results and associated error values from this study compared with the available literature.

A visual representation of diffusion coefficient values as a function of SmCl<sub>3</sub> concentration and their associated errors is displayed in Figure 47.

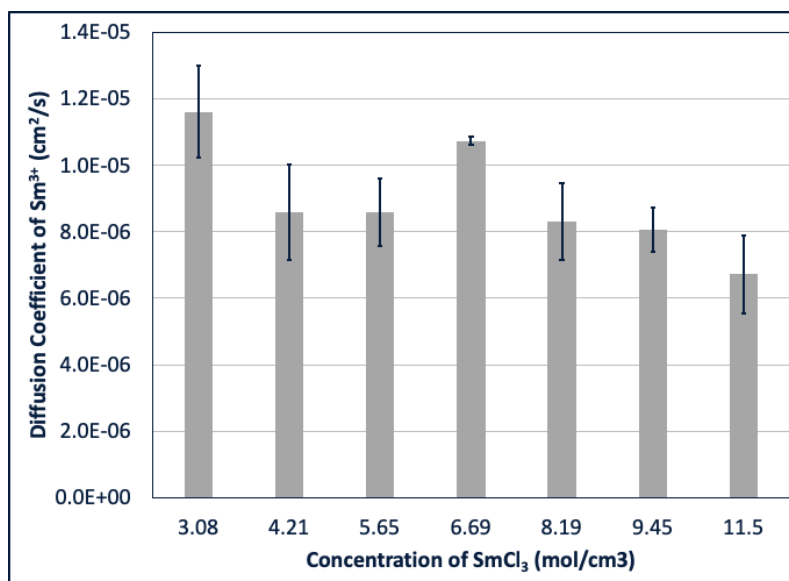


**Figure 47** Diffusion coefficient of Sm<sup>3+</sup> values and their respective errors versus SmCl<sub>3</sub> concentration.

The error in the diffusion coefficient values make it difficult to determine any dependence of the diffusion coefficient on SmCl<sub>3</sub> with certainty, but it remains feasible that the coefficient decreases with increasing analyte concentration.

Cylindrical diffusion's contribution is assumed to be less than 5% if the relationship detailed in Equation 10 holds true [42, 46, 96].

$$\frac{4D\tau}{d^2} \leq 3 \cdot 10^{-3} \text{ where } \tau = \frac{RT}{nFv} \quad (10)$$

Here  $d$  is the WE diameter in cm. An average cylindrical diffusion factor of  $4.8 \cdot 10^{-4}$  was calculated for the  $200 \text{ mV s}^{-1}$  data, indicating the effects of cylindrical diffusion are minimal but not necessarily negligible. The contribution of  $\text{Sm}^{3+}$  migration was calculated using the relationship detailed in Equation 11 and is reported for all analyzed samples in Table 12 [46].

$$t_i = \frac{|z_i|\mu_i C_i}{\sum_k |z_k|\mu_k C_k} \text{ where } \mu = \frac{zFD}{RT} \quad (11)$$

Here,  $t$  is the transference number fraction of the ion of interest,  $z$  is the species' ionic charge, and  $\mu$  is the species' mobility value.

Sample Number	Concentration of $\text{SmCl}_3$ Wt. %	Concentration of $\text{SmCl}_3$ ( $\cdot 10^{-4} \text{ mol/cm}^3$ )	$\text{Sm}^{3+}$ Transference Number (%)
1	4.66	3.08	2.34
2	6.30	4.21	2.37
3	8.39	5.65	3.16
4	9.73	6.69	4.60
5	11.9	8.19	4.36
6	13.5	9.45	4.87
7	16.3	11.5	4.94

**Table 12** Migration contribution results with respect to  $\text{Sm}^{3+}$  transference for all sample concentrations.

The migration contribution approaches 5% at the highest concentrations analyzed in this study, suggesting that the contribution is non-negligible [46]. Migration effects increase with decreasing supporting electrolyte and increasing applied potential. Molten salts such as LiCl-KCl serve as both the solvent and supporting electrolyte, meaning that migration

will play an increasing role as a direct function of increasing analyte concentration. However, it is not clear whether the dissolved lanthanide species migrate in their trivalent states. Spectroscopic studies have suggested lanthanides form  $[\text{LnCl}_6]^{-3}$  complexes when solvated in the molten LiCl-KCl eutectic [71]. The migration effect is heavily dependent the behavior of these solvated complexes and requires further investigation [46].

Errors associated with WE surface area determination and peak current response measurement undoubtedly introduce uncertainty to the diffusion coefficient results. The contribution of cylindrical diffusion and migration are small, but likely nonnegligible as previously reported in the literature for high concentration actinide [42, 46, 97]. The dependence of diffusion coefficient on concentration may play a larger role at these higher concentrations, along with the effects of approaching analyte solubility limits. Uncompensated resistance and charge transfer kinetics undoubtedly affect the CV results; however, developing a numerical method for positive feedback resistance compensation and charge transfer kinetics correction is non-trivial and would require considerable investment in adjusting the numerical solution to diffusion laws that is at the foundation of the Randles-Sevcik relationship.

## 5.4 Conclusions

CV was employed for high concentration electrochemical reversibility and diffusion analysis of  $\text{SmCl}_3$  solvated in the molten LiCl-KCl eutectic at 773 K. Published methods for repeatable CV acquisition and WE surface area determination were adjusted and applied to the  $\text{SmCl}_3$  reaction couples of interest, producing repeatable current

response data. Peak current versus the square root of scan rate correlations, along with peak current ratio analysis, was employed to determine a scan rate region with high current response repeatability, minimal WE surface effects, and maximized reversibility characteristics. The scan rate region was then utilized to conduct concentration analysis as it relates to peak current density response and the calculation of diffusion coefficients. The diffusion coefficient results were in agreement with the available literature; however, the concentration results indicated some sources of uncertainty. Peak current response error, WE surface area error, concentration dependence of the diffusion coefficient, cylindrical diffusion effects, migration effects, uncompensated resistance, and charge transfer kinetics effects were all determined to play some role in creating the observed uncertainty. Further work is required to develop accurate and reliable CV numerical methods that incorporate the effects of these phenomena before the technique can be applied to processing facilities on a commercial scale.

## Chapter 6 An Investigation of Synthesized Samarium Oxychloride in Molten LiCl-KCl Eutectic and its Nuclear Material Management Implications

### 6.1 Introduction

As the international community transitions to more sustainable and environmentally-friendly energy sources, nuclear power remains one of the cleanest sources of electricity in terms of greenhouse gas (GHG) emissions. The International Atomic Energy Agency's (IAEA) *Climate Change and Nuclear Power 2018* report projects nuclear energy's role in electricity markets to grow anywhere from 24-184 % in terms of generating capacity by 2050 [8]. Technological improvements in power plant design, passive safety features, proliferation-resistant fuel cycles, and analytical nuclear material management methodology will allow for nuclear energy to penetrate emerging electricity markets [9]. Nuclear power plants are considered to be in their second technological generation as of 2019, with a Generation-III fleet of reactors currently being constructed. Generation-IV nuclear power plants and fuel cycles drift away from aqueous systems in favor of higher-temperature materials, such as molten salts. Securing nuclear material and optimizing process conditions for economically viable power and fuel production remain the main obstacles to advanced system commercialization [99].

Molten chloride salts are candidate materials for nuclear power plant cooling, fueled-salt power reactors, and the electrochemical processing of nuclear material. Used



nuclear fuel (UNF) is not reprocessed internationally on a large scale; however, a few nations recycle UNF using a process termed PUREX (Plutonium Uranium Redox Extraction). PUREX relies on aqueous media to separate, pure uranium and plutonium streams that exhibit dangerously high enrichment levels. PUREX is riddled with problems associated with radiolysis and criticality that manifest in the form of waste management and proliferation concerns [15, 27]. The pyrochemical reprocessing of UNF employs the molten LiCl-KCl eutectic salt at 500 °C to electrochemically deposit uranium, plutonium, and transuranic (TRU) chlorides in metallic form on a combination of solid and liquid metal electrodes [27, 29]. The impure and high temperature nature of plutonium streams in the pyrochemical flowsheet create a more proliferation-resistant process [14]. Although the fuel is refined and consolidated in metallic form, electrolytic reduction unit operations can incorporate existing light water reactor (LWR) oxide fuel into a closed nuclear fuel cycle employing the pyrochemical process [29]. Electroanalytical and spectroscopic investigations of actinide and lanthanide chloride analytes in the molten LiCl-KCl eutectic produce information regarding analyte chemistry, electrochemical separation efficiency, and process scale-up [38, 40, 43, 47, 48, 62, 71, 100]. The proposed process flowsheet for the pyrochemical reprocessing of UNF, reported by Williamson et al., is shown in Figure 48 [29].

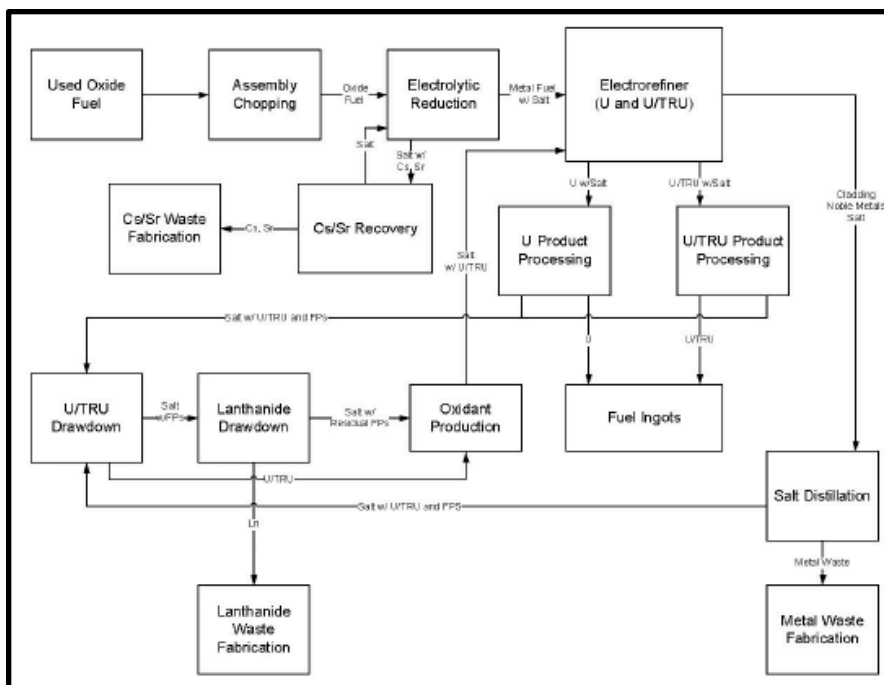


**Figure 48** Proposed pyroprocessing flowsheet published by Williamson et al. reports a variety of unit processes (electrorefiner, oxidant production, lanthanide drawdown, U/TRU drawdown) that require concrete understanding of analyte behavior before optimization can be pursued.

Oxychloride chemistry plays an important role when addressing lanthanide and actinide chemistry in molten chloride salts. Oxychloride formation, predominantly in the form of precipitates, can have negative effects on process efficiency along with creating nuclear material management concerns regarding hold up and material loss. Oxychloride precipitation has also been proposed as a method for co-precipitation and consolidation of nuclear material in molten salt [101, 102]. Furthermore, also oxychloride formation presents a potential for nuclear material buildup due to moisture or impurities in alternative electrochemical processes related to the nuclear industry, specifically the conversion of plutonium pits in high-temperature molten salt [103]. The literature data regarding oxychloride formation in the LiCl-KCl molten eutectic is limited and requires further investigation to fully understand solvation mechanisms, effects on

electroanalytical measurements, and characterization of relevant reaction products [49, 101, 102].

This paper presents a synthesis method for, and characterization of, samarium oxychloride (SmOCl) in the molten LiCl-KCl eutectic at 500 °C. Additionally, solid state characterization is reported to confirm the synthesis of SmOCl before the *in situ* analysis of the analyte using electroanalytic measurements and polarized Raman spectroscopy. Cyclic voltammetry (CV) results are reported and discussed in terms of current response and empirical relationships applicability. CV and *in situ* Raman also provide a qualitative evaluation of oxychloride formation in the molten LiCl-KCl eutectic. The results are discussed in term of engineering implications related to nuclear material management in high-temperature molten salt systems.

## 6.2 Experimental

### General features

All molten salt studies were conducted in ultra-high purity argon atmosphere (Airgas 99.99%) inside an inert glovebox maintained under 1 ppm moisture and oxygen content. The electroanalytical and *in situ* Raman spectroscopy setup has been previously presented by the authors for low concentration lanthanide studies in the same eutectic system [77, 78, 104, 105]. The experimental apparatus employed for both spectroscopic and electroanalytical molten salt investigations is shown in Figure 49.

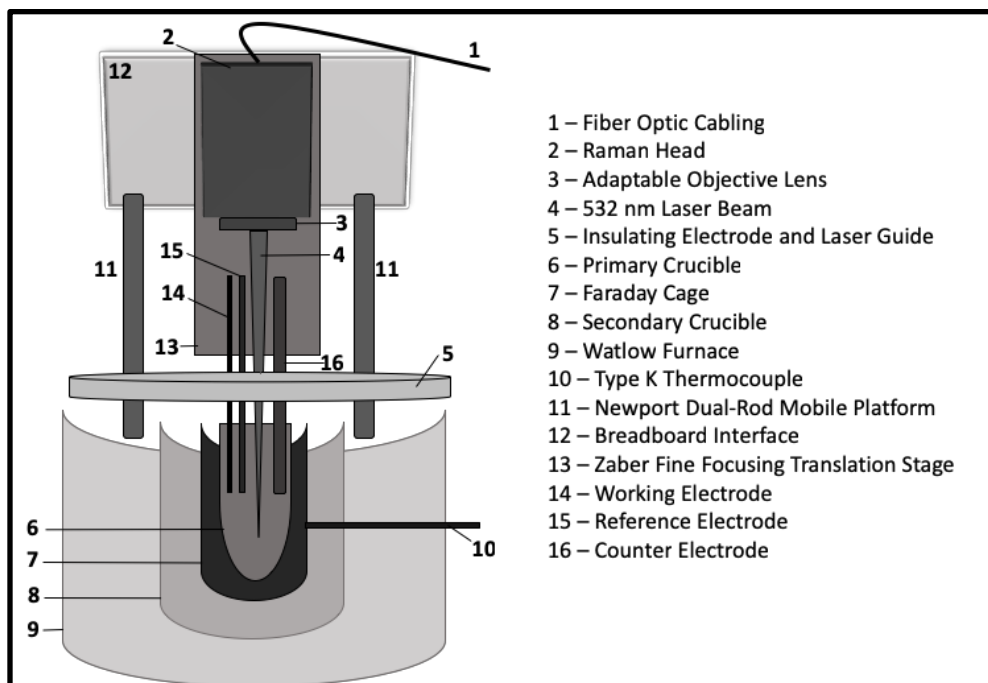


**Figure 49** Experimental setup employed for spectroscopic and electroanalytical investigations in molten LiCl-KCl eutectic consists of precision alignment stages for electrochemical and spectroscopic focusing, electrode alignment mounts, fiber cabling for 532 nm laser excitation, a polarized Raman probe, and a high-temperature ceramic cylindrical furnace.

Uncertainties associated with thermal gradients were mitigated with an insulating ceramic furnace cap fabricated with electrode alignment holes and a laser beam path for Raman analysis. Alumina tubes were installed to ensure electrode alignment is repeatable and precise. Molten salt samples were contained in 55 mL alumina crucibles nested inside stainless-steel Faraday cages that remove electrical current noise produced by the furnace heaters. The system was equipped with a three-electrode electrochemical stage and Raman probe with polarization capability. A 532 nm wavelength laser was utilized for Raman excitation. A K-type thermocouple was installed to provide feedback to the furnace controller with  $\pm 2$  °C temperature precision. Electrode positioning and Raman probe focusing were controlled by a high-resolution translation stage with a LabVIEW National Instruments software user interface to ensure accurate and repeatable

placement of electrodes inside the molten salt matrix and to ensure the laser excitation converges in the solution to excite the bonds associated with dissolved analyte complexes rather than electrodes or crucible walls.

### Cyclic Voltammetry Methods

CV is a three-electrode electrochemical method that relies on a cyclic potential sweep to scan a voltage range for analyte-specific redox reactions. Current response can be correlated to analyte concentration if the diffusion behavior of the analyte is well understood [39]. The Randles-Sevcik equation can be applied to CV data assuming all diffusion is mass transfer limited, linear in nature, and the redox reaction of interest is reversible [39]. The Randles-Sevcik relationship is reported in Equation 12. Once diffusion coefficient values are established, current response has the potential to be correlated to concentration for process monitoring and nuclear security applications [52].

$$i_p = 0.4463 \cdot n \cdot F \cdot A \cdot C_i \cdot \left(\frac{n \cdot F}{R \cdot T}\right)^{1/2} \cdot v^{1/2} \cdot D^{1/2} \quad (12)$$

Here  $i_p$  is the peak current response,  $n$  is the number of electrons transferred during the redox reaction,  $F$  is Faraday's constant,  $A$  is the surface area of the working electrode (WE),  $C_i$  is the bulk concentration of the dissolved analyte of interest,  $R$  is the ideal gas constant,  $T$  is temperature,  $v$  is the potential scan rate, and  $D$  is the diffusion coefficient of the analyte of interest [39]. The working electrode (WE) and counter electrode (CE) consisted of a 1/16" and 1/8" diameter tungsten rod, respectively. A 5 mol % Ag|AgCl reference couple encased in Pyrex which has been previously deployed for voltammetry experiments in the same eutectic was employed as a reference electrode [38]. The peak

current versus square-root of scan rate relationship was studied for both  $\text{SmCl}_3$  and  $\text{SmOCl}$ . Peak currents were measured five times at each of the following scan rates for each CV analysis: 100 mV/s, 150 mV/s, 200 mV/s, 250 mV/s, and 300 mV/s.

#### Samarium oxychloride synthesis

LiCl-KCl melts were prepared by mixing LiCl (Alfa Aesar 99% pure) and KCl (Alfa Aesar 99% pure) at 46 wt.% and 54 wt.%, respectively [26]. Precursor salts utilized to prepare the final eutectic were first baked under vacuum at 200 °C in order to minimize moisture-induced impurities. Anhydrous  $\text{SmCl}_3$  (Alfa Aesar, 99.9% pure) was dissolved directly into the molten LiCl-KCl eutectic at 500 °C and agitated for eight hours. Synthesis of  $\text{SmOCl}$  was accomplished through the dissolution of  $\text{O}^{2-}$  ions in the eutectic with the addition  $\text{Li}_2\text{CO}_3$  to the  $\text{SmCl}_3$ -LiCl-KCl solutions. The reaction mechanism for  $\text{SmOCl}$  formation and precipitation in this manner has been reported in the literature by Castrillejo et al. [49, 106]. The dissolution of  $\text{SmCl}_3$ ,  $\text{Li}_2\text{CO}_3$ , and formation of  $\text{SmOCl}$  are reported in Equations 13, 14, and 15, respectively.



After addition of  $\text{Li}_2\text{CO}_3$ , melts were agitated until  $\text{CO}_2$  gas bubbling halted, indicating the reaction had completed.

$\text{SmCl}_3$  was solvated in LiCl-KCl at a concentration of  $3.3 \times 10^{-4} \text{ mol cm}^{-3}$ , and  $\text{Li}_2\text{CO}_3$  was added to the solution in an equimolar quantity. Upon completion of the synthesis

reaction, the melt was allowed to solidify. Carboxylic acid groups on ethylenediaminetetraacetic acid (EDTA) were deprotonated in DI H<sub>2</sub>O in solution through the addition of NaOH. The deprotonated solution was used to rinse off remaining eutectic and pull any unreacted SmCl<sub>3</sub> into solution as well. The EDTA forms a 1:1 complex with the unreacted SmCl<sub>3</sub>, leaving only the SmOCl precipitate behind. Excess EDTA was present to ensure all unreacted SmCl<sub>3</sub> was fully chelated. The remaining solution containing the synthesized precipitate was then centrifuged so that precipitate powder could be consolidated. The powder was then allowed to dry before undergoing solid state characterization.

Synthesis is complete once CO<sub>2</sub> bubbling is no longer observed. Li<sub>2</sub>CO<sub>3</sub> is added in small increments while the melt is agitated to ensure the salt mixture does not overflow out of the containment crucible due to CO<sub>2</sub> bubbling. Once bubbling has halted, the melt is agitated for an extended period of time to ensure the reaction proceeds to completion. After agitation, the melt is observed to be transparent with a suspension of white precipitate, assumed to be SmOCl. After reaction completion, the melt is cooled and dissolved in the EDTA complex for separation and consolidation.

#### Solid state characterization

Synthesized precipitate was analyzed using a variety of solid-state characterization methods to confirm the formation of SmOCl. X-ray diffraction (XRD) patterns were obtained from the collected precipitates using a Rigaku Smartlab X-ray diffractometer. Diffraction patterns were analyzed using a PDXL software package. A Hitachi S-4700 field emission scanning electron microscope (SEM) equipped with energy

dispersive x-ray spectroscopy (EDS) was employed to investigate precipitate morphology and elemental makeup, respectively. Transmission electron microscopy (TEM) analysis was carried out using a JEOL-JEM 2100F Analytical TEM. A Thermo Scientific DXR Raman microscope equipped with a 10 mW, 532 nm wavelength laser was employed for solid-state Raman analysis of the precipitate.

### 6.3 Results and Discussion

#### Synthesis and Solid-State Characterization

The precipitate remains a white color throughout the separation and consolidation operations. Once dry, solid-state characterization is commenced to confirm the presence of SmOCl. The XRD pattern obtained from separated, consolidated, and dried precipitate is reported in Figure 50.

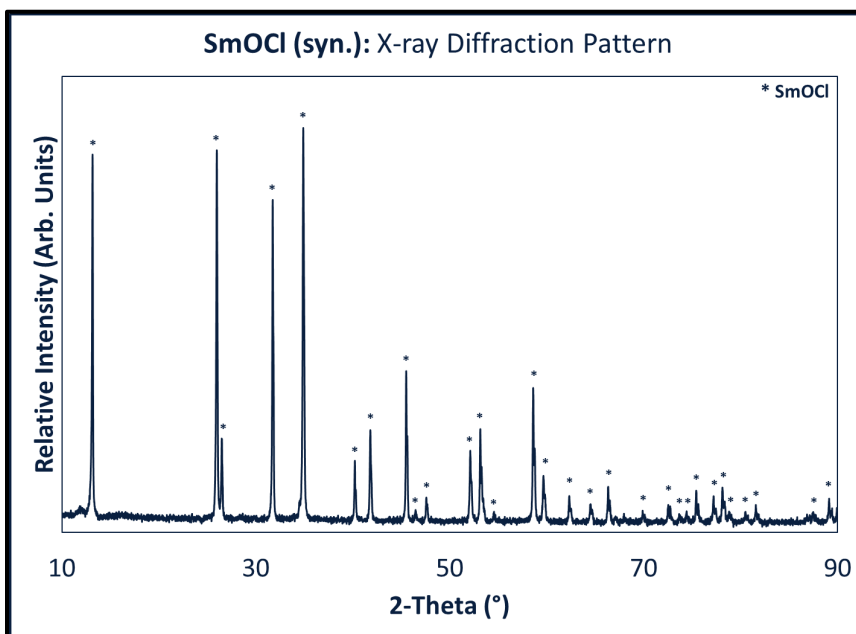


**Figure 50** The XRD pattern obtained from separated, consolidated, and dried precipitate indicates the formation of SmOCl with relatively few impurities.



XRD analysis is followed by SEM imaging and EDS elemental analysis. Two different particulate morphologies can be observed in the SEM micrographs. EDS elemental analysis is conducted with respect to the Sm:Cl atomic ratios. SmOCl should exhibit 1:1 Sm:Cl atomic ratios, while SmCl<sub>3</sub> will exhibit 3:1 Sm:Cl ratios. The oxygen ratios are not reliable due to oxygen atmospheric and mounting tape contamination. The two different morphologies observed by SEM are displayed in Figure 51, and the regions of analysis by EDS are indicated.

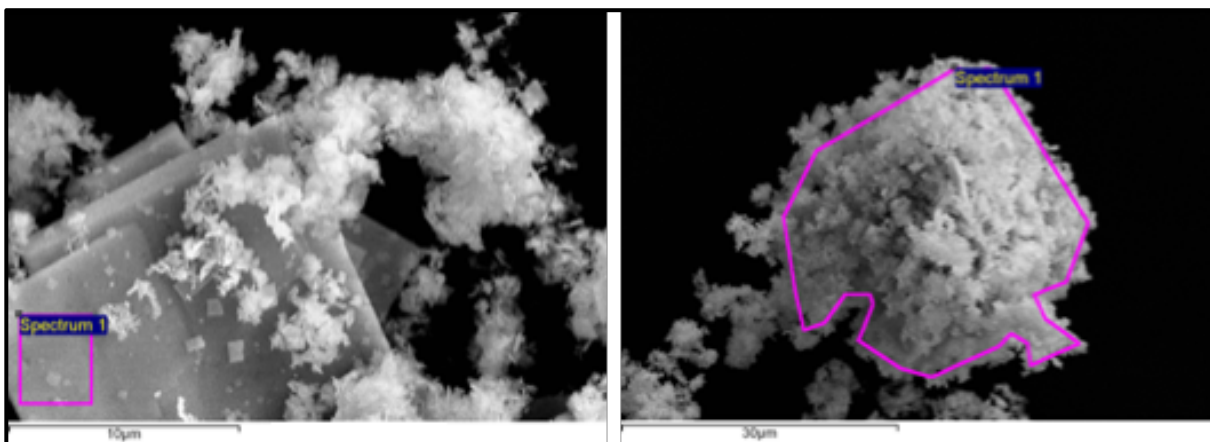


**Figure 51** SEM images of plate-like precipitate particles (left) and fluff-like precipitate particles (right) both illustrate the regions of interest (purple outline) where EDS chemical analysis was conducted.

The EDS results are reported in Table 13 for both morphologies. The platinum content is attributed to the use of platinum to sputter coat samples before SEM-EDS analysis in order to prevent sample charging.

Elemental Emission	Atomic %	
	Plate-Like Morphology	Fluff-Like Morphology
<b>O K</b>	58.61	52.44
<b>Cl K</b>	19.35	23.05
<b>Sm L</b>	20.78	23.67
<b>Pt M</b>	1.26	0.84

**Table 13** EDS chemical analysis results for both precipitate morphologies observed in SEM images indicated approximately 1:1 Sm:Cl atomic ratio values.

Both morphologies indicate Sm:Cl atomic ratios approximately 1:1, suggesting both morphologies are SmOCl. These ratios confirm that the bulk precipitate collected is indeed SmOCl as the XRD pattern also suggests.

TEM imaging allows for planar, d-spacing to be measured. TEM imaging and d-spacing measurement results obtained from the precipitate are reported in Figure 52.

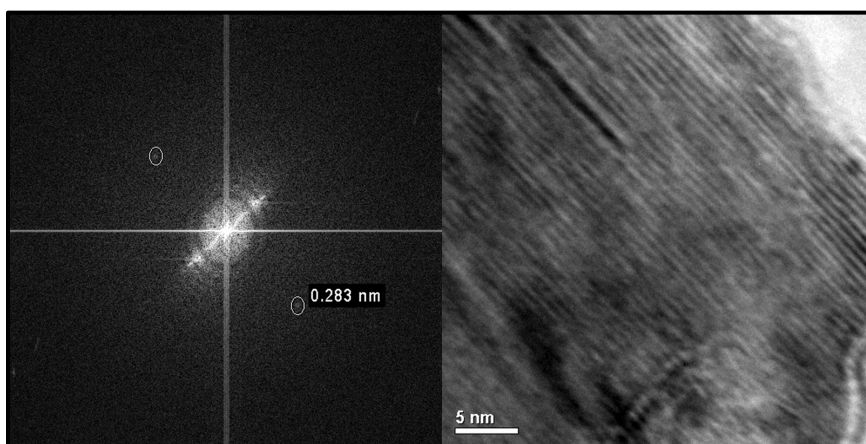


**Figure 52** TEM diffraction analysis shows the 110-plane d-spacing is in agreement with the measured XRD pattern reported in Figure 50, confirming the precipitate to be SmOCl.

Once focusing on a plane of interest is achieved, a d-spacing measurement is confirmed with the 110-plane associated with SmOCl and d-spacing values for the 110-plane measured using XRD. Solid-state Raman spectra obtained from the precipitate are reported in Figure 53.

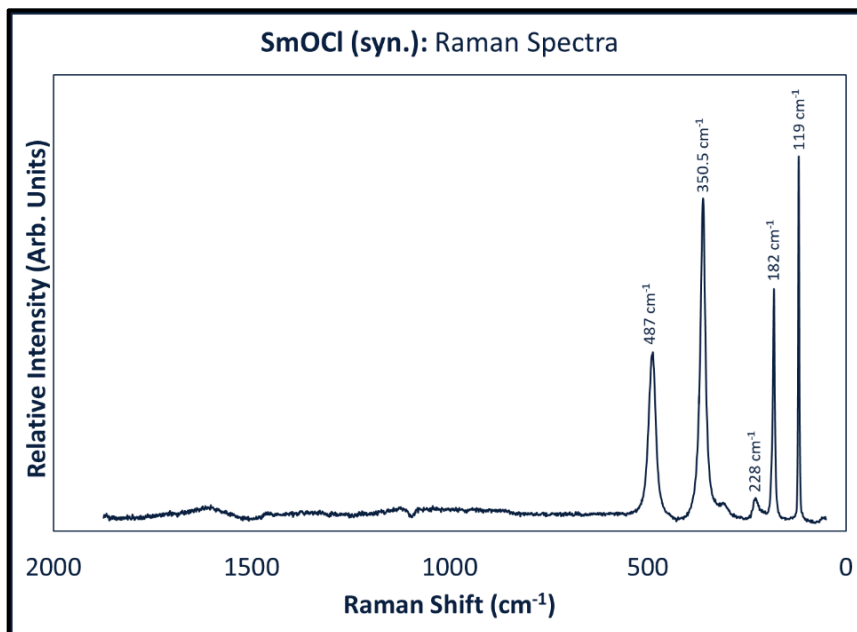


**Figure 53** Raman spectra obtained from the precipitate show five symmetry modes that confirm the precipitate to be SmOCl [107].

Raman spectra indicate the presence of five symmetrical modes labelled in Figure 53. These modes are confirmed to be consistent with the previously reported literature concerning lanthanide oxychlorides [107, 108].

Solid-state characterization results all indicate the precipitate synthesized in the molten LiCl-KCl-SmCl<sub>3</sub> solution is indeed SmOCl, as Equations 13-15 suggest. The TEM images confirm the d-spacing values reported for the 110-plane in the obtained XRD patterns, and the SEM-EDS results show the presence of two different morphologies, both of which can be attributed to SmOCl through Sm:Cl atomic ratio analysis. The solid-state Raman spectra report five symmetrical modes that are consistent with the previously published lanthanide oxychloride literature [107, 108].

#### In Situ Electrochemistry and Spectroscopy

CV experiments conducted on LiCl-KCl with  $\text{SmCl}_3$  solvated at low concentrations may produce an additional anodic peak in a slightly more oxidative region than that associated with the traditional  $\text{SmCl}_3$  redox couple. A sample CV that contains this additional anodic peak, indicated with an asterisk, is reported in Figure 54.

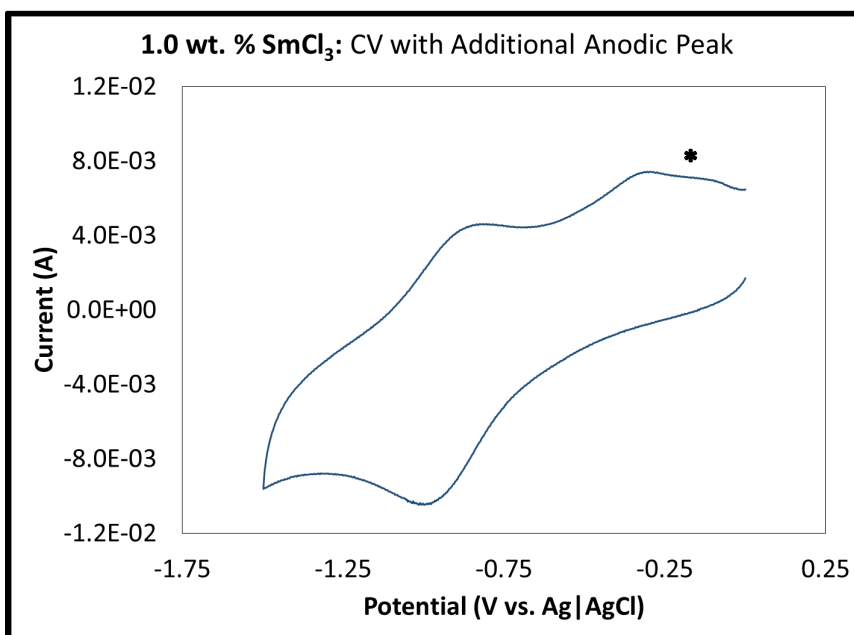


**Figure 54** An additional anodic peak (\*) manifests in a slightly more oxidative region than the traditional  $\text{SmCl}_3$  redox couple at low concentrations.

The additional anodic peak is hypothesized to be the result of  $\text{SmOCl}$  formation. The CV reported in Figure 54 is compared with a CV obtained from the molten LiCl-KCl eutectic solvated only with synthesized  $\text{SmOCl}$  in Figure 55.

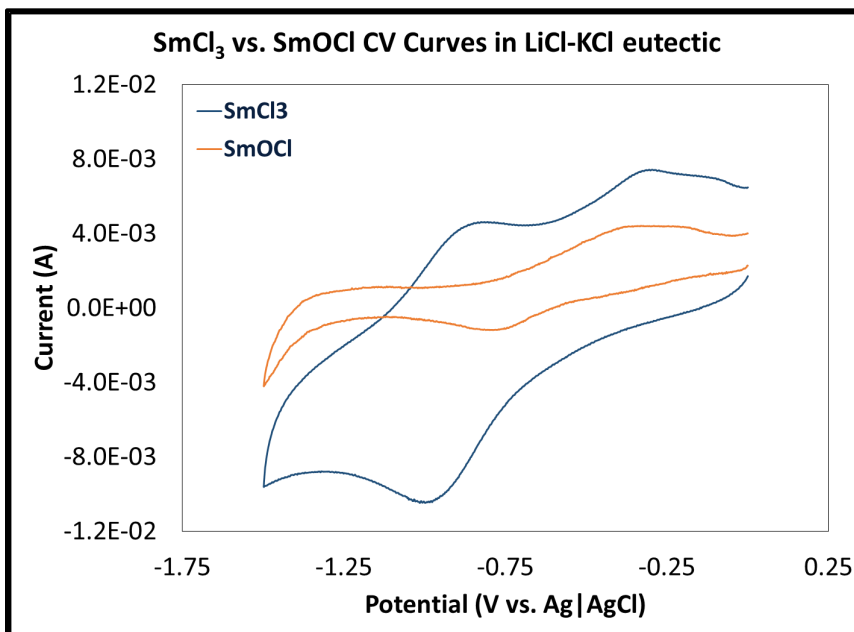


**Figure 55** A comparison of CV curves obtained from a low-concentration  $\text{SmCl}_3$  melt with the additional anodic peak and a molten LiCl-KCl melt containing synthesized SmOCl indicate the additional peak is due to SmOCl formation.

Figure 55 illustrates SmOCl is responsible for the additional anodic peak observed in molten LiCl-KCl melts solvated with low concentrations of  $\text{SmCl}_3$ . The SmOCl couple also includes a cathodic peak that manifests underneath the more prominent  $\text{SmCl}_3$  cathodic peak. The additional cathodic and anodic redox peaks that are the result of SmOCl contamination will create uncertainty in  $\text{SmCl}_3$  current response measurements which will have nuclear material management implications in terms of monitoring  $\text{SmCl}_3$  content.

In order to better understand the electroanalytical implications of SmOCl formation, the oxychloride was synthesized using the methods outlined in previous sections of this paper and then studied using CV and fiber-based Raman spectroscopy. CV and Raman analysis were first conducted on a molten LiCl-KCl melt solvated with  $\text{SmCl}_3$  at a concentration of  $3.3 \times 10^{-4} \text{ mol cm}^{-3}$ . The equimolar synthesis of SmOCl was then

conducted through  $\text{Li}_2\text{CO}_3$  solvation to convert the  $\text{SmCl}_3$  to  $\text{SmOCl}$ . CV and *in situ* Raman were conducted to confirm the  $\text{SmCl}_3$  is no longer present after synthesis is complete. A more targeted CV analysis was then conducted on the  $\text{SmOCl}$  in the LiCl-KCl melt. Figure 56 and Figure 57 respectively report *in situ* CV results and Raman spectra of  $\text{SmCl}_3$  solvated in the molten LiCl-KCl eutectic that is consistent with the reported literature, and the subsequent disappearance of  $\text{SmCl}_3$  Raman indicators post-synthesis of the  $\text{SmOCl}$  [49, 71].

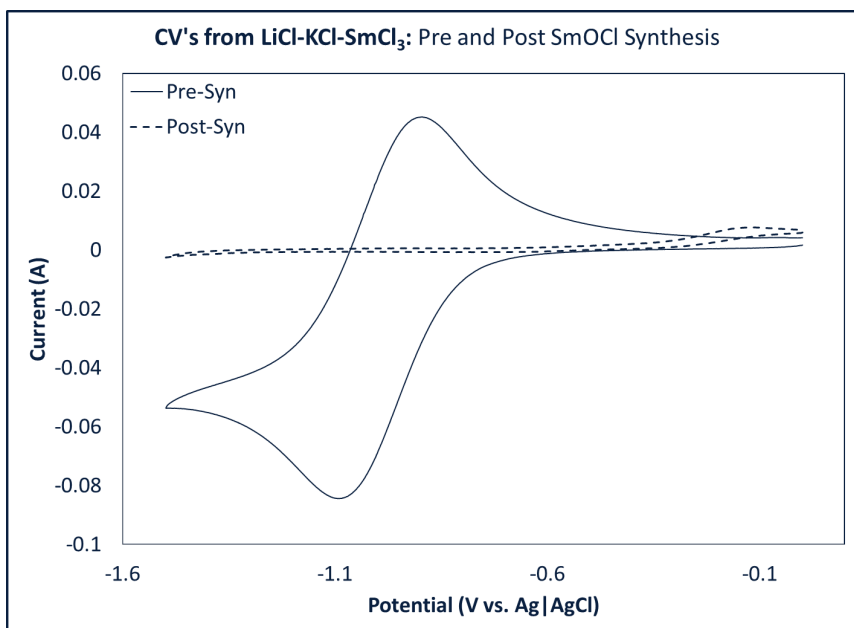


**Figure 56** A clear shift in the location and magnitude of the peak current response is observed in the CV acquired post- $\text{SmOCl}$  synthesis as compared to the CV acquired before  $\text{SmOCl}$  synthesis.

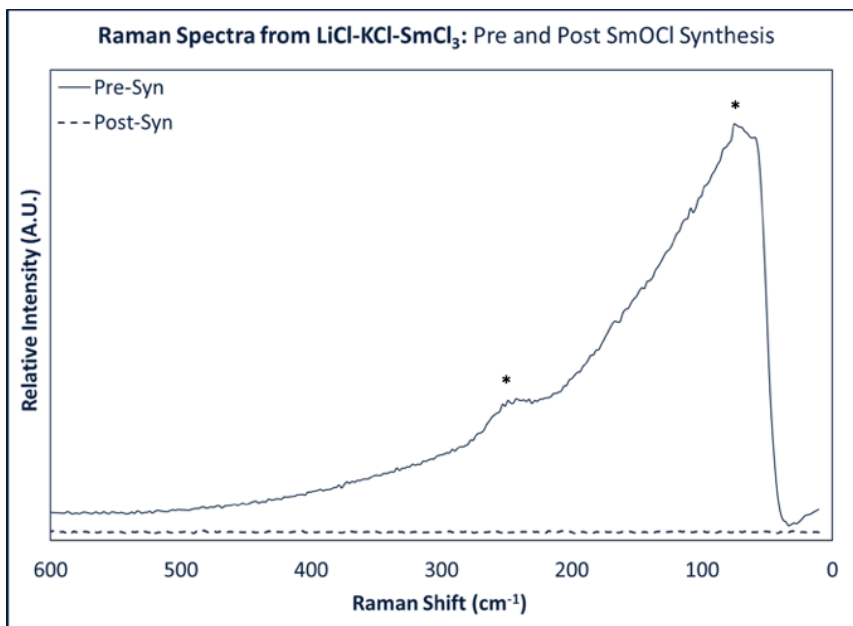


**Figure 57** The lack of features in the Raman spectra acquired after the SmOCl synthesis indicate the SmOCl is either soluble at levels below the detection limits of the Raman or does not exhibit Raman active modes when solvated in the molten LiCl-KCl eutectic.

The peak current response from SmOCl is less in terms of magnitude than the solvated SmCl<sub>3</sub>. Figure 56 illustrates this shift in magnitude as the post-synthesis, SmOCl redox peaks are barely visible compared to the prominent, pre-synthesis SmCl<sub>3</sub> peaks. This reduction in magnitude, along with the observable collection of SmOCl precipitate at the bottom of the melts suggests SmOCl is soluble at low levels in the molten LiCl-KCl eutectic. This low solubility may explain why no Raman indicators are detected post-synthesis in Figure 57; however, this lack of modes may also be attributed to dissolved SmOCl not being Raman active. There is no available literature regarding the coordination chemistry of SmOCl solvated in the molten LiCl-KCl eutectic so that its Raman activity can be determined. Investigations of fundamental coordination chemistry requires techniques such as x-ray absorption fine structure (XAFS) analysis.

The peak current responses from CV associated with  $\text{SmCl}_3$  reached values above 100 mA, while the same peak current responses all remained below 10 mA for  $\text{SmOCl}$ . This difference in magnitude further suggests the low solubility of  $\text{SmOCl}$  in the molten LiCl-KCl eutectic. The results of CV analysis as a function of scan rate are summarized for the LiCl-KCl- $\text{SmCl}_3$  (pre-synthesis) and LiCl-KCl- $\text{SmOCl}$  (post-synthesis) melts in Figure 58 and Figure 59 respectively.

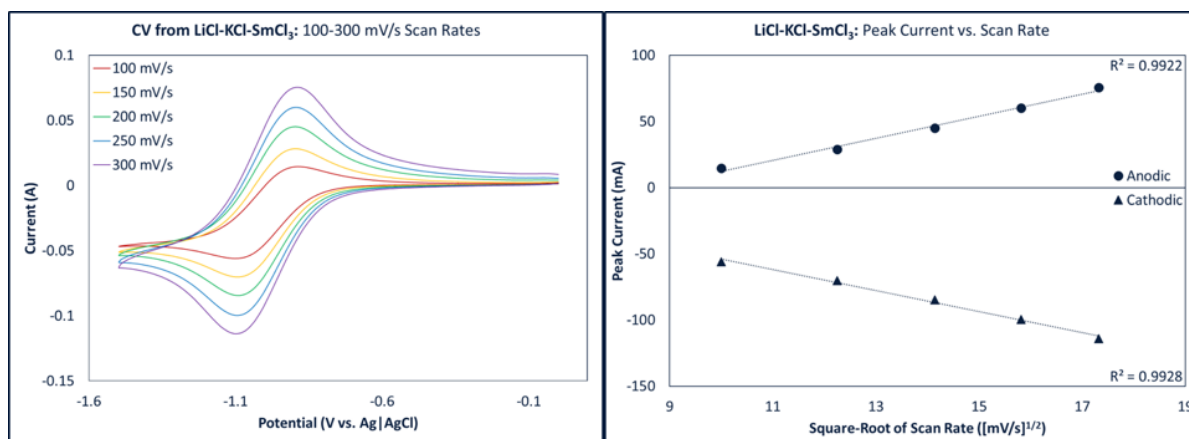


**Figure 58** CV results (left) with respect to scan rate from the LiCl-KCl- $\text{SmCl}_3$  (pre-synthesis) indicate high levels of peak current vs. scan rate linearity (right), and therefore high levels of Randles-Sevcik applicability.

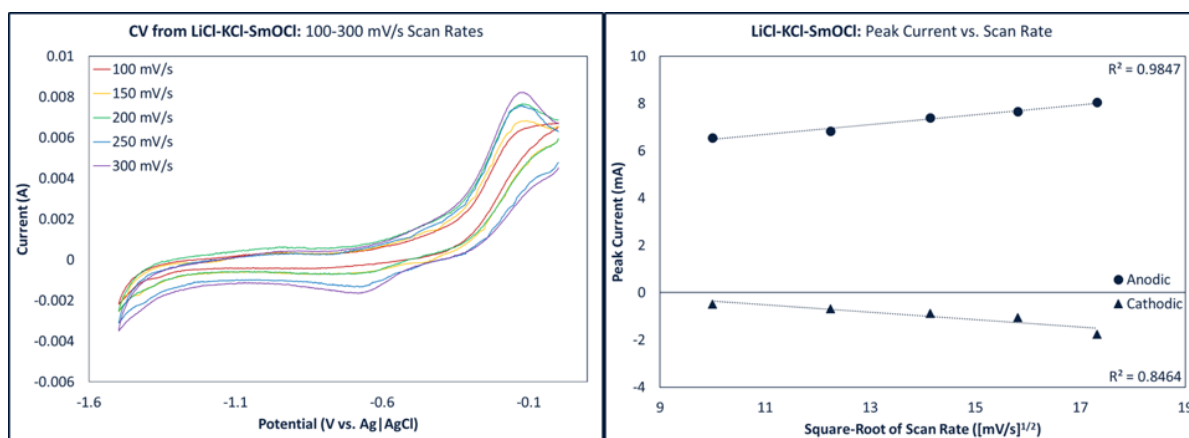


**Figure 59** CV results (left) with respect to scan rate from the LiCl-KCl- $\text{SmOCl}$  (post-synthesis) indicate lower levels of peak current vs. scan rate linearity (right), and therefore lower levels of Randles-Sevcik applicability.



The linearity of peak current vs. scan rate relationships, both for cathodic and anodic current response, is much higher for  $\text{SmCl}_3$  (pre-synthesis) samples than  $\text{SmOCl}$  (post-synthesis) samples. This difference in linearity is illustrated by the difference in  $R^2$  values reported in Figure 58 and Figure 59. Randles-Sevcik applicability for analysis is therefore less suitable for the oxychloride species than  $\text{SmCl}_3$ . The dissolution behavior in terms of ionic state equilibrium also seems to vary between the  $\text{SmCl}_3$  and  $\text{SmOCl}_3$  samples. Specifically, the  $\text{SmCl}_3$  samples produce cathodic peak current responses slightly larger than the anodic responses, suggesting the trivalent samarium that is reduced on the cathodic sweep is not fully oxidized back into solution. In comparison, the anodic current responses are much larger than the cathodic responses for the  $\text{SmOCl}$  samples. The literature is limited regarding the nature of oxychloride redox reactions, but this difference in current response relationships suggests the  $\text{SmOCl}$  could be more likely to undergo spontaneous reduction. Therefore, there is less oxidized species to reduce on the cathodic sweep, producing lower cathodic response. XAFS analysis may help elucidate these equilibrium conditions as well.

The implications of these findings regarding the application of CV for process monitoring and nuclear material management are notable. Carbonate or moisture impurities have the potential to convert solvated trichloride analytes to their oxychloride forms. Correcting for  $\text{SmOCl}$  is clearly necessary as it is electroactive and produces distinguishable redox peaks in CV curves. Current correction methods must be developed for oxychloride species to account for their contributions to solvated trichloride analysis. Developing these correction methods will not be trivial, as the applicability of Randles-

Sevcik relationship loses effectiveness when studying the oxychloride species. Elucidation of ionic states and equilibria associated with oxychloride species must first be investigated before any adjustments to the Randles-Sevcik can be accomplished. These studies would most likely require fundamental coordination chemistry investigations using methods such as XAFS.

## 6.4 Conclusions

A targeted synthesis, solid-state characterization, *in situ* electroanalytical, and *in situ* Raman spectroscopic investigation of SmOCl in the molten LiCl-KCl eutectic was completed. Synthesis was accomplished through carbonate addition to the molten LiCl-KCl-SmCl<sub>3</sub> system. SmOCl was confirmed to precipitate out of solution due to carbonate addition through a variety of solid-state characterization techniques. The SmOCl was then analyzed *in situ* using fiber-based Raman spectroscopy and cyclic voltammetry. Both the Raman and voltammetry results indicated a conversion of SmCl<sub>3</sub> to SmOCl and change in solution chemistry. The SmOCl was not detectable using Raman either due to its solubility limit being below the Raman's detection limits or its solvated form being Raman inactive. CV investigations into the SmOCl produced redox peaks that suggest current corrections will be necessary for SmOCl when using CV for process monitoring and nuclear material management purposes in the molten LiCl-KCl eutectic.

## Chapter 7 Other Relevant Results

### 7.1 Multi-Analyte Study

Preliminary studies using the SPEC system to analyze molten LiCl-KCl matrices with multiple analytes solvated were commenced in order to evaluate electroanalytical and Raman spectroscopic performance. The results from these multi-analyte studies provide insights regarding avenues for further development of the system and potential deployment scenarios of the SPEC system on an engineering scale for NMA. CV investigations were conducted on the molten LiCl-KCl eutectic solvated with  $\text{CeCl}_3$ ,  $\text{EuCl}_3$ , and  $\text{SmCl}_3$ , each at a concentration of 2.5 wt. %. This weight loading produced a total 7.5 wt. % lanthanide chloride concentrations solvated in the molten LiCl-KCl eutectic maintained at 500 °C. The Randles-Sevcik peak current response versus the square root of potential scan rate relationship was evaluated for each analyte. Raman spectroscopy experiments compared individual  $\text{SmCl}_3$  and  $\text{CeCl}_3$  spectra solvated in the molten LiCl-KCl eutectic with spectra obtained from the eutectic with both  $\text{CeCl}_3$  and  $\text{SmCl}_3$  solvated.

The CV study produced the expected electrochemical reaction responses from all three analytes. As mentioned in Chapter 3, the  $\text{CeCl}_3$  reaction couple is a three-electron transfer, converting the solvated  $\text{Ce}^{3+}$  directly to its metallic state. The  $\text{SmCl}_3$  reaction couple is a one-electron transfer, converting  $\text{Sm}^{3+}$  to  $\text{Sm}^{2+}$ . The reaction couple associated with  $\text{EuCl}_3$  is identical to  $\text{SmCl}_3$ . However,  $\text{EuCl}_3$  is known to spontaneously disproportionate to its divalent state upon solvation, which will produce some

uncertainty in trivalent concentration measurements [60, 100]. The CV curves measured at various potential scan rates from this triple-analyte matrix are overlaid in Figure 60.

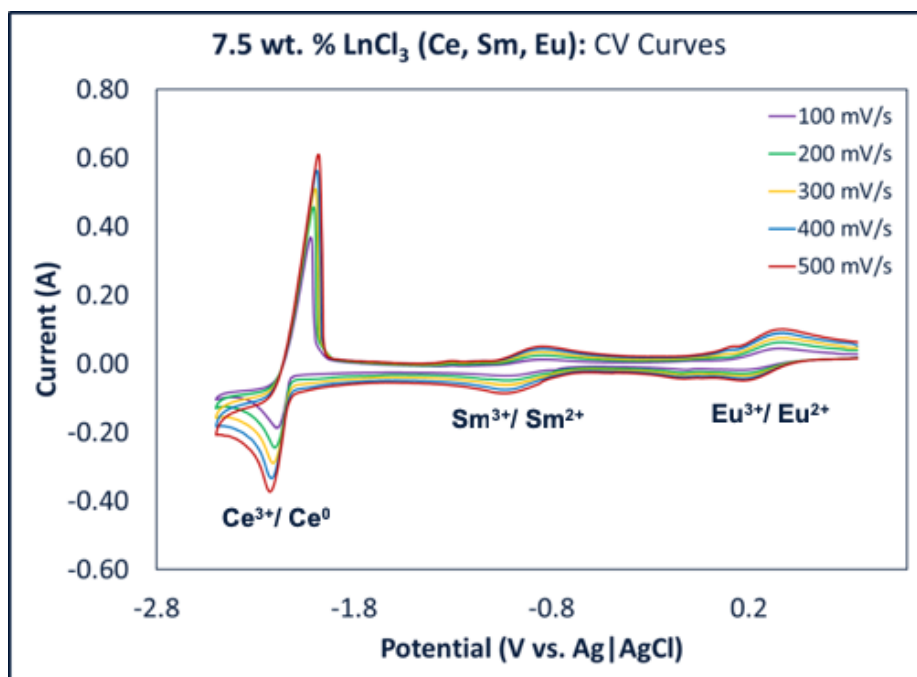


**Figure 60** Overlaid CV curves at various scan rates from the molten LiCl-KCl eutectic at 500 °C solvated with  $\text{CeCl}_3$ ,  $\text{EuCl}_3$ , and  $\text{SmCl}_3$

The electrochemical responses associated with each solvated analyte do not overlap or interfere with one another in terms of potential vs. Ag|AgCl in Figure 60. This sort of spacing is ideal but will not necessarily be the case in processing conditions, especially in the electrorefiner where SNM and fission products are present. Upon closer inspection of the  $\text{EuCl}_3$  CV curves, the cathodic current response is less than the anodic current response unlike the  $\text{SmCl}_3$  couple. This change in current response ratio is indicative of the tendency for  $\text{Eu}^{3+}$  to spontaneously disproportionate to  $\text{Eu}^{2+}$ . The peak anodic and cathodic current responses versus the square root of potential scan rate are reported in Figure 61 for each analyte.

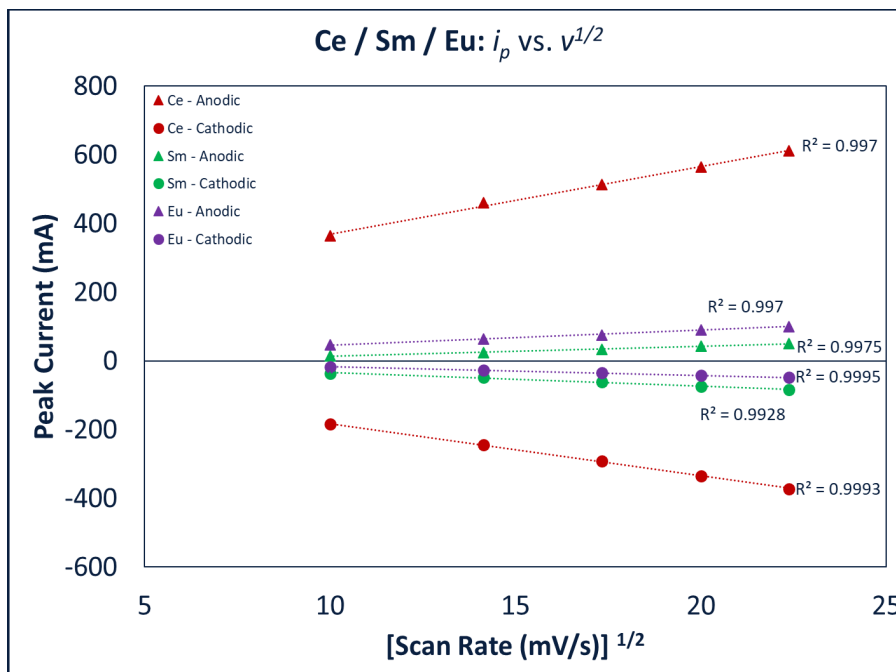


**Figure 61** Peak anodic and cathodic current response versus square root of potential scan rate data for molten LiCl-KCl eutectic solvated with CeCl<sub>3</sub>, EuCl<sub>3</sub>, and SmCl<sub>3</sub>

All three analytes produced linear anodic and cathodic current responses with respect to the square root of potential scan rate. This linearity suggests the electrochemical reactions are at minimum quasi-reversible. Furthermore, as discussed in Chapter 5, at concentrations above 5 wt. %, alternative diffusion mechanisms, like migration, and resistance compensation begin to affect the reliability of electroanalytical results. The total lanthanide concentration in this study was 7.5 wt. %. The three-electron transfer associated with CeCl<sub>3</sub> can affect the surface of the WE due to deposition and adsorption effects, which will also negatively affect the reliability of electroanalytical results [46]. Consistent with the findings in Chapter 5, the mechanism associated with alternative diffusion mechanisms and resistance compensation require further investigation to increase the reliability of CV in multi-analyte process conditions.

A comparison of Raman spectra obtained from the following sample matrices is reported in Figure 62:  $\text{CeCl}_3$ -LiCl-KCl,  $\text{SmCl}_3$ -LiCl-KCl,  $\text{CeCl}_3$ - $\text{SmCl}_3$ -LiCl-KCl.

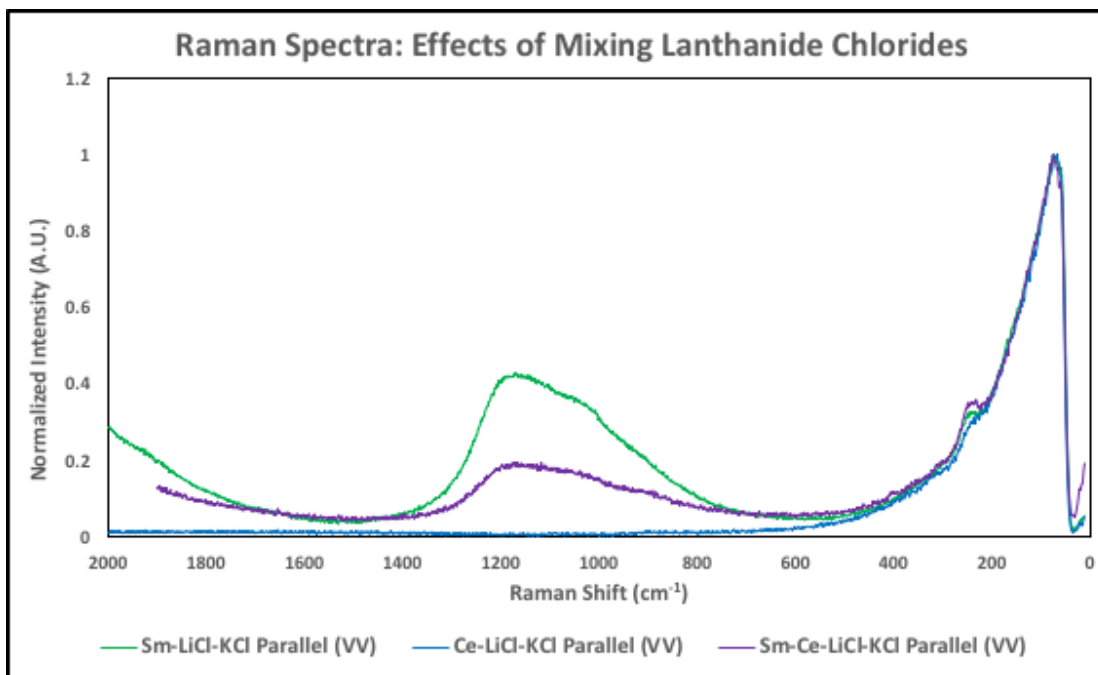


**Figure 62** Comparison of individually solvated and mixed  $\text{CeCl}_3$  and  $\text{SmCl}_3$  Raman spectra in the molten LiCl-KCl eutectic

The  $\text{CeCl}_3$  and  $\text{SmCl}_3$  Raman spectra solvated in the molten LiCl-KCl eutectic are nearly identical.  $\text{CeCl}_3$  solvated in the molten LiCl-KCl does not produce a fluorescence feature in the 800-1400  $\text{cm}^{-1}$  region, while  $\text{SmCl}_3$  clearly fluoresces. The mixed analyte spectra exhibit a moderate level of fluorescence. The  $O_n$  Raman modes on top of one another in the 0-400  $\text{cm}^{-1}$  region, requiring improvement of the signal-to-noise (STN) ratio associated with the SPEC system before deconvolution methods can be developed. The development of deconvolution protocols will be nontrivial as Raman mode manifestation is dependent on analyte identity and concentration.

## 7.2 LiCl-KCl-ZrCl<sub>4</sub> Raman Spectroscopy

Zirconium alloy is the most common fuel cladding material utilized in existing LWR fleets worldwide [109, 110]. The cladding will be solvated in the molten LiCl-KCl eutectic as part of the pyrochemical reprocessing scheme if LWR fuel is accommodated. Understanding the nature of zirconium dissolution in the molten electrolyte is therefore important, and a preliminary investigation into the nature of that solvation was conducted using the SPEC system. Polarized (VV) and depolarized (HV) Raman spectra of ZrCl<sub>4</sub> solvated in the molten LiCl-KCl eutectic are overlaid in Figure 63.

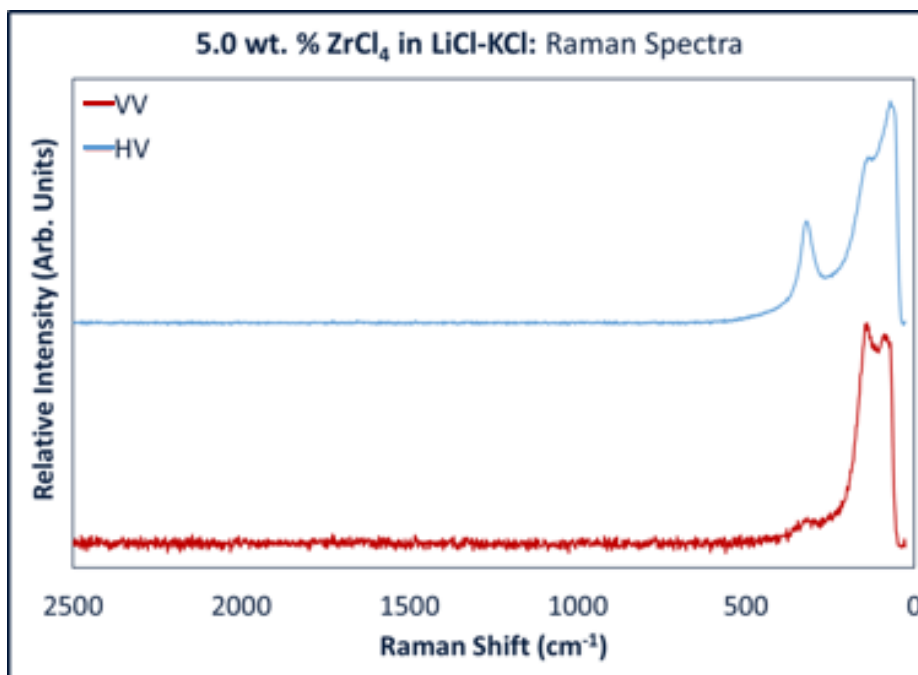


**Figure 63** Polarized (VV) and depolarized (HV) in situ Raman spectra of ZrCl<sub>4</sub> solvated in the molten LiCl-KCl eutectic

Assignment of Raman modes will require further coordination analysis. It has been reported that Th<sup>4+</sup> complexes predominantly as [ThCl<sub>6</sub>]<sup>2-</sup> but achieves equilibrium with an alternative [ThCl<sub>7</sub>]<sup>3-</sup> complex [111]. The [ThCl<sub>6</sub>]<sup>2-</sup> complex exhibits an O<sub>h</sub> symmetry consistent with the lanthanides reported in this dissertation. The [ThCl<sub>7</sub>]<sup>3-</sup> complex forms

a pentagonal bipyramid complex [111]. Whether or not  $ZrCl_4$  complexes and reaches equilibrium in the same manner will require further investigation using coordination analyses like XAFS.



## Chapter 8 Discussion of Results


### 8.1 Evaluation of Spectroelectrochemical System

The electroanalytical and spectroscopic components of the SPEC both produced promising results that have the potential to augment NMA in high temperature molten salt systems. The individual components of the SPEC system each offer their own advantages and disadvantages in terms of deployment for NMA in molten salt systems.

The electroanalytical CV method has the potential to produce real-time quantitative data concerning analyte concentration in molten salt for NMA. The continued development of an accurate diffusion coefficient library remains the prerequisite for deployment of CV for real-time NMA. The diffusion coefficient library must continue to incorporate high concentration effects, mixed analyte scenarios, system resistance, and alternative diffusion mechanisms. A drawback of CV is the need for improved understanding of valence state speciation and dissolved analyte complex formation before diffusion coefficients and migration contributions can be determined with higher certainty. Furthermore, the reference electrodes used for CV require at least five hours to equilibrate in the system, presenting a challenge to online, real-time monitoring goals. The CV method presents a more promising and immediate path to mixed-analyte application than the Raman spectroscopy unit as the standard reduction potentials of dissolved analytes are more discernable than their respective Raman modes.

The Raman spectroscopy method produces qualitative data than elucidates the complexation of analytes when solvated in molten salt. These insights can provide

information regarding valence state which is important for both electrochemical processing of nuclear material and may help elucidate the remaining questions associated with CV disproportionation and migration. Solvated analytes are more difficult to deconvolute using Raman spectroscopy compared to CV because the analytes' respective spectra are extremely similar. Peaks associated with the  $O_h$  complex's vibration modes fall in the same area. The Raman unit requires the improvement of signal-to-noise ratio before deconvolution protocols can be developed. Table 14 summarizes the advantages, disadvantages, and synergies associated with the SPEC system's components.

	<b><u>CV</u></b>	<b><u>Synergies</u></b>	<b><u>Raman</u></b>
<b><u>Pros</u></b>	<ul style="list-style-type: none"> <li>Quantitative concentration profiles</li> <li>Multi-analyte resolution</li> </ul>		<ul style="list-style-type: none"> <li>Qualitative process monitoring</li> <li>Speciation insights</li> </ul>
<b><u>Cons</u></b>	<ul style="list-style-type: none"> <li>Lack of clarity regarding dissolved analyte speciation</li> </ul>		<ul style="list-style-type: none"> <li>Multi-analyte, identical valence state systems difficult to analyze</li> </ul>

**Table 14** Summary of advantages, disadvantages, and synergies of the SPEC system's analytical components

Table 14 illustrates the ways in which the SPEC system's individual components can maintain a synergistic relationship to address one another's weaknesses. The uncertainties associated with speciation during CV analysis may be addressed using Raman spectroscopy. Similarly, the deconvolution and quantitative weaknesses of Raman spectroscopy may be addressed by CV's strengths.

## 8.2 Nuclear Material Accountancy Applications

Chapter 6 introduces a brief and process specific application the SPEC system for NMA in the pyrochemical reprocessing of UNF. The SPEC system was demonstrated to produce information regarding solvent content and alternative chemistry formation in the molten LiCl-KCl eutectic. There are a number of molten salt engineering-scale applications that would benefit from the continued development of the SPEC system for NMA. Fueled molten salt reactors will contain a molten salt matrix that serves as both the heat transfer medium and nuclear fuel solvent [23]. Once fully developed, the SPEC system has the potential to provide real-time data concerning fuel concentration in the salt, formation of fission products, and burnup in real-time. This information would ensure accurate NMA logs can be produced to record SNM concentrations and reactor operation history. If a leak forms and SNM begins to leak from containment vessels or heat exchanger loops, the SPEC system could potentially alert operators to such an event and prevent the loss of SNM in substantial volume. Furthermore, if leaks introduce moisture or oxygen impurities to the fueled salt, the SPEC system can detect the formation of alternative chemistries *in situ*.

Alternative chemistry formation is a concern in the domestic nuclear weapons complex as well. Oxide and oxychloride formation are common when reducing plutonium in molten chloride electrolytes [18, 93, 106]. The formation of these alternative chemistries affects process efficiency but can present a potential for SNM precipitation and holdup in the refining vessels. The SPEC system has shown the capability to detect

oxychlorides *in situ*, and the detection of alternative chemistry formation in real-time would help account for holdup in these processes and improve the accuracy of NMA logs associated with those processes.

There are many molten chemistries that may benefit from the SPEC system's deployment as an NMA technique. Plutonium electrorefining in molten  $\text{CaCl}_2$  may benefit from the voltammetry component so that plutonium concentration and americium decay daughter buildup can be monitored in real-time. Uranium electrorefining in the  $\text{LiCl-KCl}$  system may benefit in the same manner. Both of these electrorefining schemes are essential unit operations in the United States' nuclear weapons complex. The Raman component of the SPEC system may help elucidate the coordination chemistry characteristics of dissolved analytes in the same systems.

Since the SPEC system conducts analyses in a nondestructive manner, it can greatly reduce the time and costs associated with NMA for the pyrochemical reprocessing of UNF. Each unit operation of the pyrochemical reprocessing scheme is discrete. This discrete nature means the products from one operation would most likely be removed and individually transported to their next operation. Destructive analysis of these transported samples would not only be time consuming, but also expose radiological control technicians to substantial radiation dosage. A developed SPEC system could be installed on the necessary unit operations and produce data in real-time. The electroanalytical and spectroscopic components can both be operated in a remote fashion using basic instrument controls, reducing both the time and dosage associated with producing NMA logs in this processing scheme.

## Chapter 9 Conclusions and Future Work

### 9.1 Conclusions

An electroanalytical system for the analysis of high temperature LiCl-KCl molten salt was constructed and tested using samarium and cerium as the solvated analytes of interest. CV analysis produced relatively repeatable data over a broad concentration range of dissolved analyte. The uncertainty associated with low concentrations was attributed to the formation of oxychloride species that are quasi-soluble in nature. The reported diffusion coefficients for trivalent samarium and cerium were relatively consistent with the previously published literature and exhibited similar magnitudes of variation.

Variation in electrochemical data was attributed to the many variables affecting diffusion coefficient calculations: WE surface area, alternative diffusion mechanism, and uncompensated resistance. Multi-analyte CV studies are promising in that they clearly separate redox features associated with different analytes when their standard reduction potential are relatively separated. Further evaluation is required to determine CV effectiveness when analyte standard reduction potentials overlap.

A fiber-based Raman system was coupled to the electroanalytical apparatus to produce a spectroelectrochemical (SPEC) suite. The SPEC system allows for simultaneous electrochemical and Raman spectroscopic investigations to be conducted, and preliminary engineering concerns regarding Raman objective working distance and cooling were addressed. The SPEC system was employed for the study of samarium ion

chemistry in molten LiCl-KCl eutectic. The trivalent complex symmetry and spectra were indicative of octahedral  $\text{SmCl}_6^{3-}$  complexes. Chemical reduction experiments produced spectra similar to those reported for divalent neodymium in the literature. To our knowledge, this is the first Raman spectrum of divalent samarium in molten LiCl-KCl eutectic. The divalent vibration modes disappeared one hour after their initial manifestation, suggesting spontaneous reactions associated with  $\text{Sm}^{2+}$  as the literature suggests. Electrochemical reduction experiments produced Raman spectra dissimilar to the chemically reduced spectra. This discrepancy is likely due to the variation in  $\text{SmCl}_3$  concentration but remains unclear. Raman spectra of  $\text{CeCl}_3$  in molten LiCl-KCl was found to be identical to that obtained from  $\text{SmCl}_3$  in molten LiCl-KCl except for the fluorescence features. Spectra obtained from mixed analytes (mixture of Sm and Ce in molten LiCl-KCl) showed that differentiating mixed analytes will require additional investment in lowering the focal length of fiber probes and engineering high temperature cooling methods. The location of vibration modes associated with different analytes are very similar and can also be affected by  $\text{Li}^+$  concentration due to its large polarizing power.

The coupled SPEC system was shown to have promising application for NMA in high temperature molten salt, including the formation of alternative chemistries, such as oxychloride compounds. The individual analytical components of the SPEC system each presented their own advantages and disadvantages. However, the two analytical methods (CV and Raman spectroscopy) form a synergistic relationship that accounts for each other's weaknesses and presents a promising path forward for chemical-based sensing and NMA using the SPEC system.

## 9.2 Future Work

Avenues for future work concerning this dissertation can be separated into two major categories: electroanalytical and spectroscopic methodology.

### 1.) Electroanalytical methodology

- a. The Randles-Sevcik relationship is a numerical solution to Fick's 2<sup>nd</sup> Law that requires adjustment to account for the following phenomena: cylindrical diffusion, migration, and convection.
- b. Positive feedback (PF) resistance compensation must be implemented into the experimental protocols. PF compensation is more effective than the traditional *ex post facto* method as it will address any concerns that system resistance is a function of analyte identity, analyte concentration, or applied potential.
- c. A WE with a fixed surface area must be engineered to reduce the uncertainty associated with calculating current response density.

### 2.) Spectroscopic methodology

- a. The continued investigation of valence state implications on complexing behavior of solvated analytes will help address uncertainties associated with migration correction of electroanalytical results.
- b. Improvements in signal-to-noise ratio must be made to establish a better understanding of spectroscopic characteristics of species at electrode surfaces during electrorefining operations. The continued development of

these protocols will require working distances to decrease, probe heating to be further mitigated, and higher resolution spectrometer implementation.

Even with above improvements, the system may have challenges as the Raman features from several analytes might look very similar (like Sm and Ce) and the effect of salt concentration may be more (in terms of peak positions) than the peaks from various analytes. However, future work avenues summarized above will allow for the continued development of the SPEC system and consideration in deployment in engineering-scale operations using high temperature molten salt for nuclear material processing or power production purposes.



## References

- [1] Safely Managing Used Nuclear Fuel: Fact Sheet, Nuclear Energy Institute, 2016. <https://www.nei.org/resources/fact-sheets/safely-managing-used-nuclear-fuel>
- [2] J.E. Doyle, Nuclear Safeguards, Security, and Nonproliferation, Elsevier, 30 Corporate Drive, Suite 400, Burlington MA 01803, USA. Linacre House, Jordan Hill, Oxford OX2 8DP, UK, 2008.
- [3] D.H. Joyner, Interpreting the Nuclear Non-Proliferation Treaty, 1<sup>st</sup> ed., Oxford University Press, New York, USA, 2011.
- [4] N. McCarthy, The Countries With The Biggest Nuclear Arsenals, 2015. <https://www.statista.com/chart/3653/the-countries-with-the-biggest-nuclear-arsenals/>.
- [5] N. Tsoulfanidis, The Nuclear Fuel Cycle, American Nuclear Society, 555 North Kensington Avenue; La Grange Park, Illinois 60526 USA, 2013. ISBN 978-0894484605
- [6] IAEA Safeguards: Stemming the Spread of Nuclear Weapons, IAEA 2001 Annual Report "Nuclear Security & Safeguards" 43(4) (2001) 4.
- [7] Guidance for States Implementing Comprehensive Safeguards Agreements and Additional Protocols, International Atomic Energy Agency Service Series (21) (2016) 102.
- [8] I.A.E. AGENCY, Climate Change and Nuclear Power 2018, International Atomic Energy Agency, Vienna, 2018. <https://www.iaea.org/publications/13395/climate-change-and-nuclear-power-2018>
- [9] S. Saito, Role of nuclear energy to a future society of shortage of energy resources and global warming, Journal of Nuclear Materials 398(1-3) (2010) 1-9.
- [10] B. Christiansen, D. Serrano, J. Serp, R. Malbeck, J.P. Glatz, Advanced reprocessing technologies, Technical Specialists Meeting on 'Inno-Innovative nuclear fuel cycles technologies, which would potentially meet user requirements in the area of economy, safety, environment and waste, proliferation resistance and cross-cutting issues', IAEA, Vienna (2003). <https://www.iaea.org/sites/default/files/inpro0812.pdf>
- [11] J. Randolph, G.M. Masters, Energy for Sustainability: Technology, Planning, Policy, Island Press, Washington, D.C., 2008. ISBN 978-1597261036

- [12] P.N. Alekseev, V.V. Ignatiev, S.A. Konakov, L.I. Menshikov, N.N. Ponomarev-Stepnoi, V.N. Prusakov, V.A. Stukalov, S.A. Subbotine, Harmonization of fuel cycles for nuclear energy system with the use of molten salt technology, *Nuclear engineering and design* 173(1) (1997) 151-158.
- [13] T.L. Burr, C.A. Coulter, J. Howell, L.E. Wangen, Solution monitoring: quantitative and qualitative benefits to nuclear safeguards, *Journal of nuclear science and technology* 40(4) (2003) 256-263.
- [14] M.T. Cook, Hybrid K-edge Densitometry as a Method for Materials Accountancy Measurements in Pyrochemical Reprocessing. Ph.D. Dissertation. University of Tennessee, Knoxville, 2015.
- [15] P.L. Lafreniere, D.S. Rappleye, R.O. Hoover, M.F. Simpson, E.D. Blandford, Demonstration of Signature-Based Safeguards for Pyroprocessing as Applied to Electrorefining and the Ingot Casting Process, *Nuclear Technology* 189(2) (2015) 173-185.
- [16] N.A. Smith, J.A. Savina, M.A. Williamson, Application of Laser Induced Breakdown Spectroscopy to Electrochemical Process Monitoring of Molten Chloride Salts. Poster presented at: International Atomic Energy Agency (IAEA) Symposium on International Safeguards, 2014.
- [17] R. Natarajan, Reprocessing of spent nuclear fuel in India: Present challenges and future programme, *Progress in Nuclear Energy* 101 (2017) 118-132.
- [18] L.J. Mullins, J.A. Leary, A.N. Morgan, W.J. Maraman, Plutonium electrorefining, *Industrial & Engineering Chemistry Process Design and Development* 2(1) (1963) 20-24.
- [19] K.E. Dodson, Molten salt extraction (MSE) of americium from plutonium metal in CaCl<sub>2</sub>-KCl-PuCl<sub>3</sub> and CaCl<sub>2</sub>-PuCl<sub>3</sub> salt systems, LLNL UCRL-LR-110870 (1992).
- [20] C.W. Forsberg, P.F. Peterson, H. Zhao, An advanced molten salt reactor using high-temperature reactor technology, *Proceedings of ICAPP*. Vol. 4. 2004, pp. 13-17.
- [21] M.K.M. Ho, G.H. Yeoh, G. Braoudakis, Molten salt reactors, *Materials and Processes for Energy*, Formatex (2013) 761-768.
- [22] E. Merle-Lucotte, D. Heuer, M. Allibert, V. Ghetta, C. Le Brun, R. Brissot, E. Liatard, L. Mathieu, The thorium molten salt reactor: Launching the thorium cycle while closing the current fuel cycle, *European Nuclear Society*, pp. 48-53.

- [23] D.E. Holcomb, G.F. Flanagan, B.W. Patton, J.C. Gehin, R.L. Howard, T.J. Harrison, Fast spectrum molten salt reactor options, ORNL/TM-2011/105 (2011).
- [24] D. Ludwig, L. Olson, K. Sridharan, M. Anderson, T. Allen, High temperature electrochemistry of molten fluoride salt for measurement of dissolved chromium, Corrosion Engineering, Science and Technology 46(4) (2011) 360-364.
- [25] C.E. Till, Y.I. Chang, Plentiful energy: the story of the integral fast reactor, CreateSpace Independent Publisher, (2011) 1-394. ISBN 978-1466384606
- [26] K. Sridharan, T. Allen, M. Anderson, M. Simpson, Thermal Properties of LiCl-KCl Molten Salt for Nuclear Waste Separation, USDOE (United States); Nuclear Energy University Programs (United States), United States of America, 2012.
- [27] J.L. Willit, W.E. Miller, J.E. Battles, Electrorefining of uranium and plutonium — A literature review, Journal of Nuclear Materials 195(3) (1992) 229-249.
- [28] C.C. McPheeters, R.D. Pierce, T.P. Mulcahey, The Technology of the Integral Fast Reactor and its Associated Fuel Cycle Application of the pyrochemical process to recycle of actinides from LWR spent fuel, Progress in Nuclear Energy 31(1) (1997) 175-186.
- [29] M.A. Williamson, J.L. Willit, Pyroprocessing flowsheets for recycling used nuclear fuel, Nuclear Engineering and Technology 43(4) (2011) 329-334.
- [30] J.P. Ackerman, Chemical basis for pyrochemical reprocessing of nuclear fuel, Industrial & Engineering Chemistry Research 30(1) (1991) 141-145.
- [31] J. Uhlir, Pyrochemical reprocessing technology and molten salt transmutation reactor systems, Nuclear Energy Agency, Organisation for Economic Co-operation and Development, p. 73. <https://www.oecd-nea.org/science/pubs/2001/2988-pyrochemical-separations.pdf#page=76>
- [32] H.P. Nawada, K. Fukuda, Role of pyro-chemical processes in advanced fuel cycles, Journal of Physics and Chemistry of Solids 66(2-4) (2005) 647-651.
- [33] U. Gat, J.R. Engel, Non-proliferation attributes of molten salt reactors, Nuclear engineering and design 201(2) (2000) 327-334.

- [34] H. Lee, G.-I. Park, J.-W. Lee, K.-H. Kang, J.-M. Hur, J.-G. Kim, S. Paek, I.-T. Kim, I.-J. Cho, Current Status of Pyroprocessing Development at KAERI, Science and Technology of Nuclear Installations 2013 (2013) 11.
- [35] T. Inoue, H. Tanaka, Recycling of actinides produced in LWR and FBR fuel cycles by applying pyrometallurgical process. International conference on future nuclear systems. Challenge towards second nuclear era with advanced fuel cycles. Proceedings. 1997.
- [36] T. Koyama, K. Kinoshita, T. Inoue, M. Ougier, J.-P. Glatz, L. Koch, Demonstration of pyrometallurgical processing for metal fuel and HLW, pp. 9-13.
- [37] J. Zhang, Safeguards in Pyroprocessing: an Integrated Model Development and Measurement Data Analysis, The Ohio State University, Columbus, OH (United States). Research Foundation, 2017.
- [38] M.M. Tylka, J.L. Willit, J. Prakash, M.A. Williamson, Method Development for Quantitative Analysis of Actinides in Molten Salts, Journal of The Electrochemical Society 162(9) (2015) H625-H633.
- [39] A.J. Bard, L.R. Faulkner, J. Leddy, C.G. Zoski, Electrochemical methods: fundamentals and applications, wiley New York 1980. ISBN 978-0471043720
- [40] M. Iizuka, T. Inoue, O. Shirai, T. Iwai, Y. Arai, Application of normal pulse voltammetry to on-line monitoring of actinide concentrations in molten salt electrolyte, Journal of Nuclear Materials 297(1) (2001) 43-51.
- [41] S. Paek, T.-J. Kim, G.-Y. Kim, D.-H. Ahn, S. Kim, Y. Jung, Determination of Lanthanide Ions in a LiCl-KCl Molten Salt by Square Wave Voltammetry, International Journal of Electrochemical Science 9(9) (2014) 4925-4931.
- [42] Z.-h. Wang, D. Rappleye, M.F. Simpson, Voltammetric Analysis of Mixtures of Molten Eutectic LiCl-KCl Containing LaCl<sub>3</sub> and ThCl<sub>4</sub> for Concentration and Diffusion Coefficient Measurement, Electrochimica Acta 191 (2016) 29-43.
- [43] C. Zhang, D. Rappleye, M.F. Simpson, Development and Optimization of Voltammetry for Real Time Analysis of Multi-Component Electrorefiner Salt, ECS Transactions 75(15) (2016) 95-103.

- [44] D. Rappleye, S.-M. Jeong, M. Simpson, Electroanalytical measurements of binary-analyte mixtures in molten LiCl-KCl eutectic: gadolinium (III)-and lanthanum (III)-chloride, *Journal of The Electrochemical Society* 163(9) (2016) B507-B516.
- [45] D. Rappleye, M.F. Simpson, Application of the rotating cylinder electrode in molten LiCl-KCl eutectic containing uranium (III)-and magnesium (II)-chloride, *Journal of Nuclear Materials* 487 (2017) 362-372.
- [46] D. Rappleye, K. Teaford, M.F. Simpson, Investigation of the effects of uranium (III)-chloride concentration on voltammetry in molten LiCl-KCl eutectic with a glass sealed tungsten electrode, *Electrochimica Acta* 219 (2016) 721-733.
- [47] G. Cordoba, C. Caravaca, An electrochemical study of samarium ions in the molten eutectic LiCl + KCl, *Journal of Electroanalytical Chemistry* 572(1) (2004) 145-151.
- [48] A. Samin, Z. Wang, E. Lahti, M. Simpson, J. Zhang, Estimation of key physical properties for LaCl<sub>3</sub> in molten eutectic LiCl-KCl by fitting cyclic voltammetry data to a BET-based electrode reaction kinetics model, *Journal of Nuclear Materials* 475 (2016) 149-155.
- [49] Y. Castrillejo, C. de la Fuente, M. Vega, F. de la Rosa, R. Pardo, E. Barrado, Cathodic behaviour and oxoacidity reactions of samarium (III) in two molten chlorides with different acidity properties: The eutectic LiCl-KCl and the equimolar CaCl<sub>2</sub>-NaCl melt, *Electrochimica Acta* 97 (2013) 120-131.
- [50] J. Zhang, Electrochemistry of actinides and fission products in molten salts—Data review, *Journal of Nuclear Materials* 447(1–3) (2014) 271-284.
- [51] C. Caravaca, G. de Córdoba, M.J. Tomás, M. Rosado, Electrochemical behaviour of gadolinium ion in molten LiCl-KCl eutectic, *Journal of Nuclear Materials* 360(1) (2007) 25-31.
- [52] M.M. Tylka, J.L. Willit, J. Prakash, M.A. Williamson, Application of voltammetry for quantitative analysis of actinides in molten salts, *Journal of The Electrochemical Society* 162(12) (2015) H852-H859.
- [53] K.B. Oldham, Analytical expressions for the reversible Randles-Sevcik function, *Journal of Electroanalytical Chemistry and Interfacial Electrochemistry* 105(2) (1979) 373-375.

- [54] M.F. Simpson, Developments of Spent Nuclear Fuel Pyroprocessing Technology at Idaho National Laboratory, Idaho National Laboratory, INL/EXT-12-25124, Idaho Falls, ID, USA (2012).
- [55] S.P. Fusselman, J.J. Roy, D.L. Grimmett, L.F. Grantham, C.L. Krueger, C.R. Nabelek, T.S. Storvick, T. Inoue, T. Hijikata, K. Kinoshita, Thermodynamic properties for rare earths and americium in pyropartitioning process solvents, *Journal of the Electrochemical Society* 146(7) (1999) 2573-2580.
- [56] Y. Castrillejo, M.R. Bermejo, E. Barrado, A.M. Martinez, P.D. Arocas, Solubilization of rare earth oxides in the eutectic LiCl–KCl mixture at 450° C and in the equimolar CaCl<sub>2</sub>–NaCl melt at 550° C, *Journal of Electroanalytical Chemistry* 545 (2003) 141-157.
- [57] K.C. Marsden, B. Pesic, Evaluation of the electrochemical behavior of CeCl<sub>3</sub> in molten LiCl–KCl eutectic utilizing metallic Ce as an anode, *Journal of The Electrochemical Society* 158(6) (2011) F111-F120.
- [58] M. Iizuka, Diffusion Coefficients of Cerium and Gadolinium in Molten LiCl–KCl, *Journal of the Electrochemical Society* 145(1) (1998) 84-88.
- [59] D. Yamada, T. Murai, K. Moritani, T. Sasaki, I. Takagi, H. Moriyama, K. Kinoshita, H. Yamana, Diffusion behavior of actinide and lanthanide elements in molten salt for reductive extraction, *Journal of Alloys and Compounds* 444–445 (2007) 557-560.
- [60] K.E. Johnson, J.R. Mackenzie, J.N. Sandoe, Spectra of samarium (II), europium (II), and ytterbium (II) in molten lithium chloride–potassium chloride, *Journal of the Chemical Society A: Inorganic, Physical, Theoretical* (1968) 2644-2647.
- [61] Y. Castrillejo, P. Fernández, J. Medina, P. Hernández, E. Barrado, Electrochemical extraction of samarium from molten chlorides in pyrochemical processes, *Electrochimica Acta* 56(24) (2011) 8638-8644.
- [62] S.-E. Bae, T.S. Jung, Y.-H. Cho, J.-Y. Kim, K. Kwak, T.-H. Park, Electrochemical Formation of Divalent Samarium Cation and Its Characteristics in LiCl–KCl Melt, *Journal of the ACS, Inorganic chemistry*, 57(14), 2018.
- [63] J.R. Ferraro, *Introductory raman spectroscopy*, Elsevier 2003. ISBN 978-0122539909
- [64] D.C. Harris, M.D. Bertolucci, *Symmetry and spectroscopy: an introduction to vibrational and electronic spectroscopy*, Courier Corporation 1989. ISBN 978-0486661445

[65] D.C. Harris, Quantitative chemical analysis, 7th ed., W.H. Freeman and Co, New York, NY, 2007.

[66] G.J. Janz, D.W. James, Raman spectra and ionic interactions in molten nitrates, *The Journal of Chemical Physics* 35(2) (1961) 739-745.

[67] G.J. Janz, Y. Mikawa, D.W. James, Light Source, Excitation, and High Temperature Cell Assembly For Raman Spectroscopy, *Appl. Spectrosc.* 15(2) (1961) 47-52.

[68] A. Chrissanthopoulos, G.N. Papatheodorou, Probing the structure of GdCl<sub>3</sub>-KCl melt mixtures by electronic absorption spectroscopy of the hypersensitive f<sub>7</sub> ← f<sub>6</sub> transitions of Ho<sup>3+</sup> and by Raman spectroscopy, *Physical Chemistry Chemical Physics* 2(16) (2000) 3709-3714.

[69] V. Dracopoulos, B. Gilbert, B. Brrensen, G.M. Photiadis, G.N. Papatheodorou, Vibrational modes and structure of rare earth halide-alkali halide binary melts YBr<sub>3</sub>-ABr (A= Li, K, Cs) and YF<sub>3</sub>-KF, *Journal of the Chemical Society, Faraday Transactions* 93(17) (1997) 3081-3088.

[70] G.N. Papatheodorou, Raman spectroscopic studies of yttrium (III) chloride-alkali metal chloride melts and of Cs<sub>2</sub>NaYCl<sub>6</sub> and YCl<sub>3</sub> solid compounds, *The Journal of Chemical Physics* 66(7) (1977) 2893-2900.

[71] T. Uda, T. Fujii, Y. Iwadate, A. Uehara, H. Yamana, Raman Spectroscopic Study of Rare Earth Chlorides in Alkali Chloride Eutectic Melts, *Zeitschrift für anorganische und allgemeine Chemie* 639(5) (2013) 765-769.

[72] V.M. Rodríguez Betancourt, Raman spectroscopic study of high temperature rare earth metal-rare earth halide solutions: Ln-Ln<sub>x</sub>3- and Ln<sub>x</sub>2-Ln<sub>x</sub>3-(Li<sub>x</sub>-K<sub>x</sub>)Eu systems (Ln: Nd, Ce; x: Cl, I), ProQuest Dissertations Publishing U6, 2004.

[73] V.M. Rodriguez-Betancourt, D. Nattland, Raman spectroscopic study of mixed valence neodymium and cerium chloride solutions in eutectic LiCl-KCl melts, *Physical Chemistry Chemical Physics* 7(1) (2005) 173-179.

[74] A. Merwin, W.C. Phillips, M.A. Williamson, J.L. Willit, P.N. Motsegood, D. Chidambaram, Presence of Li Clusters in Molten LiCl-Li, *Scientific Reports* 6 (2016) 25435.

- [75] W. Phillips, A. Merwin, V. Singh, D. Chidambaram, Characterization of the Electrochemical Behavior of a Li-Bi Reference Electrode for the Molten LiCl-Li, The Electrochemical Society, pp. 3441-3441.
- [76] V. Singh, D. Chidambaram, In Situ Raman Spectroscopy for Nuclear Material Monitoring in Molten Salt Systems, The Electrochemical Society, pp. 765-765.
- [77] V. Singh, D. Chidambaram, Electrochemical Studies of Lanthanide Chlorides in Molten Eutectic LiCl-KCl, Materials Science and Technology 2016, ASM International, Salt Lake City, Utah, 2016.
- [78] V. Singh, D. Chidambaram, Electrochemical Techniques for Nuclear Safeguards in Molten Salt, 146th Annual Meeting of the Minerals, Metals and Materials Society, ASM International, San Diego, California, 2017.
- [79] V. Singh, D. Chidambaram, Electrochemical Behavior of Samarium in Molten LiCl-KCl, Abstract 3519 in: T.E. Society (Ed.) Pacific Rim International Meeting on Electrochemistry, The Electrochemical Society, Honolulu, HI, 2016, pp. 3519-3519.
- [80] K. Summers, Corrosion Behavior Of Potential Structural Materials For Use In Nitrate Salts Based Solar Thermal Power Plants, M.S. Thesis, University of Nevada, Reno 2016.
- [81] H.R. Chandrasekhar, G. Bhattacharya, R. Migoni, H. Bilz, Infrared and Raman spectra and lattice dynamics of the superionic conductor  $\text{Li}_3\text{N}$ , Physical Review B 17(2) (1978) 884-893.
- [82] Y. Iwadate, 2 - Raman Spectroscopy and Pulsed Neutron Diffraction of Molten Salt Mixtures Containing Rare-Earth Trichlorides: Trial Approaches from Fundamentals to Pyrochemical Reprocessing A2 - Lantelme, Frédéric, in: H. Groult (Ed.), Molten Salts Chemistry, Elsevier, Oxford, 2013, pp. 17-31.
- [83] A. Merwin, Material Interactions with Molten LiCl-Li<sub>2</sub>O-Li, Materials Science and Engineering, Ph.D. Dissertation, University of Nevada, Reno, Reno, NV, 2016, p. 241.
- [84] V. Singh, D. Chidambaram, In Situ Raman Spectroscopy for Nuclear Material Monitoring in Molten Salt Systems, Abstract 765 in Corrosion Session, 232nd Meeting of the Electrochemical Society, ECS, National Harbor, MD USA, 2017, p. 765.



- [85] W.J. Glover, P.A. Madden, Raman spectra of ionic liquids: a simulation study of  $\text{LaCl}_3$  and its mixtures with alkali chlorides, *The Journal of chemical physics* 121(15) (2004) 7293-7303.
- [86] Y. Okamoto, S. Suzuki, H. Shiwaku, A. Ikeda-Ohno, T. Yaita, P.A. Madden, Local coordination about  $\text{La}^{3+}$  in molten  $\text{LaCl}_3$  and its mixtures with alkali chlorides, *The Journal of Physical Chemistry A* 114(13) (2010) 4664-4671.
- [87] K. Fukasawa, A. Uehara, T. Nagai, T. Fujii, H. Yamana, Electrochemical and spectrophotometric study on neodymium ions in molten alkali chloride mixtures, *Journal of Alloys and Compounds* 509(16) (2011) 5112-5118.
- [88] V. Singh, D. Chidambaram, *Electrochemical Studies of Lanthanide Chlorides in Molten Eutectic LiCl-KCl*, Materials Science and Technology 2016, ASM International, Salt Lake City, Utah, 2016.
- [89] V. Singh, D. Chidambaram, *Electrochemical Techniques for Nuclear Safeguards in Molten Salt*, 146th Annual Meeting of the Minerals, Metals and Materials Society, ASM International, San Diego, California, 2017.
- [90] V. Singh, D. Chidambaram, *Electrochemical Behavior of Samarium in Molten LiCl-KCl*, Abstract 3519 in: T.E. Society (Ed.) Pacific Rim International Meeting on Electrochemistry, The Electrochemical Society, Honolulu, HI, 2016, pp. 3519-3519.
- [91] A. Merwin, W.C. Phillips, M.A. Williamson, J.L. Willit, P.N. Motsegood, D. Chidambaram, Presence of Li Clusters in Molten LiCl-Li, *Scientific Reports* 6 (2016) 25435.
- [92] S. Rayaprolu, D. Chidambaram, Electrochemical deposition of terbium from molten salts, *ECS Transactions* 58(45) (2014) 51-66.
- [93] D. Lambertin, S. Ched'homme, G. Bourgès, S. Sanchez, G. Picard, Plutonium chemical properties in NaCl-KCl and CaCl<sub>2</sub> at 1073K, *Journal of Nuclear Materials* 341(2-3) (2005) 124-130.
- [94] D. Yoon, S. Phongikaroon, Measurement and analysis of exchange current density for U/U<sup>3+</sup> reaction in LiCl-KCl eutectic salt via various electrochemical techniques, *Electrochimica Acta* 227 (2017) 170-179.

- [95] M.F. Simpson, Projected salt waste production from a commercial pyroprocessing facility, *Science and Technology of Nuclear Installations* 2013 (2013). <https://www.hindawi.com/journals/stni/2013/945858/>
- [96] C. Zhang, J. Wallace, M.F. Simpson, Electrochemical measurement of high concentrations of  $\text{UCl}_3$  and  $\text{GdCl}_3$  in molten  $\text{LiCl-KCl}$  eutectic, *Electrochimica Acta* 290 (2018) 429-439.
- [97] N.C. Hoyt, J.L. Willit, M.A. Williamson, Communication—Quantitative Voltammetric Analysis of High Concentration Actinides in Molten Salts, *Journal of The Electrochemical Society* 164(2) (2017) H134-H136.
- [98] D.-H. Kim, S.-E. Bae, T.-H. Park, J.-Y. Kim, C.-W. Lee, K. Song, Real-time monitoring of metal ion concentration in  $\text{LiCl-KCl}$  melt using electrochemical techniques, *Microchemical Journal* 114 (2014) 261-265.
- [99] K.L. Murty, I. Charit, Structural materials for Gen-IV nuclear reactors: Challenges and opportunities, *Journal of Nuclear Materials* 383(1) (2008) 189-195.
- [100] T.J. Kim, Y. Jung, S.H. Kim, S.W. Paek, D.H. Ahn, Elucidation of Electrode Reaction of  $\text{EuCl}_3$  in  $\text{LiCl-KCl}$  Eutectic Melts through CV Curve Analysis, *BULLETIN OF THE KOREAN CHEMICAL SOCIETY* 32(3) (2011) 863-866.
- [101] H.C. Eun, Y.Z. Cho, S.M. Son, T.K. Lee, H.C. Yang, I.T. Kim, H.S. Lee, Recycling of  $\text{LiCl-KCl}$  eutectic based salt wastes containing radioactive rare earth oxychlorides or oxides, *Journal of Nuclear Materials* 420(1) (2012) 548-553.
- [102] H.C. Eun, J.H. Choi, N.Y. Kim, T.K. Lee, S.Y. Han, S.A. Jang, T.J. Kim, H.S. Park, D.H. Ahn, A study of separation and solidification of group II nuclides in waste salt delivered from the pyrochemical process of used nuclear fuel, *Journal of Nuclear Materials* 491 (2017) 149-153.
- [103] S.J. Zygmunt, C.F.V. Mason, W.K. Hahn, The US plutonium materials conversion program in Russia, (2000). <https://inis.iaea.org/collection/NCLCollectionStore/Public/32/033/32033985.pdf>
- [104] V. Singh, D. Chidambaram, In Situ Raman Spectroscopy for Nuclear Material Monitoring in Molten Salt Systems, Abstract 765 in Corrosion Session, 232nd Meeting of the Electrochemical Society, ECS, National Harbor, MD USA, 2017, p. 765.

- [105] V.J. Singh, C.D. Bruneau, D. Chidambaram, In situ Raman spectroscopy of samarium ions in molten LiCl-KCl eutectic, (2019). <https://ecsarxiv.org/qpsr3/>
- [106] J.-F. Vigier, A. Laplace, C. Renard, M. Miguiritchian, F. Abraham, Uranium (III)-Plutonium (III) co-precipitation in molten chloride, *Journal of Nuclear Materials* 499 (2018) 394-400.
- [107] H. Haeuseler, Normal coordinate analysis of lanthanide oxychlorides and oxybromides with Matlockite-type structure, *Spectrochimica Acta Part A: Molecular Spectroscopy* 38(4) (1982) 505-507.
- [108] G.D. Del Cul, S.E. Nave, G.M. Begun, J.R. Peterson, Raman spectra of tetragonal lanthanide oxychlorides obtained from polycrystalline and single-crystal samples, *Journal of Raman spectroscopy* 23(5) (1992) 267-272.
- [109] C. Greene, A Snapshot of U.S. Spent Fuel Management Policy and Status, *Journal of Nuclear Materials Management* 44(6) (2016) 7.
- [110] C. Greene, Spent Fuel Management Issues Highlighted at 31st Spent Fuel Seminar, *Journal of Nuclear Materials Management* 44(4) (2016) 9.
- [111] G. M. Photiadis, G. N. Papatheodorou, Co-ordination of thorium(IV) in molten alkali-metal chlorides and the structure of liquid and glassy thorium(IV) chloride, *Journal of the Chemical Society, Dalton Transactions* (20) (1999) 3541-3548.

## Appendix

### A.1 Oxychloride Synthesis Method

#### Day 1

1. Required materials:
  - a. 150 mL alumina crucible (vacuum baked)
  - b. Alumina stir rod
  - c. LiCl-KCl eutectic (baked, ~125 grams)
  - d.  $\text{SmCl}_3$  at desired concentration
  - e.  $\text{Li}_2\text{CO}_3$  in equimolar ratio to samarium
2. Fire alumina components overnight at 750°C.
  - a. Hot end of alumina rod will be used for stirring.
3. Melt eutectic at a temperature 550 – 600 °C.
  - a. Remove film from eutectic once molten.
4. Dissolve  $\text{SmCl}_3$  into eutectic once salt is molten, stirring with alumina rod.
  - a. Allow for melt to sit overnight and solvate samarium.

#### Day 2

5. Add equimolar amount of  $\text{Li}_2\text{CO}_3$  in small increments.
  - a. Stir vigorously to manage  $\text{CO}_2$  bubble formation.
6. Occasionally stir solution throughout day and cool down overnight.
  - a. If overflow occurred, remove crucible while hot to prevent immobilization.
7. Prepare EDTA-NaOH solution overnight while melt cools down.

- a. 3x molar excess EDTA massed for complexation.
- b. 4x molar excess NaOH to fully deprotonate EDTA.

**Day 3**

8. Add cooled crucible to complexing solution next morning.
  - a. Allow salt to dissolve throughout day.
9. Remove crucible and allow solution to stir overnight at end of day.

**Day 4**

10. Turn off agitation next morning and allow solution to settle for 24 hours.
  - a. Remove stir bar now.

**Day 5**

11. Decant EDTA-NaOH solution off of precipitate using plastic tubing.
  - a. Save to rinse beaker with during precipitate collection.
12. Collect precipitate into centrifuge tubes.
  - a. Use excess EDTA-NaOH solution to consolidate precipitate.
  - b. Limit centrifuge tube total to twelve.
13. Centrifuge samples for 6 hours at ~3000 rpm.
  - a. Pour solution into waste as deprotonated EDTA-NaOH.
  - b. Begin 2-day vacuum bake of clean alumina crucible for precipitate drying.
14. Dry open centrifuge in fume hood overnight.
  - a. Allow for adequate air flow over tubes.

**Day 6**

15. Consolidate precipitate into dried alumina crucible.

- a. Do not include any precipitate that is not white or beige in nature.

16. Bake precipitate under vacuum for 3 days.

- a. Execute highest heat setting.

**Day 7**

17. Confirm SmOCl formation using X-ray diffraction (XRD).

## A.2 Technical Meeting Abstracts

Abstract #3441, PRIME 2016/230th ECS Meeting, © 2016 The Electrochemical Society

### Characterization of the Electrochemical Behavior of a Li-Bi Reference Electrode for the Molten LiCl-Li

William Phillips<sup>a</sup>, Augustus Merwin<sup>a</sup>, Vickram Singh<sup>a</sup>, Dev Chidambaram<sup>a</sup>

<sup>a</sup>University of Nevada Reno

In order to maximize uranium resources and minimize the need to store radioactive material in geologic repositories, it is necessary to reprocess used nuclear fuel (UNF) to recycle the fissile material and transuranic isotopes that remain. The pyroprocessing operation developed by Argonne National Laboratory as part of the integral fast reactor project was designed to accomplish this goal while minimizing the risk of proliferation (1). Inclusion of oxide based UNF from the current light water reactor fleet into the metallic fuel based fast reactor cycle will require electrolytic oxide reduction in a LiCl-Li<sub>2</sub>O electrolyte (2). As a side reaction during the electroreduction of U, Li is codeposited on the cathode surface and subsequently dissolves, forming a ternary LiCl-Li<sub>2</sub>O-Li electrolyte (3, 4). The presence of metallic Li in the electrolyte negates the possibility of using the reference electrodes typically used for molten salt electrochemistry. The Li-Bi couple has been used as a reference electrode previously but has not yet been well characterized (5, 6). This work investigates the stability of the Li-Bi reference couple in varying solution chemistries typical of those found during electrolytic reduction of UO<sub>2</sub>.

**Acknowledgements:** This work was performed under the auspices of the Department of Energy (DOE) under contracts DE-NE0008262 and DE-NE0008236, and the US Nuclear Regulatory Commission (NRC) under contracts NRCHQ-11-G-38-0039, NRC-HQ-10-G-38-0027, NRC-HQ-13-G-38-0027. W.P. and A.M. acknowledge the Fellowship Award from the USNRC. Dr. Kenny Osborne serves as the program manager for the DOE award and Ms. Nancy Hebron-Isreal serves as the grants program officer for the NRC awards.

**References:**

1. J. J. Laidler, J. E. Battles, W. E. Miller, J. P. Ackerman, E. L. Carls, Development of Pyroprocessing Technology. *Progress in Nuclear Energy*31, 131-140 (1997).
2. S. D. Hermann, S. X. Li, M. F. Simpson, S. Phongikaroon, Electrolytic Reduction of Spent Nuclear Oxide Fuel as Part of an Integral Process to Separate and Recover Actinides from Fission Products. *Separation Science and Technology*41, 1965-1983 (2006).
3. T. Takenaka, K. Shigeta, H. Masuhama, K. Kubota, Influence of Some Factors upon Electrodeposition of Liquid Li and Mg. *ECS Transactions*49, 441-448 (2009).
4. A. S. Dworkin, H. R. Bronstein, M. A. Bredig, Miscibility of Metals with Salts. VI. Lithium-Lithium Halide Systems. *The Journal of Physical Chemistry*66, 572-573 (1962).
5. M. Iizuka, Y. Sakamura, T. Inoue, Electrochemical reduction of (U-40Pu-5Np)O<sub>2</sub> in molten LiCl electrolyte. *Journal of Nuclear Materials*359, 102-113 (2006).
6. X. Ning et al., Self-healing Li-Bi liquid metal battery for grid-scale energy storage. *Journal of Power Sources*275, 370-376 (2015).

**Electrochemical Behavior of Samarium in Molten LiCl-KCl**Vickram Singh<sup>a</sup>, Dev Chidambaram<sup>a</sup><sup>a</sup>University of Nevada Reno

The mass transport behavior of samarium was investigated in molten eutectic LiCl-KCl in order to develop real-time concentration monitoring capabilities for the pyrochemical reprocessing of used nuclear fuel. Pyrochemical reprocessing relies on electrolysis in molten LiCl-KCl to recycle fissile material from used nuclear fuel. Without the capabilities to monitor concentrations of various actinides and fission products, pyrochemical reprocessing cannot be commercialized due to strict material accountability requirements set by the International Atomic Energy Agency (IAEA) [1]. Therefore, physical electrochemical properties of these species in molten salts is extremely important. Cyclic voltammetry was utilized to investigate electrochemical behavior of samarium in LiCl-KCl. By establishing valid relationships between these parameters and the peak current, the diffusion coefficient of samarium in our system can be reported with confidence [2]. Experiments were conducted in a high-purity argon atmosphere glove box using a three-electrode cell contained in an alumina crucible inside a resistive furnace. A high-resolution translation stage equipped with ceramic electrode mounts was used to accurately control electrode positions inside the melt. Tungsten was used as the counter and working electrodes, and a silver wire was used as a quasi-reference ( $\text{Ag}|\text{AgCl}_2$ ). The variation in peak current that resulted from changing the concentration, scan rate and electrode surface area will be reported, along with calculated diffusion coefficient values for samarium in molten LiCl-KCl at 500°C. The effects of using molybdenum as a working electrode will also be reported and compared to results obtained using tungsten. A comparison between reported diffusion coefficient values obtained by separate research organizations and results obtained in these studies will also be discussed.

**Acknowledgements:** This work was performed under the auspices of the Department of Energy (DOE) under contracts DE-NE0008262 and DE-NE0008236 as well as the US Nuclear Regulatory Commission (USNRC) under contracts NRCHQ-11-G-38-0039. Dr. Kenny Osborne serves as the program manager for the DOE award and Ms. Nancy Hebron-Isreal serves as the grants program officer for the NRC awards.

**References**

1. Izuka, M., et al., Application of normal pulse voltammetry to on-line monitoring of actinide concentrations in molten salt electrolyte. *Journal of Nuclear Materials*, 2001, **297**(1): p. 43-51.
2. Tylka, M.M., et al., Method Development for Quantitative Analysis of Actinides in Molten Salts. *Journal of The Electrochemical Society*, 2015, **162**(9): p. H625-H633.

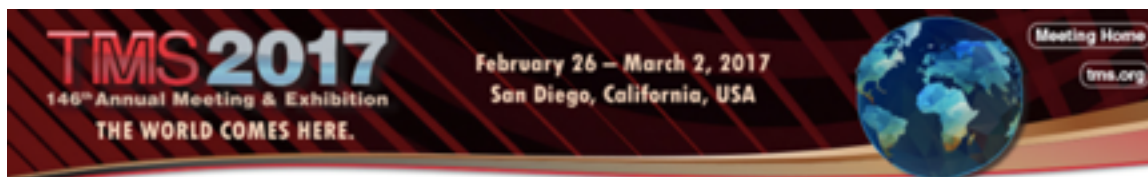


## Materials Science & Technology 2016

October 23-27, 2016: Salt Lake City, UT

### About this Abstract

Meeting	<a href="#">Materials Science &amp; Technology 2016</a>
Symposium	Materials Issues in Nuclear Waste Management in the 21st Century
Presentation Title	Electrochemical Studies of Lanthanide Chlorides in Molten Eutectic LiCl-KCl
Author(s)	Vickram St Singh, Dev Chidambaram
On-site Speaker (Planned)	Vickram St Singh
Abstract Scope	The mass transport characteristics of various lanthanide chlorides were studied in molten eutectic LiCl-KCl as they pertain to the pyrochemical reprocessing of used nuclear fuel. Electrochemical testing was performed to quantify the diffusion coefficient of lanthanide chlorides in the molten salt system. Cyclic voltammetry was utilized as an in-situ technique to measure electrochemical responses, and inductively coupled plasma optical emission spectroscopy was used to determine lanthanide concentrations in the melts. The diffusion coefficients of lanthanides were determined using cyclic voltammetry at varying composition and temperature. The findings of these experiments will be used to develop a method for in-situ monitoring of various species' concentrations during the pyrochemical reprocessing of used nuclear fuel.



**TMS 2017**  
146<sup>th</sup> Annual Meeting & Exhibition  
THE WORLD COMES HERE.

February 26 – March 2, 2017  
San Diego, California, USA

Meeting Home  
tms.org

### About this Abstract

<b>Meeting</b>	<a href="#">2017 TMS Annual Meeting &amp; Exhibition</a>
<b>Symposium</b>	High Temperature Electrochemistry III
<b>Presentation Title</b>	Electrochemical Techniques for Nuclear Safeguards in Molten Salt
<b>Author(s)</b>	Vickram Jit Singh, Dev Chidambaram
<b>On-Site Speaker (Planned)</b>	Vickram Jit Singh
<b>Abstract Scope</b>	<p>Molten salt systems are expected to play a significant role in next generation nuclear reactor designs and pyrochemical fuel reprocessing. Thus, nuclear safeguards techniques must continue to accommodate these new systems. Most safeguards techniques currently in use were developed for aqueous rather than for molten salt systems. The electrochemical technique of cyclic voltammetry may offer an approach to material monitoring in molten salt systems. Electrochemical testing was conducted on a eutectic UCl-KCl system containing lanthanide chlorides serving as actinide surrogates. Since most assumptions associated with cyclic voltammetry and its applications were also developed for aqueous systems, some preliminary studies were conducted to study the reversibility and oxidation tendencies of the above molten-salt system before applying any mathematical relationships to the collected data. Lanthanide surrogate testing was then conducted to evaluate our system and compare results to the literature.</p>

## Nuclear Material Monitoring in Molten Salt Systems using Cyclic Voltammetry

Vickram Singh and Dev Chidambaram\*

Materials Science and Engineering, University of Nevada, Reno  
 1664 N. Virginia St., Reno, NV 89557 MS 0388  
 \*dccc@unr.edu

## INTRODUCTION

As designs for the next generation of nuclear power plants and reprocessing facilities develop, molten salt based systems are receiving increasing attention as fuel containment, cooling and reprocessing media. Traditionally, aqueous systems for power production and fuel reprocessing are associated with well-developed methods for the monitoring and accountability of nuclear material. Many of these techniques are proving insufficient in providing the same information in molten salt systems [1].

The International Atomic Energy Agency (IAEA) has called for the continued evaluation of advanced measurement techniques in systems such as molten salt as part of the Generation IV International Forum (GIF) and International Project on Innovative Nuclear Reactors and Fuel Cycles (INPRO). Cyclic voltammetry (CV) is an electrochemical technique that offers promising applications in molten salt systems for the *in situ* monitoring of nuclear material.

A technique such as CV offers a method for monitoring nuclear material in a system relying on molten salt for power production, cooling or reprocessing. Cyclic voltammetry has been shown to provide information regarding the diffusion of electroactive species in molten salt. Once a diffusion coefficient data base is assembled, CV can be performed on molten salt systems to determine concentrations of species *in situ* [2].

## DESCRIPTION

CV experiments were conducted in a molten LiCl-KCl system associated with the pyrochemical reprocessing of used nuclear fuel (UNF). Pyrochemical reprocessing utilizes a molten eutectic LiCl-KCl electrolyte to electrochemically separate uranium, plutonium and other transuranic (TRU) elements from UNF [3].

The diffusion behavior of samarium in molten LiCl-KCl at 500°C was investigated using CV. Samarium was utilized as an electrochemical surrogate for materials of higher proliferation concern.

Diffusion coefficients at various concentrations, temperatures and potentials sweep rates can be determined from peak current values using the Randles-Sevcik relationship [1].

$$i_p = 0.4463nFAC \left( \frac{nFvD}{RT} \right)^{1/2} \quad (1)$$

## EXPERIMENTAL

CV experiments were conducted at varying samarium concentrations and potential sweep rates. Linear correlation between potential sweep rates and peak currents was investigated, followed by the correlation between peak current and concentration of electroactive species. Diffusion coefficients were then calculated from the obtained CV data.

Tungsten wire and rod served as the working and counter electrode, respectively. A Ag/AgCl (5 mol%) served as a reference electrode. All experiments were conducted in an argon atmosphere with oxygen and moisture levels under 1 ppm. Experiments were automated and sequenced in an attempt to obtain precise and accurate data.

## RESULTS

Preliminary results obtained during CV testing indicated a clear relationship between increasing potential sweep rate and peak currents.

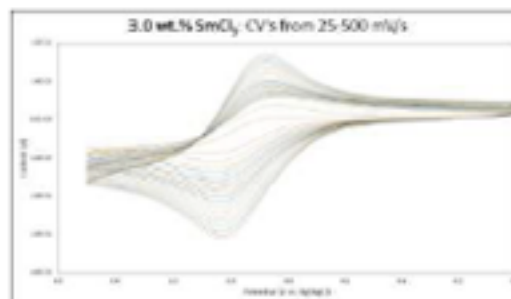


Fig. 1. CV curves obtained at potential sweep rates ranging from 25-500 mV/s for a 3.0 wt. % Sm sample.

The correlation between potential sweep rate and peak current values indicated a strong linear characteristic as well.

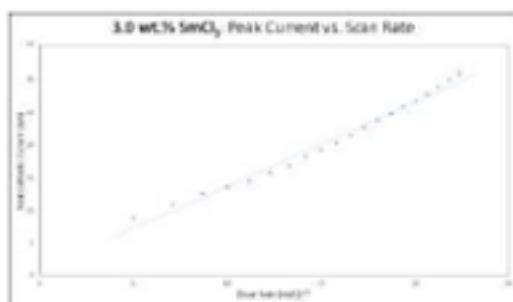


Fig. 2. Peak current vs. the square root of potential sweep rate results for a 3.0 wt. % Sm sample.

Results indicated a high level of repeatability and confirmed linear correlations associated with the Randles-Sevcik relationship.

### CONCLUSIONS

Cyclic voltammetry is a potential *in situ* method for monitoring actinide concentrations inside molten salt systems emerging as part of the next generation of nuclear technology. Although most relationships employed for cyclic voltammetry are associated with aqueous systems, a high level of repeatability and correlation was achieved using the Randles-Sevcik relationship inside a molten eutectic LiCl-KCl sample containing SmCl<sub>3</sub> as an active nuclear material surrogate. Further investigation is required to better understand the limits of Randles-Sevcik applicability in high temperature, molten salt systems.

### ACKNOWLEDGEMENTS

This work was performed under the auspices of the Department of Energy (DOE) under contracts DE-NE0008572, and the US Nuclear Regulatory Commission (NRC) under contract NRCHQ-11-G-3E-0039. V.S. acknowledges the Fellowship Award from the USNRC. Dr. Kenny Osborne and Ms. Nancy Hebron-Irsal serve as the program managers for the DOE and NRC awards, respectively.

### NOMENCLATURE

$A$  = surface area of working electrode  
 $C$  = concentration of electroactive species  
 $D$  = diffusion coefficient  
 $F$  = Faraday's constant  
 $i_p$  = peak current  
 $n$  = number of electron transfers  
 $R$  = ideal gas constant  
 $T$  = temperature  
 $v$  = potential sweep rate

### REFERENCES

1. TYLKA, M.M., et al., *Method Development for Quantitative Analysis of Actinides in Molten Salt*, Journal of The Electrochemical Society, 2015, 162(9): p. H625-H633.
2. WILLIT, J.L., W.E. MILLER, and J.E. BATTLES, *Electrorefining of uranium and plutonium — A literature review*, Journal of Nuclear Materials, 1992, 195(3): p. 229-249.
3. WILLIAMSON, M.A. and J.L. WILLIT, *Pyroprocessing flowsheets for recycling used nuclear fuel*, Nuclear Engineering and Technology, 2011, 43(4): p. 329-334.

**232<sup>nd</sup> ECS MEETING****National Harbor, MD**

October 1-5, 2017

Gaylord National Resort and Convention Center

**765****In Situ Raman Spectroscopy for Nuclear Material Monitoring in Molten Salt Systems***Wednesday, 4 October 2017: 16:20**Camellia 3 (Gaylord National Resort and Convention Center)**V. Singh (University of Nevada, Reno) and D. Chidambaram (University of Nevada, Reno, Nevada Institute for Sustainability)*



Molten salt systems are under consideration for both energy generation and used fuel processing as part of the nuclear fuel cycle. Generation IV nuclear reactor designs use molten salts as both coolants and fuel media. Advanced reprocessing technologies, such as the pyrochemical reprocessing of used nuclear fuel, rely on molten chloride melts as the electrolyte during electrochemical processing of used nuclear fuel. Before any of these technologies can reach the industrial scale, techniques for the monitoring of nuclear material in a nondestructive and *in situ* manner must be further developed for molten salt systems. Real-time monitoring of nuclear material allows for process optimization, along with addressing nuclear security concerns associated with the diversion of actinide materials. In this study, we explore the use of Raman spectroscopy, employed using a fiber-coupled system, as a method for the *in situ* analysis of molten salt. We present the development of an automated, *in situ*-Raman system for analysis of electroactive species in molten LiCl-KCl. The Raman modes of lanthanide chlorides, serving as actinide surrogates, were investigated in LiCl-KCl eutectic at 500°C and compared with the available literature. This work was performed under the auspices of the US Department of Energy (DOE) under contracts DE-NE0008262, DE-NE0008236 and DE-NE0008572, and the US Nuclear Regulatory Commission (NRC) under contract NRC-HQ-13-G-38-0027. Dr. Kenny Osborne serves as the program manager for the DOE awards and Ms. Nancy Hebron-Isreal serves as the grants program officer for the NRC award.

[See more of: Spectroscopy and Characterization 3](#)[See more of: C03: State-of-the-Art Surface Analytical Techniques in Corrosion 3: In Honor of Hugh Isaacs](#)[See more of: Corrosion Science and Technology](#)[Previous Abstract](#) | [Next Abstract >>](#)

# A.3 University of Nevada, Reno 2016 Graduate Student Poster Contest

## Nuclear Security Applications of Electrochemistry in Molten Salt Systems

Vickram Singh, Aaron Unger and Dev Chidambaram  
 Materials Science and Engineering, University of Nevada, Reno, NV 89557-0388  
 dcc@unr.edu

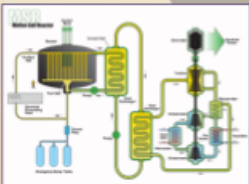
**ABSTRACT**

Molten salt systems are becoming an increasingly common medium for nuclear fuel transport and containment as design for advanced nuclear reactors and used nuclear fuel reprocessing facilities emerge. Fuel transport and containment media have traditionally been aqueous in nature. The techniques utilized to monitor and secure nuclear material inside these systems have therefore been developed for aqueous systems as well. The International Atomic Energy Agency (IAEA) is charged with maintaining the safe and monitored proliferation of nuclear technology, and has called for the advancement of nuclear material accountability techniques to meet the advanced systems emerging as part of the next generation of nuclear power. Cyclic voltammetry is an electrochemical technique that may offer a method for monitoring actinide and lanthanide content inside molten salt systems in real-time. Preliminary studies were conducted to develop an automated and hands-free system for studying the mass transport behavior of lanthanides inside molten LiCl-KCl eutectic. The effectiveness of the system developed was evaluated through comparisons of obtained results with the literature.

**INTRODUCTION**

Nuclear material accountability (NMA) is the backbone of the IAEA's international security regime.

- The IAEA must have the ability to monitor nuclear material inside the nuclear facilities.
- NMA is the monitoring and reporting of nuclear material amounts and locations.
- Aids in the prevention of theft, diversion or clandestine weapons program<sup>[1]</sup>.



Designs are transitioning from traditionally aqueous systems to molten salt systems.

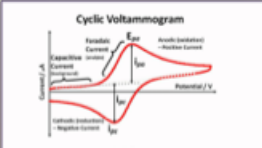
- Advanced NMA techniques must be developed for application in these molten salt systems.

**Cyclic Voltammetry (CV)**

- A potential sweep, reversal technique that provides information regarding the diffusion of electroactive species in electrolytes.
- The Randles-Sevcik relationship can be used to study diffusion coefficient values for species in molten salt systems<sup>[2]</sup>.

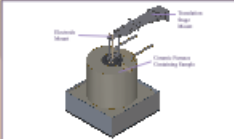
$$I_p = 0.4463nFAC \frac{n^2 D^{1/2}}{\pi^{1/2} t^{1/2}}$$

**EXPERIMENTAL**



**EXPERIMENTAL APPARATUS**

- All experiments were conducted in an argon atmosphere glove box.
- Automated using LabVIEW to allow for hands-free operation of Gamry potentiostat, Watlow furnace and Zaber translation stage.

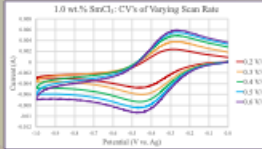
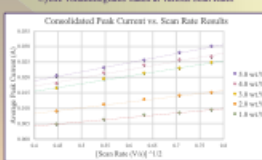
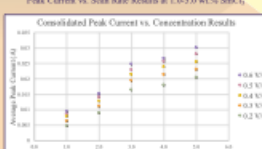



**Samarium Chloride in Molten LiCl-KCl**

- Randles-Sevcik peak current vs. scan rate and concentration correlations were investigated.
- A high level of reproducibility as it pertains to the engineering-scale application of these methods was also a goal of this study.

**RESULTS**

Below are the SmCl<sub>3</sub> results of the investigation into the peak current correlations at 500°C.

**CONCLUSIONS**

**Evaluation of Diffusion Coefficient Values**

- Results were similar to the literature values for SmCl<sub>3</sub>.
- High level of variability in the literature due to the many parameters (temperature, concentration, surface area, etc.) in the Randles-Sevcik relationship.

Source	Diffusion Coefficients (cm <sup>2</sup> /s)
Conditka, G. et al. [3]	(0.43 - 2.70) · 10 <sup>-6</sup>
Castillo, E. et al. [6]	(4.3 - 11.0) · 10 <sup>-6</sup>
Zhang, J. [7]	5.34 · 10 <sup>-6</sup> - 1.92 · 10 <sup>-5</sup>
This Study	(2.68 - 5.35) · 10 <sup>-6</sup>

**Literature Comparison of Diffusion Coefficients of SmCl<sub>3</sub>**

- Peak current vs. concentration results indicate a possible shift away from Randles-Sevcik applicability or two linear regions.
- Preliminary results do indicate a potential application of CV to the IAEA's NMA regime.

**REFERENCES**



- IAEA Handbook: Securing the Supply of Nuclear Weapons. IAEA 1981 Annual Report "Nuclear Security & Safeguards", 2001, 0811 p. 4.
- Guidance for States Developing Comprehensive Safeguards Agreements and Additional Protocols. International Atomic Energy Agency Technical Series, 2002/23 p. 160.
- Isner, D.H., Integrating the Nuclear Non-Proliferation Treaty. 1st, 2011, New York, UN Global University Press, 224.
- Maly, M. et al. (2015). "Method Development for Quantitative Analysis of Actinides in Molten Salts." *Journal of Electroanalytical Chemistry*, 180(1), 1802-1815.
- Conditka, G. and C. Cameron (2008). "An electrochemical study of uranium ions in the molten eutectic LiCl-KCl." *Journal of Electroanalytical Chemistry*, 675(1), 103-110.
- Castillo, E. et al. (2013). "Cyclic Voltammetry and Chronoamperometry of Uranium Ion in Two Molten Chlorides with Different Solubility Properties." *The Electrochimica Acta*, 107, 128-134.
- Zhang, J. (2016). "Electrochemistry of actinides and fission products in molten salts." *Chem Review*, *116*(16), 4971-5016.

**ACKNOWLEDGMENTS**

This work was conducted under the following funding contracts:

- Department of Energy (DOE) contracts DE-NE0006262, DE-NE0006236 and DE-NE0008572
- US Nuclear Regulatory Commission (NRC) contracts NRC-HQ-11-G-38-0039 and NRC-HQ-13-G-38-0027.

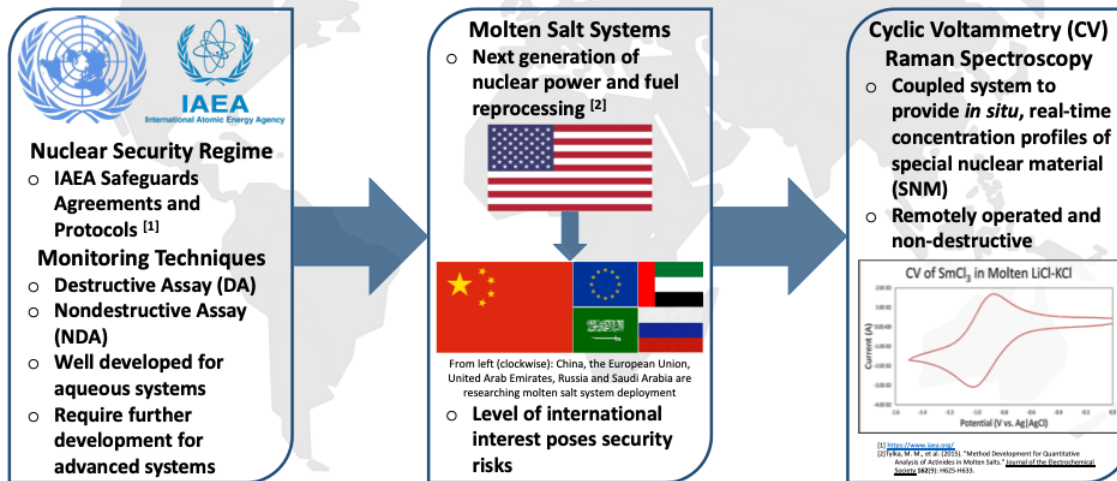
Dr. Kenny Osborne serves as the program manager for the DOE award. Ms. Nancy Habron-Irrel serves as the grants program officer for the NRC grants.

## A.4 University of Nevada, Reno 2018 3 Minute Thesis

# NUCLEAR MATERIAL ACCOUNTANCY

## A Safe and Secure Future



Vickram Singh – PhD Student – Materials Science & Engineering